

**OPTOELECTRONIC STUDIES ON CdS AND Zn-DOPED CdS
THIN FILMS FOR PHOTO SENSING DEVICES**

Thesis Submitted for the Award of the Degree

of

DOCTOR OF PHILOSOPHY

in

(Physics)

By

Rekha Rani

(Reg no: 11919209)

Under the Supervision of

Prof. Rajesh Kumar




LOVELY PROFESSIONAL UNIVERSITY, PUNJAB

2024

DECLARATION

I, hereby declared that the presented work in the thesis entitled “**OPTOELECTRONIC STUDIES ON CdS AND Zn-DOPED CdS THIN FILMS FOR PHOTSENSING DEVICES**” in fulfilment of degree of **Doctor of Philosophy (Ph. D.)** is outcome of research work carried out by me under the supervision Prof. Rajesh Kumar, Department of Physics, School of chemical engineering and physical sciences at Lovely Professional University, Punjab, India. In keeping with general practice of reporting scientific observations, due acknowledgements have been made whenever work described here has been based on findings of other investigator. This work has not been submitted in part or full to any other University or Institute for the award of any degree.

(Signature of Scholar)



Name of the scholar: Rekha

Registration No.: 11919209

Department/school: Physics

Lovely Professional University,
Punjab, India

CERTIFICATE

This is to certify that the work reported in the Ph. D. thesis entitled “**OPTOELECTRONIC STUDIES ON CdS AND Zn-DOPED CdS THIN FILMS FOR PHOTSENSING DEVICES**” submitted in fulfillment of the requirement for the reward of degree of **Doctor of Philosophy (Ph.D.)** in the department of Physics, is a research work carried out by Rekha (Reg. no-11919209), is bonafide record of his/her original work carried out under my supervision and that no part of thesis has been submitted for any other degree, diploma or equivalent course.

(Signature of Supervisor)

Name of supervisor: Dr. Rajesh Kumar (12236)

Lovely Professional University

Jalandhar-Delhi, G.T. Road (NH-1), Phagwara

Punjab (INDIA) -144411

Abstract

Photodetectors are the devices that convert light signal in to electrical signals. They are widely used in Imaging, communication, sensing and electronic devices. The development of photodetectors has reduced the consumption of electrical energy and are helpful to save the energy sources. CdS is one of the stable and promising material for the photovoltaic applications. In solar cells, it is commonly used as window layer material. This work was performed to improve the optoelectronic properties of the CdS and Zn:CdS thin-films for the photosensors. The optoelectronic properties of the prepared thin films were improved through the optimization of the process parameters during the synthesis process, deposition of thin films and post deposition also. The prepared thin films were annealed at different temperatures to study their structural and optical properties. Post deposition thin films were analyzed through different characterizations such as X-ray diffraction, UV-Visible spectroscopy, Field emission spectroscopy, Raman spectroscopy. The optical band-gap of the thin-films varied in the range 2.43-2.44 eV. The photosensitivity of thin films was also calculated through electrical studies carried out with the help of Keithley source meter. The sensitivity of CdS thin decreased due to formation of Cadmium oxide impurity phase. Thus, CdS thin films annealed at 400 °C showed good electrical results under the illumination conditions. Subsequently, Zn has been incorporated during the synthesis process to improve various optoelectronic properties of Zn: CdS thin films and results were compared with undoped CdS thin films. The work was performed for the different concentration of Zn dopant (1, 2 and 3 weight percent). No additional impurity phase such as ZnO or ZnS was observed in XRD and Raman spectroscopy. In XRD studies, diffraction patterns corresponding to (100), (002), (101), (110) and (201) planes were observed. The obtained patterns depicted the hexagonal phase of CdS. Improvements in optoelectronic properties of Zn:CdS thin films were noticed for CdS thin films with Zn 3% by weight. Further increase in Zn Concentration introduced distortion in the structural characteristics of thin films and also reduced the photosensitivity of the thin film elements due the formation of deep level defects. In order to increase the scope of applications of photodetectors, CdS and Zn: CdS thin films were also deposited on the flexible substrates made up of Polyethylene Terephthalate (PET). Photosensors fabricated on flexible substrates are widely used nowadays to reduce the size of optoelectronic devices. Subsequently, structural, optical and electrical characterizations of thin films on flexible substrates were carried out. Thin films were annealed at 300 °C for 120 minutes. The observed results for CdS thin films on PET were comparable with thin films deposited on glass substrate while distortion was observed

for Zn:CdS thin-films deposited on PET. The results obtained during this research investigation shows that these type of photodetectors are quite beneficial for biomedical applications, digital cameras and process control in various industries.

Acknowledgements

First of all I would like to thank Almighty who kept on guiding me during this journey. The spirituality and peace are two connected terms which made me capable to overcome the anxiety and difficulties faced during this tough journey. I feel self blessed. I could complete this task well on time.

The completion of this work could not be possible without the expertise of Dr. Rajesh Kumar, Professor at Lovely Professional University Jalandhar(Punjab). I would like to thank him for his consistent supervision. During this journey he shared his knowledge and experiences to accomplish this thesis. I shall ever remain indebted for his corporation which inculcated in me profound scientific knowledge.

I would also like to thank the Dr. Kailash chandra juglan, “Head of the school of chemical sciences and engineering”, Lovely Professional University, Jalandhar (Punjab) for his guidance and availing all the required resources, providing well equipped research labs and instrumentation facilities for the research purpose. All this could be possible due to his determination and consistent lab visits.

I would like to thank all my family members, specially husband (Mr. Ritesh Aggarwal) and my only son (Rithvik Aggarwal) who supported me throughout this journey without complaining.

I would like to express my gratitude to Dr. Naveen kumar, Assistant Professor at Lovely Professional University, Jalandhar (Punjab) for his support and corporation. I really grateful to him as he supported and guided us a lot whenever required. We are really thankful to him for providing his precious time and guidance.

Rekha
(11919209)

Table of Contents

<i>1.1</i>	<i>Introduction</i>	<i>1</i>
<i>1.2</i>	<i>Type of photodetectors</i>	<i>2</i>
<i>1.3</i>	<i>Principle of Photodetectors</i>	<i>2</i>
<i>1.4</i>	<i>Characteristics parameters of a photodetector</i>	<i>3</i>
<i>1.4.1</i>	<i>Photocurrent and Dark current</i>	<i>3</i>
<i>1.4.2</i>	<i>Rise and Recovery Time</i>	<i>3</i>
<i>1.4.3</i>	<i>Photosensitivity</i>	<i>3</i>
<i>1.4.4</i>	<i>Quantum efficiency</i>	<i>4</i>
<i>1.4.5</i>	<i>Responsivity</i>	<i>4</i>
<i>1.5</i>	<i>Preferred Materials</i>	<i>4</i>
<i>1.6</i>	<i>Chemical and Physical Structure</i>	<i>6</i>
<i>1.7</i>	<i>Previously reported literature</i>	<i>8</i>
<i>1.8</i>	<i>Thin films synthesis</i>	<i>17</i>
<i>1.9</i>	<i>Applications</i>	<i>18</i>
<i>1.10</i>	<i>Aim of the Present work</i>	<i>19</i>
<i>1.11</i>	<i>Proposed Objectives</i>	<i>20</i>
<i>2.1</i>	<i>Introduction</i>	<i>22</i>
<i>2.2</i>	<i>Synthesis</i>	<i>22</i>
<i>2.3</i>	<i>Thin- films fabrication</i>	<i>25</i>
<i>2.4</i>	<i>Characterization Techniques</i>	<i>26</i>
<i>2.4.1</i>	<i>UV-Visible Spectroscopy</i>	<i>26</i>
<i>2.4.2</i>	<i>X-Ray Diffraction Technique</i>	<i>28</i>
<i>2.4.3</i>	<i>Raman spectroscopy</i>	<i>30</i>
<i>2.4.4</i>	<i>FESEM</i>	<i>31</i>
<i>2.4.5</i>	<i>Electrical Characterization</i>	<i>32</i>
<i>3.1</i>	<i>Introduction</i>	<i>34</i>
<i>3.2</i>	<i>Results and discussion</i>	<i>35</i>
<i>3.2.1</i>	<i>Thermal annealing effect on structural and optical properties</i>	<i>35</i>
<i>3.2.2</i>	<i>Structural and optical properties of CdS thin films synthesised at pH-10</i>	<i>46</i>
<i>3.2.3</i>	<i>Study the Molar concentration effect on structural and optical properties</i>	<i>50</i>
<i>3.2.4</i>	<i>Structural and optical study of thin films deposited on flexible substrate</i>	<i>56</i>
<i>3.3</i>	<i>Summary</i>	<i>59</i>

4.1	<i>Introduction</i>	61
4.2	<i>Results and discussion</i>	62
4.2.1	<i>Structural and optical studies of Zn:CdS thin films fabricated on SLG</i>	62
4.2.2	<i>Structural and optical properties of Zn:CdS thin films deposited on flexible substrate</i>	69
5.1	<i>Introduction</i>	74
5.2	<i>Results and discussion</i>	74
5.3	<i>Photoconductivity</i>	75
6.1	<i>Summary</i>	85
6.2	<i>Conclusion</i>	86
6.3	<i>Future scope</i>	87

List of Figures

<i>Fig.1. 1 Shows the absorption of Direct and In-direct band gap materials</i> -----	6
<i>Fig. 1. 2-CdS-Hexagonal</i> -----	7
<i>Fig. 1.3 - CdS- fcc cubic</i> -----	7
<i>Fig.1. 4 The above image represents the Applications of Phtoto-sensors</i> -----	18
<i>Fig. 1. 5 Represents the different types of sensors used in biomedical commonly</i> -----	19
<i>Fig. 2.1 Sol-gel preparation methodology</i>	24
<i>Fig. 2.2 Represents the Photograph of thin films deposition set-up Spin- coaterattached with vacuum pump</i>	25
<i>Fig. 2.3 Represents the photograph of UV-visible spectrophotometer (UV- 1900i)</i>	26
<i>Fig. 2. 4 Photograph of Bruker X-ray diffractometer (AXS D8 ADVANCE A25)</i>	28
<i>Fig. 2.5 Represents the X-ray diffraction pattern images for crystalline, semicrystalline and amorphous materials [85].</i>	29
<i>Fig. 2. 6 Represents the Photograph of Raman spectrophotometer available withlaser source of 488 and 532 nm wavelength</i>	31
<i>Fig. 3. 1 The above diagram shows the XRD-diffraction patterns of samples coded 1a-1c annealed at different temperatures for 30 minutes with pH-8</i>	36
<i>Fig. 3. 2 The above diagram shows the X-ray diffractograms of CdS thin filmsannealed at different temperatures for 60 minutes with pH-8</i> -----	37
<i>Fig. 3. 3 The above diagram shows the X-ray diffractograms of thin-film samples coded 3a- 3c (Refer table 3-A)</i> -----	37
<i>Fig. 3.4 The above diagram shows annealing temperature and time effect on the surface micrographs for thin film samples coded as 1a-1c</i> -----	38
<i>Fig. 3.5 The above diagram shows the surface micrographs for thin films annealed for 60 minutes at different temperatures</i> -----	39
<i>Fig. 3. 6 The above diagram shows the surface micrographs for thin films annealed for 90 minutes at different temperatures</i> -----	40
<i>Fig. 3. 7The above diagram shows the transmission spectra of thin films samples 1a-3c with pH-8 annealed at different temperatures 400 °C ,450 °C and500 °C for 30 min, 60 min and 90 min</i> -----	42
<i>Fig. 3. 8The above diagram shows the Energy gap (E_g) of samples coded as 1a-1c.</i> -----	42
<i>Fig. 3.9 The above diagram shows the Energy gap (E_g) of samples coded as 2a-2c.</i> -----	43

<i>Fig. 3. 10 The above diagram shows the Energy gap (E_g) of samples coded as 3a-3c</i>	<i>44</i>
<i>Fig. 3. 11 The above diagram represents the observed Longitudinal modes of (A) 1a-1c shows 30 minutes annealed samples, (B) 2a-2c shows 60 minutes annealed samples and (C) 3a-3c shows the LO modes of 90 minutes annealed samples.</i>	<i>45</i>
<i>Fig. 3. 12 The above diagram shows the X-ray diffractograms of thin film samples coded 4a-4c annealed for 60 minutes</i>	<i>47</i>
<i>Fig. 3. 13 The above diagrams represent the W-H plots of thin film samples coded as 4a, 4b, 4c annealed for 60 minutes.</i>	<i>47</i>
<i>Fig. 3. 14 The above diagram shows the observed (A) transmittance spectra and (B) TAUC-plot for thin films samples coded as 4a-4c annealed for 60 minutes.</i>	<i>49</i>
<i>Fig. 3. 15 The above diagram represents the Raman spectra of thin film samples coded as 4a-4c annealed for 60 minutes with pH-10.</i>	<i>50</i>
<i>Fig. 3.16 The above diagram shows the X-ray diffractograms of CdS thin-films prepared with (5a) 0.2M, (5b) 0.3M, and (5c) 0.4 M molar concentrated sol and annealed at 400°C for 180 minutes.</i>	<i>52</i>
<i>Fig. 3. 17 The above diagram represents the W-H plots of thin film samples prepared by varying the molar concentration of the sol where (5a) 0.2M, (5b) 0.3M, (5c) 0.4M</i>	<i>53</i>
<i>Fig. 3. 18 The above diagram shows the surface micrographs and thickness for CdS thin- films having different molar concentration of precursors</i>	<i>54</i>
<i>Fig. 3. 19 The above diagram shows the transmittance of CdS thin films coded as 5a,5b and 5c with different molar concentration of the solution</i>	<i>55</i>
<i>Fig. 3. 20 The above diagram represents the calculated optical band gap of thin-films samples coded 5a,5b and 5c with different molar concentration of the solution</i>	<i>56</i>
<i>Fig. 3. 21 The above diagram shows the diffraction patterns of thin-films deposited on PET.</i>	<i>57</i>
<i>Fig. 3. 22 Surface morphology of CdS thin-films deposited on PET</i>	<i>57</i>
<i>Fig. 3. 23 The above diagram shows the transmittance graph of CdS thin films deposited on flexible substrate prepared with 0.3 Molar concentrated solution.</i>	<i>58</i>
<i>Fig. 3. 24 The above diagram shows the optical band gap of CdS thin-films deposited on flexible substrate prepared with 0.3 Molar concentrated solution.</i>	<i>58</i>
<i>Fig. 4. 1 The above graph represents the X-ray diffractograms of Zn: CdS thinfilms coded as 6a, 6b and 6c prepared by varying the dopant concentration</i>	<i>64</i>
<i>Fig. 4. 2 Represents the Surface micrographs of Zn: CdS thin films prepared with different</i>	

concentrations(6a) Zn=0.01, (6b) Zn= 0.03 and (6c) Zn= 0.05 of dopant and annealed at 400°C.....	65
Fig. 4.3 Represents the transmittance of $CdxZn1-xS$ thin films (where 6a, 6b and 6c corresponds to $x=0.01, 0.03, 0.05$)	67
Fig. 4. 4 Optical band gap of $CdxZn1-xS$ (where 6a, 6b and 6c corresponds to $x = 0.01, 0.03, 0.05$) thin films annealed at 400°C.....	67
Fig. 4. 5 The above graphs 6a,6b and 6c represents the optical phonon modes of Zn: CdS thin films.	69
Fig.4. 6 The above graph represents the X-Ray diffraction pattern for $CdxZn1-xS$ (where $x=0.03$) thin film deposited on PET	70
Fig. 4. 7 The above graph represents the W-H plot for thin film sample codedas 7b deposited on PET	70
Fig. 4. 8 Represents the Surface micrograph of $CdxZn1-xS$ (where $x=0.03$) thin films deposited on PET	71
Fig. 4. 9 Represents the transmittance curve for $CdxZn1-xS$ (where $x = 0.03$) thinfilms deposited on PET	72
Fig. 4. 10 The above graph represents the Optical band gap of $CdxZn1-xS$ (where $x0.03$) thin films deposited on PET	72
Fig. 5. 1 Represents the I-V characteristics of thin films annealed at (4a) 400°C,(4b) 450 °C and (4c) 500°C for 60 minutes.	76
Fig. 5. 2 Represents the Photoconductivity of thin films samples coded as 4a, 4band 4c annealed at 400 °C, 450°C and 500 °C. -----	77
Fig.5. 3 Represents the I-V characteristics of $CdxZn1-xS$ where 6a,6b and 6c are the graphs of thin films prepared with different concentration of Zn i.e. $x=0.01,0.03$ and 0.05 -	78
Fig. 5. 4 Represents the Photoconductivity of $CdxZn1-xS$ where 6a,6b and 6c arethe graphs of thin films prepared with different concentration of Zn i.e. $x=1 \%,2 \%$ and 3% and prepared thin films were annealed at 400 °C.-----	79
Fig 5. 5 Represents the I-V characteristics of CdS thin films deposited on PETannealed at 300 °C-----	80
Fig. 5.6 Represents the I-V characteristics of $CdxZn1-xS$ ($x=2\%$) thin filmsdeposited on PET.-----	81
Fig. 5. 7 Represents the Photoconductivity of CdS and $CdxZn1-xS$ (where $x=0.03$)thin films on PET substrate. -----	82

List of Tables

<i>Table 2- 1 Represents the chemical used for the synthesis of CdS solution.....</i>	<i>23</i>
<i>Table 3- A Represents the composition, annealing temperature and annealing-time and figure coding for the prepared samples of CdS thin films -----</i>	<i>34</i>
<i>Table 3- B Shows the Calculated optical band gap for thin films 1a-3c from Tauc-plot----</i>	<i>44</i>
<i>Table 3- C Shows the observed values for peak position (2θ), FWHM (β), Crystallite size (D) and Lattice strain -----</i>	<i>48</i>
<i>Table 3- D Shows the Peak position (2θ), FWHM(β), Crystallite size (D) and the value of lattice strain.-----</i>	<i>53</i>
<i>Table 4- A The table below represents the pH-values, annealing temperature and annealing time and sample coding for the prepared samples of Zn doped CdS thin films deposited on SLG and PET -----</i>	<i>62</i>
<i>Table 4- B Represents the d-spacing between different Plane orientations for Zn: CdS thin films. -----</i>	<i>63</i>
<i>Table 4- C Lattice parameter of Zn: CdS thin films -----</i>	<i>63</i>
<i>Table 4- D Represents the 2θ, FWHM, Crystallite size(D), dislocation density(δ) -----</i>	<i>64</i>
<i>Table 5- A Represents the photocurrent, dark current, rise time and decay time for CdS thin films coded as 4a,4b and 4c -----</i>	<i>77</i>
<i>Table 5- B Represents the Photocurrent, dark current, Photosensitivity, Responsivity, response time and recovery time for Zn doped CdS thin films coded as 6a, 6b and 6c. -----</i>	<i>80</i>
<i>Table 5- C Represents the calculated values of Photocurrent, dark current, sensitivity, response time and recovery time for maximum intensity for thin films coded as- 7a and 7b deposited on PET substrate -----</i>	<i>81</i>
<i>Table 5- D Represents the Previous work reported -----</i>	<i>83</i>

List of symbols

1)	Peak position	2θ
2)	Full width half maxima	β
3)	Crystallite size	D
4)	Lattice strain	ϵ
5)	Dislocation density	δ
6)	Interplanar spacing	d
7)	Transmittance	T
8)	Absorption cofficeint	α
9)	Thickness	d
10)	Energy gap	E_g
11)	Intensity of light	I
12)	Power of light	P
13)	Photocurrent	I_{ph}
14)	Dark current	I_d
15)	Photo sensitivity	S
16)	Responsivity	R



Chapter-1

Introduction

1.1 Introduction

Human lives are completely dependent on various forms of energy such as mechanical energy, heat energy, gravitational energy, electrical energy etc. World-wide increase in population raised the demand of industrialization and automation to full fill the daily needs of the society. Thus, the huge demand of energy sources also raised. Coal, fossil fuel, crude oils are the preferable sources of energy used by human beings to make their work faster and easy. Due to limited availability of these energy sources and their high usage will surely lead to energy crises in coming years. To overcome this problematic situation, early decision of preferable use of natural sources of energy in various fields was taken. Solar energy and water are considered as main natural resource of energy. Since 54.6% of total workforce are dependent on agriculture for their lives and contributes 17.7% to our economy. Thus, a huge amount of water is used in harvesting, for daily activities, for the production of electricity in hydrothermal plants also. At the same time the occupation of land for making houses, to establish industries and deforestation disturbed the nature cycle. This cause the global warming which affects the rain cycle and many rivers, ponds natural sources of water are became dried. Ground level water also became very low. Thus, the production of electricity through photodetection helped us to limit the usage of available energy sources and save them.

Now the days, Photon detection is considered as an integral technology in various fields such as industries, automobiles, fiber optics telecommunication, research etc. It is widely accepted technology which also opens up the door for researcher to explore devices such as photodiodes phototransistors, cameras for sensing images, photomultiplier tube, enormous arrays used by astronomers to detect radiation from the universe etc. As many novel photodetector materials still suffer from limited photocurrent and photo-response speed. Photodetectors are the photon sensing devices which convert light signals into electrical signals [1]. Photodetectors are categorized depending on their light detection mechanism that is photoelectric effect, thermal effect, photo-chemical effect etc. In semiconductor-based photodetectors, the photogenerated charge carriers are collected at the electrodes. Photogeneration takes place if energy of the incident photon is more than band-gap of the semi-conducting material. In order to gain the electric signal external electric field is required which help to keep electrons and holes apart from each other. In the absence of electric field after some time ($\sim 10^{-8}$ sec) electron will automatically come back to its initial state. The evolution of photodiodes is associated with development of the PN junction diode that started in early 1940s. Later PIN structure was first

investigated and published by[2]. Silicon has been the favoured material for photodiode and the use of germanium was also demonstrated by[3]. In 1960 the first commercial semiconductor photodiode was appeared, particularly for the processing in the visible spectral region. A growth in spectral region was shown in 1964 that operation of a silicon device was possible in the Visible-UV region. Designs that were satisfactory in the visible spectral region proved, however, to have problems at somewhat shorter wavelengths [4].

1.2 Type of photodetectors

With the passage of time different type of photodetectors are developed with improved technology. Photodetectors are mainly divided into two categories on the basis of light detection mechanism.

❖ *Thermal photodetectors*

This case, radiation is absorbed by active material which rises temperature of the active material. The rise in temperature causes change in resistance. The current moves in circuit due to difference in temperature of two metals in contact.

❖ *Photon detectors*

Photon detectors are wavelength dependent; if incident photon energy is more than the band gap of the semiconductor then electron hole pair (EHP) generation takes place. The photogenerated carriers can be detected as electronic signal further with the help of external electric field before they recombine. The rate of EHP generation is proportional to the intensity of light. Performance of the photo detectors depends on wavelength, power and duration of incident photon.

1.3 Principle of Photodetectors

- *Photoelectric effect*
- *Photoconductive effect*
- *Photovoltaic effect*

In photoconductors single layer of semiconducting material is used and ohmic contacts are developed by using a metal at both of its ends. Under the illumination free charge carriers (electron- hole pairs) generates in single layer material which are collected at electrodes by applying some external voltage through the circuit.

Photovoltaic and Photoconductive: Semiconductor based photodetectors mainly work on either photoconductive or photovoltaic principle to generate the electric current [5]. In photovoltaic case, photogenerated electron-hole pairs are separated apart by applying external voltage and

whereas in photoconductive case, internal inbuilt field separates the electron-hole pairs. In semiconductor photodiode, a p-n junction is formed by either different type of materials or same materials but different doping that is same material will act as p-type and n-type. Thus, former photodiodes are known as heterojunction photodiodes and latter are homojunction photodiodes.

1.4 Characteristics parameters of a photodetector

There are many factors which decide the performance of a photodetector. Few parameters are discussed below:

1.4.1 Photocurrent and Dark current

The current measured under the illumination conditions is known as Photocurrent (I_{ph}) while the current under the dark conditions is known as dark current (I_d). The photocurrent is given as

$$I_{ph} = I_{ph(\text{measured})} - I_d \quad (1)$$

1.4.2 Rise and Recovery Time

Rise time and recovery time are very well-known essential parameters. Rise time is defined as time taken by the device to raise its current from 10 % to 90 % under the illumination conditions and time taken by the device to fall the current from 90% to 10 % when light switched off, is known as recovery time. Both parameters decide how quick is the response of prepared device.

1.4.3 Photosensitivity

It is defined as ratio of Photocurrent to dark current. Photocurrent is the current under the illumination while dark current is the value of current without any light exposure. It is represented by(S).

$$S = \frac{I_{ph} - I_d}{I_d} \quad (2)$$

Based on the characteristic parameters, it turns out that intrinsic photoconductor has the maximum internal gain ($> 10^4$), Schottky barrier photodiodes have the shortest response time ($\sim 10^{-11}$ s) and largest bandwidth. APD shows the highest gain bandwidth product among all photodetectors. Along with the advancement in science and technology, size and structure of devices also modified. Nano-sciences brought this transformation in material science. The

properties of a bulk material can be attained and improved in a nano scale material also. Nanowires, nanotubes, nanosheets, nanoparticles and thin films of various materials are under focus.

1.4. 4 Quantum efficiency

It is the ratio of photogenerated carriers to the incident photons. It is also known as internal quantum efficiency. However, external quantum efficiency is often used to assess the performance of a photodetector. It is ratio of photogenerated carriers those are collected at the electrodes to the number of incident photons.

The quantum efficiency is given by:

$$\eta = \frac{I_{ph}}{e\phi} = \frac{I_{ph}}{e} \left(\frac{h\nu}{P} \right) \quad (3)$$

where, ν is frequency of the incident photon, I_{ph} is photocurrent, ϕ is photon flux, and this is related to the optical power (P). In the above relation, reflection of photons from the photodetector is assumed to be zero. Quantum efficiency is high for direct band semiconductor; for GaAs $\eta > 70\%$ whereas for Si (indirect band) $\eta \sim 20\% - 40\%$.

1.4. 5 Responsivity:

The responsivity of photodetector is the ratio of photocurrent generated to the optical power in linear region of response [6]. It may be defined as the measure of sensitivity to the light.

(4)

$$R = \frac{\eta\lambda}{1240} \text{ or } \frac{I_{ph}}{P}$$

where ‘ λ ’ is the wavelength (nm) and ‘ η ’ is quantum efficiency. Responsivity is directly proportional to the wavelength region with light energy greater than the band gap energy. The responsivity decreases with increase in doping concentrations.

1.5 Preferred Materials

Periodic table consists of different types of materials such as metals, semiconductors and

insulators. Insulators are the material with wide band gap and unavailability of free charge carriers. Due to which insulators could not be considered for electronic devices. Semiconductors are the materials with intermediate band gap such that sufficient energy for the generation of free charge carriers and band to band transitions can be absorbed through illumination. In periodic table from group II-VI are known as semiconductors. Semiconductors are preferred for optoelectronic devices as their conductive properties can be enhanced through various ways such as through formation of compound semiconductor, doping of any suitable material, or by forming p-n junction like structures. Compound semiconductors of group III-V and II-VI are mainly used to form Metal oxides and Metal-sulphides such as ZnO, CdS, CdSe, CdTe, ZnS, CuO, PbS, PbSe, In₂S₃, InGaAs etc [7–15]. Apart from metal oxides metal chalcogenide-based compound semiconductors are under intense investigation for various photonic devices such as Photodetectors, Photocatalyst, Photosensors, Photocells, Phototransistors etc. Metal-chalcogenide are great of interest due to their easy and low-cost fabrication, chemically stability and enormous optoelectronic properties [16–20]. Another important aspect of preference depends on the process of absorption of light at a certain wavelength. The absorption needs to be strong and fast to improve the responsivity of photonic devices. On the behalf of that direct band gap materials are always preferred for optoelectronic devices as they show strong absorption under illumination. On the other-hand in case of indirect band gap materials absorption is a slow process as showing in Fig.1.1 . Absorption coefficient also helpful for the estimation of penetration depth(δ) givenby

$$\delta = 1/\alpha \quad (5)$$

Intensity of light varies as

$$I = I_0 e^{-\alpha x} \quad (6)$$

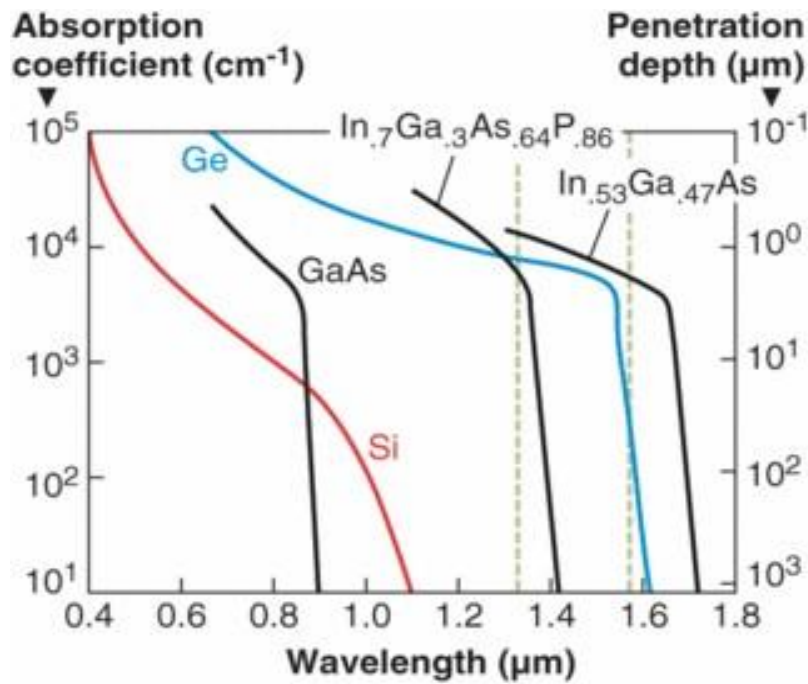


Fig.1. 1 Shows the absorption of Direct and In-direct band gap materials

Cadmium sulphide(CdS) one of the promising semi-conductor. CdS is used as a window layer material in solar cell application [21,22]. It is considered as one of the promising material due to its high transparency greater than 90%. It is yellowish in color. It is polycrystalline in nature. CdS exists in two forms either Zinc blend cubic or hexagonal phase as shown in (Fig. 1.2-1.3). Zinc blend cubic structure is considered as low temperature metastable phase while hexagonal phase is high temperature stable phase. Pure CdS has E_g of 2.42 eV which signifies that it is also suitable to work as photodetector in visible range of electromagnetic spectrum. Due to its n-type intermediate and direct band it shows good optical and electrical properties.

1.6 Chemical and Physical Structure

Physical appearance of CdS is yellowish color powder. CdS possess two different crystal structures as shown in Fig 1.2 - 1.3

- **Zinc Blend cubic**
- **Hexagonal**

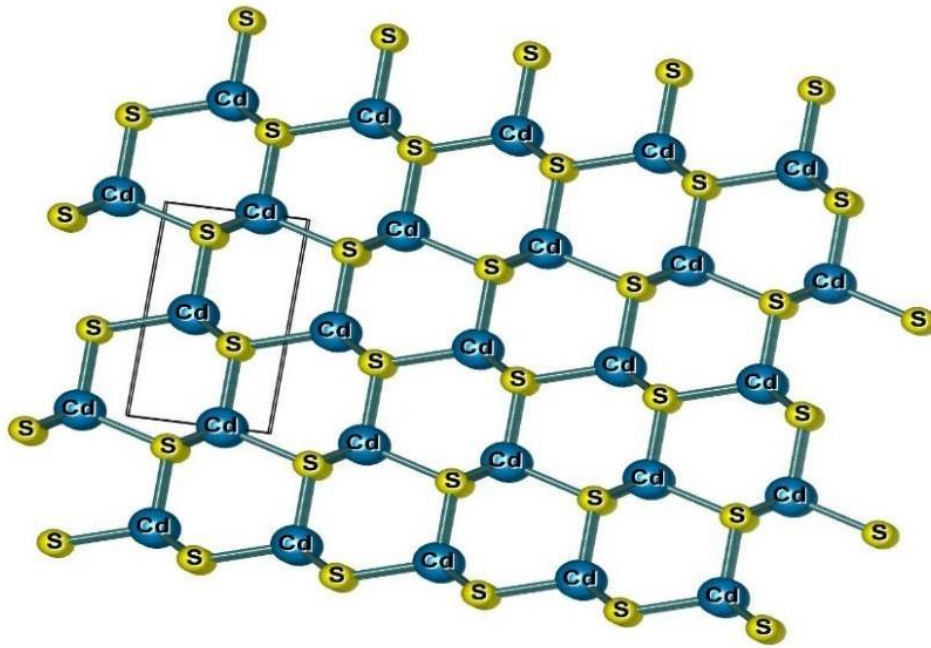


Fig. 1. 2-CdS-Hexagonal

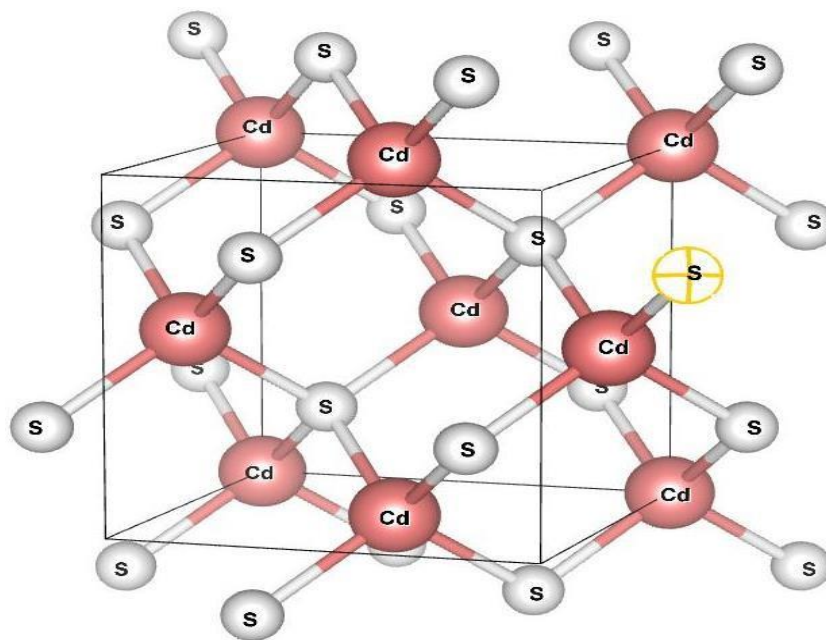


Fig. 1.3 - CdS- fcc cubic

Zinc-blend cubic phase is known as low temperature and unstable phase while hexagonal is known as stable phase. It has been observed in many literature reports that at high temperature cubic phase turns into hexagonal stable phase due to improvement in various lattice parameters. Material in bulk has their own properties but various nanostructures such as thin-films, quantum dots, nanorods etc. has made it possible to attain all the properties of bulk in nanosized

material also. In this work we have synthesized CdS in thin-film mode. Thin-films were preferred as it has large surface to volume ratio. More number of free charge carriers can be avail for the photodetection. As a result, various characteristics parameters such as quantum efficiency, responsivity, sensitivity, photoconductivity can be improved.

1.7 Previously reported literature

Qwens, 2005[23] have reported photodetectors semiconductors belong to group III-V (GaAs, InP) and group II-VI (CdTe) compounds. Compound semiconductor materials are preferred over the elemental semiconductor materials due to wideband gap ranges from 1.35 eV to 2.6 eV. The band-gap energy and the energy of defect formation in $\text{Cd}_{(1-x)}\text{Zn}_x\text{Te}$ could be increased by doping. Doping results in higher leakage currents and resistivity.

Korneva et al., 2006 [24] reported copper antimony sulphides thin films prepared by CVD and a thermal evaporation for visible-infrared photodetector. The photo detection properties were measured by LED and laser, using three different Cu thicknesses (20 nm, 30 nm and 40 nm). 30 nm and 40 nm thin films displayed better photodetector characteristics in a visible region, whereas the 20 nm thin film showed better performance in the NIR region. 20 nm films showed the greatest responsivity for all applied voltages under illumination at various wavelengths. The sensitivity of thin films gradually increases with intensity of 532 nm laser. The highest responsivity was observed for 20 nm, 30 nm and 50 nm at 2 mW, 10 mW and 6 mW respectively.

Scales et al., 2010 [25] Thin film based Schottky barrier photodetectors were developed in three different ways. Photons of energy less than the band gap of semiconductor material but greater than the Schottky barrier energy used to study the internal Quantum efficiency through photoemission process. Schottky barrier was developed between one thick metal layer on semiconductor substrate, second thin layer on semiconductor substrate, thin metal film buried between semiconductor in the third configuration and two Schottky barrier were developed between metal and semiconductor. Thin film-based configuration had shown the finest quantum efficiency and double barrier based Schottky barrier detector had shown greatest quantum efficiency due to double barrier emission process. Such models were designed to investigate the photoemission of the hot carrier because of multiple reflections in metal film. The internal quantum efficiency~2.4 for single barrier photodetector and 4.6 for double barrier was reported.

Frank, 2008; Saravanan et al., 2012[26,27] In this work coprecipitation method was used to synthesis the CdS nanoparticles. Effect of dopant concentration was analysed through

photoluminescence study and Raman spectroscopy. It has been found that dopant will not change the crystal structure. It will only cause the interstitial or substitutional defects. Do Reduction in particle size of the nanomaterials can be attained through doping of rare earth elements. System with rare earth element as a dopant mainly reflect the properties of the dopant.

Roshima et al., 2012[28] had studied the Different type vacancy related defects of CdS thin films deposited by CBD. The role of interstitial Cd, interstitial Sulphur and Sulphur vacancy defects of as prepared sample on emission spectra discussed by studying the PL. A blue shift observed in as prepared thin films due to the presence of defects. Heat treatment effect on as prepared samples also discussed. No change was found in band gap or nanoparticle size due to heat treatment. The point defects moved to the surface due to heating and quenches band edge emission.

Zhang et al., 2013 [29] introduced the trapping centers in quantum dot like structures which raise the carrier life time and by this way responsivity credibly increased from visible to IR (0.4 A/W in mid-IR). For the high-speed electronics, high mobility and narrow band gap is necessary and PtX₂ provides the high mobility 1000 cm²V⁻¹s⁻¹. Experimentally it has been found that mobility, band gap and sensitivity are layer thickness dependent for a 9 nm PdSe₂ films, its bandgap is about 0.16 eV.

Tan et al., 2017 [30] have demonstrated 2D PbI₂ and PbFI based UV photodetectors. The bandgap of crystallized PbF_{2-x}I_x nanosheets was varied from 2.3 eV (PbI₂) to 5.8 eV (PbF₂). The responsivity and speed of PbI₂ photodetectors was 1 × 10⁻⁴ AW⁻¹ and 110 μs respectively. Presence of large trap states due to surface absorbents and defects, a high responsivity of 8 AW⁻¹ and a response speed of 400 ms was observed. At the other hand PbI₂ nanosheets inherent carriers were dominant in electrical conductivity due to high crystallinity and less number of shallow states. The large number of defects in PbFI may lead to parasitic carriers which enables the larger dark current value of PbFI as compared to PbI₂. The decrease of responsivity was also observed at higher power illumination due to filling of all trapped states by photogenerated carriers that leads to saturation of photocurrent.

Alvi & Khan, 2013 [31] synthesized (PbSe)_{100-x}Cd_x nanoparticle thin film by thermal evaporation method at different concentration of Cd in PbSe. A blueshift in the emission peak was observed at 360 nm with decrease in the film (with thickness 20 nm). The addition of Cd to PbSe originated a new peak at 380 nm and further blueshift was observed in these peaks with the increase of Cd. The absorption coefficient of 10⁵cm⁻¹ was observed.

Zhou et al., 2014 [32] The effect of impurities on the responsivity was investigated for pure and tin doped CdS nanostructured based photodetectors at different wavelengths. The synthesized nanowires were found to be sensitive for two different wavelengths i.e. 532 nm and 650 nm wavelengths.

Muthusamy et al., 2014 [33] undoped and Al-doped (0-8% Al) Cadmium Sulphide's thin-films were fabricated through CBD method. The dopant concentration effect on electrical, optical properties and on morphology was studied. The change in nature of defects due to the change concentration of dopant also discussed. At lower concentration (0-4%) substitutional defects were introduced beyond that same dopant cause the interstitial defects in the lattice. The increased dopant concentration directly affected the optical band gap. Red shift was observed.

Husham et al., 2016 [34] nanocrystalline CdS thin film based self-powered photodetector has been fabricated and evaluated by studying different parameters like dark current value, photocurrent, responsivity at zero bias voltage. Photo-luminescence had shown an emission peak at 500 nm and a broader peak at 680 nm which may be due to sulphur vacancies. High ratio of band edge intensity to the defect emission intensity is observed which shows high crystallinity of prepared thin films. I-V characteristics were also studied at low power 1.20 mW/cm^2 at 500 nm.

Pandya, 2016 [35] had prepared CdS thin films by dip coating method. XRD, SEM, UV-spectroscopy and hot probe characterization techniques are used to study optical, electrical and morphological studies. 80% transmission is reported above 530 nm. The direct band gap energy of 2.56 eV and cubic structure has been found.

Zhao et al., 2017 [36] demonstrated the increase of carrier density in ID CdS nanowires with illumination intensity. The photodetector showed higher photocurrent under stronger illumination. The 0.82 s and 0.84 s were recorded as mean response time and recovery time respectively. The 450 nm was observed as better response wavelength than 500 nm by the measurement of photocurrent and responsivity for the CdS nanorods. The enhanced crystalline quality reduced recombination rate.

Suganthi et al., 2017 [37] have reported the structural properties of dip coated CdS thin films. Structural properties were characterized by XRD and SEM and optical study was carried out through UV-Visible spectroscopy. The reported band gap was 2.56 eV with high transmittance about 80%.

Bishop et al., 2017 [38] had investigate Zn-doped CdS thin films by PVD method on glass substrate at 100°C . Thin films are characterized by XRD, SEM and EDAX. No change has been found in crystal structure of CdS. But crystallite size has been decreased with rise in Zn

content. Surface characterization is suggested for future work.

Z. Makhdoumi-Kakhaki et al., 2017 [39] had fabricate CdS thin films by CBD methodology. Zn, Sn and Al were used as a dopant for CdS thin-films and optoelectronic properties were compared. The spherical and elongated grains were observed in FESEM The highest improvement in Electrical and photosensitivity reported for Sn-doped CdS thin films and $E_g \sim 2.78$ eV was observed which is greater than for undoped CdS thin films.

Wang et al., 2016; Fong et al., 2019 [40,41] had checked the applicability of GaN thin-films for the UV-photodetection by measuring the contrast ratio, responsivity i.e. 1.36 and 1.68 $\mu\text{A/W}$ respectively. The Rare earth element (La, Ce, Pr) doped GaN thin-films were prepared by sol-gel spin coating method and photoluminescence properties were studied. Spectral range of GaN thin films enhanced from UV region to near infrared. SEM is also done and it has been found that doping may change the grain size.

J.Wang et al., 2018 [42] CdS-Se heterojunction based self-powered photodetector was fabricated. The photodetector demonstrated fast response time, 300-700 nm photo-response and maximum peak responsivity of 40 mA/W.

Zheng et al., 2018 [43] synthesized high performance 1-D NW of SnSe and SnS by Chemical vapour deposition method. Different parameters like photo-response, I-V characteristics, dark current, photocurrent fall and rise time, carrier life time, specific detectivity were studied under the low incident light intensity of 0.05 mW cm^{-2} . Results conclude that p-type SnSe and SnS Nws has potential for optoelectronic devices application and observed values were comparable with existing values of Si, Ge based photodetectors.

Late et al., 2019 [44] explored the Molybdenum disulfide (band gap ~ 1.83 eV) based devices phototransistor and it has been found although they were efficient but they were totally optical power dependent it was observed if the light of wavelength > 670 nm falls on material value of photocurrent gets lowered. It is also observed that monolayered Mo-TMD is much more efficient than multilayer. Further 2D graphene /Mo-TMD were found to possess better internal quantum efficiency 85%. It is apparent that photodetectors based on semi-conductive layered materials display a wide variance (about 10 orders of magnitude) in their responsivity. Limiting dark current and enhancing system performance were the novel features of TMD-based photodetector design variations. In the case of 2D heterostructures, the photon energy for the visible range is larger than the bandgap of the individual TMD materials and each layered material produces sufficient quantities of photogenerated free carriers, resulting in a significantly higher photo response.

P. Wang et al., 2019 [45] found IR photodetector can be developed from 2D materials with narrow band gap as wavelength in this region is high and energy is low so for wide gap materials energy would not be sufficient for the transition. Thus, narrow band gap materials used to construct IR photodetector such as InGaAs, Hg-CdTe and materials also fascinated in to artificial structures such as quantum well, supper lattice to achieve narrow band gap which have low volume which reduces the dark current and enhances the responsivity as compared to thin films ($E_g < 1$ eV). IR photodetectors has been explored MX_2 ($M=Mo$, $X=S$, Se , Te). TMDs, black phosphorous and narrow band gap rediscovered layered materials and arsenic alloys has been found to detect mid-IR. Graphene has been found first layered material capable to work as IR detector efficiently even to terahertz. The graphene-based detectors show the responsivity <10 mA/W.

Yip et al., 2019 [46] reported development of flexible photodetectors. Unique properties like large surface to volume ratio to have high photo-response are exhibited by 1D nanostructures. Due to their low dimensions 1D nanostructure materials can lasts with larger bending without cracking as compared to their bulk counterparts. Branched CdS NWs were modified into the flexible photodetector, the device performance was comparable to the rigid photodetectors and also demonstrated the electrical stability, good flexibility and good endurance. Sb_2S_3 with narrow band gap (1.21 eV) is also considered as another interesting material due to its stability. Sb_2S_3 NW based flexible photodetector showed good flexibility and stability.

Najim et al., 2019 [47] Thermal evaporation method was used to prepare thin-films and Ag is usedas dopant. Study is done to study the consequences of doping by varying the concentration. it has been found that addition of Ag reduced the grain size and cubic phase was observed. Thus, it reduced the band gap (2.4 - 2.25 eV) of CdS and photocurrent is increased with increase in concentration of dopant. The highest responsivity 0.43 A/W is observed for 0.05 M Ag.

Poulomi Roy et al., 2006 [48] have studied the variation in thickness because of complexing-agent. The thickness of the films increased from $0.8\mu m$ (with deposition time 15 minutes) to $1.3\mu m$ (with deposition time 90 minutes) there after thickness got saturated however in previously reported literature with ammonia as complexing agent thickness variedfrom $0.24\mu m$ (with deposition time 30 minutes) to $0.34\mu m$ (with deposition time 120 minutes).

N.T. Shelke et al., 2006 [49] Optoelectronic properties were studied by XRD which confirmed the Pure thin film formation as no other peak was there with hexagonal phase and morphology was studied by SEM, EDX was also performed to study the present concentration of Cd and Se. Characteristic parameters like photo response, photoconductivity, detectivity, I-V

characteristics were studied. T

he direct band gap found to be 1.75 eV and high responsivity of 4.9A/W reported.

S.R. Gosavi et al., 2015 [50] Effect of synthesis time on the thickness and formation of defect states has been studied. Blue shift in absorption edge was observed by decreasing the synthesis time which affects the thickness of CdS thin film also. Growth rate of reaction mechanism is found to be increased with respect to synthesis time (80 min). beyond that no effect was seen due to unavailability of free Cations or anions. CdS thin-films were changed from crystalline to porous nature due to increase in synthesis time. Further increase in synthesis time (100 min) formation of Oxide phase was also reported. Photoconductivity dependence on temp., wavelength and applied voltage also studied. A linear dependence of photocurrent (I_{ph}) with applied voltage is found which supports the deposited CdS films are free from traps as reported earlier.

Borse et al., 2007 [51] Investigated the effect of temperature (40 and 90 °C) and deposition time (30&90 minutes) on the growth rate of film and molar concentration impact on thickness. Thickness was linearly dependent on time. The maximum thickness was attained in 60 minutes and no significant deposition beyond the 60 minutes. It was due to so unavailability of free ions as reaction rate increased at high temperature. Thin-films annealed. The optical band gap of thin-films annealed at 70 °C was varied in the range 2.34 - 3.43 eV as composition varied from $x = 0.0$ to 1.0.

Elilarassi et al., 2010 [52] prepared CdS nanoparticles by chemical reaction method. Wurtzite phase has been reported by XRD. A blue shift in absorption spectra was observed at 480nm which is slightly different from bulk CdS (512nm) it may be due to quantum confinement. Purity of CdS has been reported by EDAX no additional peak was observed.

Liu et al., 2010 [53] has studied the effect of deposition conditions on film thickness and transmission spectra. The temperature varied from 55-85°C. At 55°C it has been found that only one cubic or hexagonal phase exist and grain size observed was 55nm which reveals poor crystallinity. At 65 °C both phases exist so it was difficult to say whether film was purely hexagonal or cubic. At 75 °C peaks correspond to hexagonal phase exist and crystallinity is also improved. Another effect on absorption edge also studied a shift towards higher wavelengths was observed which may be due to film thickness suggesting that the band gap value decreases 2.56-2.38eV with rise in deposition temperature. Thus, increasing the deposition temperature increases the grain size and avoid the void.

S. PRABAHAR et al., 2009 [54] studied the electrical property resistivity relation with deposition time and temperature. it is found that resistivity is minimum for deposition time 38

min increases linearly with increase in time and inversely proportional to temp.

Bakiyaraj et al., 2011 [55] performed the thermal annealing processes in an open horizontal tubular furnace in the temperature range of 300 - 500 °C for a fixed time of 1 hour. For as deposited thin film diffraction peak observed at 26.5° which may be due to either hexagonal phase or cubic phase but after annealing hexagonal phase is confirmed due to increase in intensity of (002) phase peak which confirms the hexagonal phase at the same time presence of other peak at $2\theta=28.1^\circ$ which corresponds to (101) confirmed hexagonal phase. This may be due to increase in crystallinity and band gap decreases from 3.5-2.9 eV due to annealing due to quantum confinement.

I.Rathinamala., 2014 [56] has prepared the thin films by sol-gel spin coating method and the effect of aging time as well as of annealing temperature effect on the stoichiometry and optical properties is studied. Hexagonal phase was reported. At high annealing temperature crystallinity levels became better. Band gap decreased with increase in sol-aging time from 24 hrs to 48 hrs. Spherical shaped grains observed through FESEM were uniformly distributed over the entire surface of the substrate.

Samarasekara et al., 2017 [57] prepared the thin films at spin speed 900 rpm for 30 sec. All the samples were annealed at 300 °C for 20 min. CdS thin films prepared by electrodeposition method and effect of Cu concentration as dopant was studied. No change in structure was found but little change in lattice parameters like grain size, lattice strain and band gap has been reported due to addition of Cu.

Devi et al., 2020 [58] explored that variation in concentration didn't affect the band gap value but surface morphology was altered. 0.4 A/W photosensitivity and 8.46×10^{10} Jones detectivity reported degradation in all peaks was reported for molar concentration $>0.1M$ degradation in crystallinity. CdO phase occurrence was also reported.

Mohamed Shaban et al., 2015 [59] has deposited CdS thin films on glass substrate through spin coating. Thickness of CdS thin films were varied. Highly dense and agglomerated CdS thin films covering whole surface were obtained. Sharp absorption edge was observed at 295 nm.

F. Y. Al-Shaikley., 2011 [60] Electrical and optical study was done with respect to annealing temperature (523 K, 623 K, 723 K). Increasing and decreasing trend of optical band gap due to thermal annealing in air was reported. The band gap of as deposited CdS thin film was more as compare to annealed thin films. The variation in band gap was due to improvement in crystalline properties, defect states, dislocation densities and strain present within thin film.

C. Doroody et al., 2021 [61] had done comparative study of RF magnetron sputtering and CBD

method grown CdS thin films. The optical band gap 2.40 eV and 2.32 eV was reported. Hexagonal phase corresponds to (002) plane examined to find out various characteristic parameters of synthesized CdS thin films. Better crystallinity and electrical properties due to higher concentration of free charge carriers were found for the films prepared through sputtering while formation of cluster was reported for the films grown by CBD synthesis route. **A.I. Oliva et al., 2001** [62] prepared the CdS thin by following two technique Chemical Bath Deposition (CBD) and closed space sublimation (CSS). Long deposition time reduced the formation of defects in CdS thin films. The optical band gap was found to be 2.31-2.32 eV. Higher values were reported for fast rate of deposition.

N. K. Ponon et al., 2015 [63] had studied the effect of annealing temperature and annealing time post deposition. The prepared thin films were annealed in nitrogen atmosphere. Recrystallization and growth rate improved due to annealing. As result resistivity of annealed thin films was less as compared to as-deposited tin nitride thin films. Annealed thin films were thermally and electrically stable.

Ravangave et al., 2015 [64] prepared at spin speed 900 rpm for 30 sec. all the samples were annealed at 300°C for 20 minutes. CdS thin films prepared by electrodeposition method and effect of Cu concentration as dopant was studied. No change in structure was found but little change in lattice parameters like grain size, lattice strain and band gap has been reported due to addition of Cu.

S.S. Shaikh et al., 2019 [65] had prepared the CdS thin films at 300 °C by spray pyrolysis methodology. Optical, structural, morphological and vibrational study was carried out. The optical band gap 2.43 eV was reported. Longitudinal optical phonon modes reported at 297 cm⁻¹ and 580 cm⁻¹ through vibrational study. Average crystallite size of 15 nm was confirmed through XRD.

Al-Dujayli et al., 2012 [66] had grown the CdS thin films on glass substrate by spray pyrolysis method. Optical, structural properties were studied by varying the ratio of Cd and S concentration. Hexagonal phase was found and optical band gap found to be varied from 2.40-2.45 eV. Optical band gap was decreased with decrease in Cd concentration in solution and crystallinity also improved.

J.Podder et al., 2014 [67] CdS thin films were prepared under optimum conditions (300°C) and molar concentration of both the precursors were varied (0.1 M- 0.4M). The optical band gap varied from 2.44 -2.55 eV.

Jie Xing et al., 2012 [68] fabricate the SrTiO₃ thin films on fused quartz wafer through RF magnetron sputtering. Various optical and electrical properties were studied. The transient

photovoltaic signals were observed with rise time 330 ps and fall time 480 ps. The quantum efficiency 42.1 % correspond to wavelength 310 nm was reported and maximum responsivity found to be 105 mA/W.

Zhe Liu et al., 2013 [69] synthesized ZnTe thin films on rigid silicon substrate which were highly sensitive in visible range of electromagnetic spectrum. Responsivity (1.85×10^5 A/W) and quantum efficiency ($4.36 \times 10^7\%$) two characteristic parameters to be a photodetector were also found. Polarization sensitivity of photodetector also studied by varying polarizing angle of incident light and photocurrent response noted. Maximum photocurrent was recorded when angle of incident light is 0° or 180° with respect to axis of ZnTe nanowire.

M.THAMBIDURAI et al., 2011 [70] investigated the optical properties Uv-Visible spectroscopy and Photoluminescence of CdS thin films by varying the annealing temperature. Quantum confinement was found to be responsible for the variation in optical band gap, crystallite size was found to be 5-8.2 nm greater than Bohr radius~ 3.5 nm of CdS through XRD. In PL green and Yellow band emission peaks were found at 486 nm and 542 nm. The presence of defects states was confirmed due to presence of emission peak at 486 nm while main peak is at 542 nm. The FWHM decreased with rise in sintering temperature from 150°C to 450°C which confirms the increase in crystallite size.

C.P. Nikam et al., 2014 [71] had deposited CdS thin films of FTO coated glass substrate for photosensor application. CdS thin films were characterized by UV- Visible spectroscopy, XRD and Keithley source meter 2400 is used for electrical study in dark and under illumination of light in visible range. Polycrystallinity observed through XRD and optical band gap 2.15 eV was noted. Resistance of CdS thin films found to be very less in presence of light ($0.88 \times 10^2 \Omega\text{-cm}$) as compared to dark ($1.42 \times 10^2 \Omega\text{-cm}$). Resistivity decreased with increase in light intensity.

M. Reddy et al., 2013 [72] had prepared CdS thin films by CBD method. Optical and structural study was carried out by varying the complexing agent ammonia concentration from (0.1-3.0 M) in bath solution. No grains could be seen for lower concentration. Maximum crystallinity and grains with fine boundaries could be seen for CdS thin films prepared from the solution consist of 2.0 M ammonia. For further increase in concentration decrease in carrier concentration and increase in band gap was noticed. Cd/S ratio confirmed by EDX and its value reported was 1.04.

Eya et al., 2016 [73] had studied the optical properties of CdS thin films deposited by chemically route method. Transmittance found to be maximum 79% and 71% for as grown and annealed thin films in IR region at wavelength 100 nm. Maximum absorbance was noted in UV region of electromagnetic spectrum. thickness of films varied from 280 nm to 500 nm

after annealing at 423 K. Energy gap varied in the range of 2.59 -3.11 eV.

Munaga Venkata Veera Prasad et al., 2020 [74] had observed the optical and thermo-electrical behaviour of sol-gel spin coated CdS thin films deposited on glass substrate.

Cubic phase of CdS thin films observed for all concentrations of dopants. The agglomeration of particles was observed in all SEM micrographs while no grain boundaries were observed for 2% of Zn doping further increase in Zn concentration increases the crystallite size and fine grain boundaries could be seen. Presence of Zn in CdS thin films were confirmed through EDS. Two longitudinal modes of optical phonon were reported shift in frequency was noted which was in agreement with XRD results. The increase in Zn content leads to increase free charge carrier concentration. As a result, electrical conductivity also enhanced.

1.8 Thin films synthesis

Thin films can be synthesized by various methods such as chemical bath deposition [75], chemical vapour deposition [9], thermal evaporation [76], physical vapour deposition [39], spray pyrolysis [77], RF magnetron sputtering [61], pulsed vapour deposition method [78], solution processed methods such as dip coating and spin coating [41]. Chemical bath deposition is commonly used technique in which ion to ion deposition on the substrate takes place. Due to which there might be possibility of numerous defect formation and uneven morphology of obtained thin films. we adopt sol-gel spin coated chemical route method in which various parameters such as spin speed, deposition time, thickness of thin films and post deposition temperature can be controlled. It is easily available and low-cost method. For the fabrication of good quality uniform thin films homogeneous solution is preferred.

1.9 Applications

Since electrical and optical behaviour of a semiconducting material can be varied thus It can be preferred for various photonic devices. such as biosensors, light emitting diode, wave guide, photocells and lasers [31,33,79,80]. As these materials can shows sharp absorption and band to band transition under illumination.

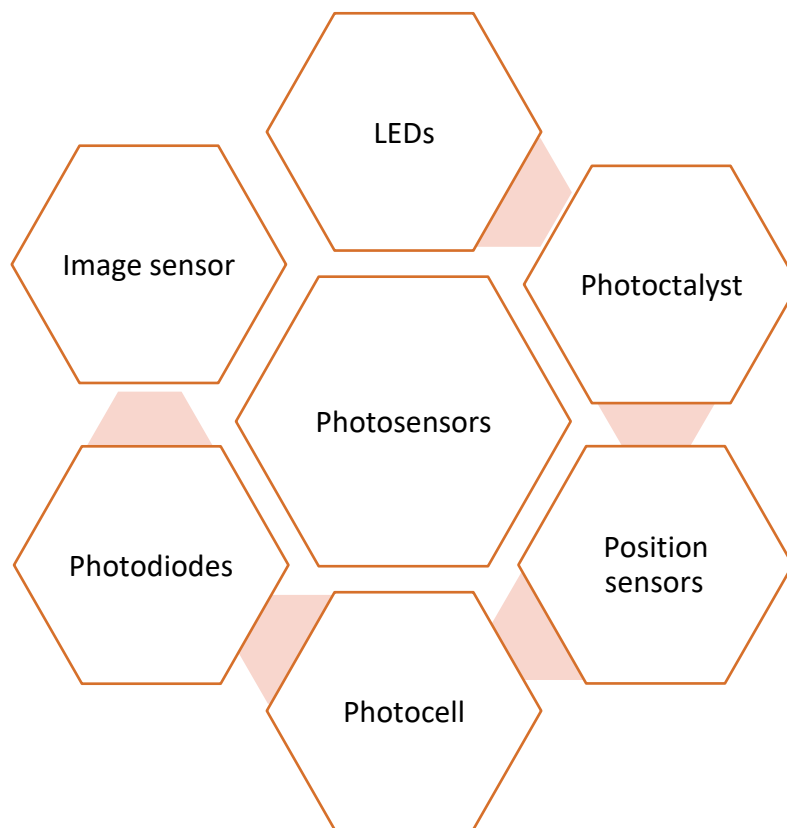


Fig.1. 4 The above image represents the Applications of Phtoto-sensors

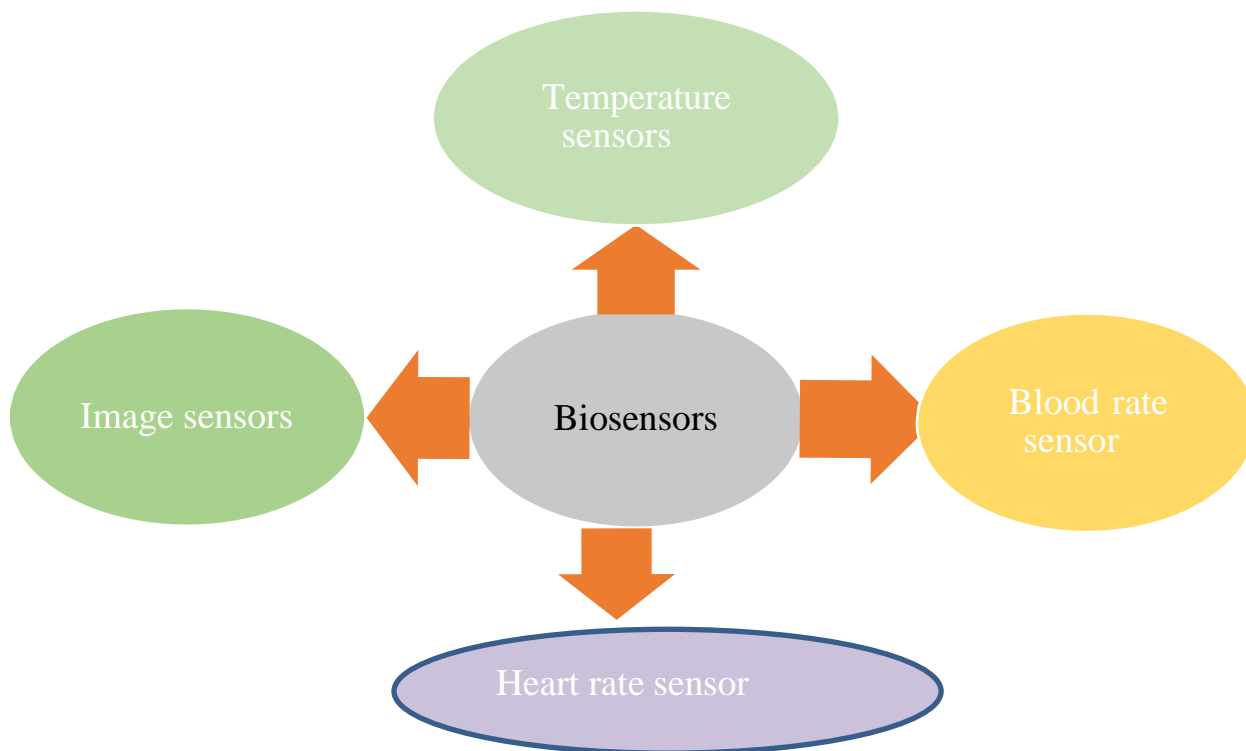


Fig. 1. 5 Represents the different types of sensors used in biomedical commonly

1.10 Aim of the Present work

The aim of the present work is to synthesize CdS and Zn:CdS thin films. At the same time various parameters need to be optimise during the synthesis process. The main motive to do the optimization is to reduce the sintering temperature so that we can maintain the quality of thin films at flexible substrate also. In this work optical, structural and electrical properties of preferred material (CdS) were studied through nano-thin film fabrication. CdS and Zn:CdS thin-films were prepared by sol-gel spin coating methodology. Glass was used as substrate for the deposition of the thin films. At the same time efforts has been done to synthesis CdS thin films on the flexible substrate and maintain their quality as well as characteristic parameters.

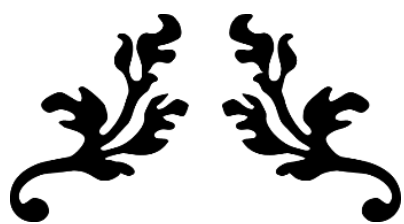
1.11 Proposed Objectives

O1: Optimization of process parameters to synthesize CdS thin-films.

O2: Study of optoelectronic properties of CdS thin films by varying the process parameters.

O3: Tailoring optoelectronic properties by appropriate doping in CdS.

O4: Study of optoelectronics properties of CdS and doped CdS thin films grown on flexible substrates.



Chapter-2

Synthesis and characterizations techniques

2.1 *Introduction*

In this chapter the process followed for the synthesis of compound semiconductor and fabrication of nanostructured thin films is discussed. Synthesis route is very crucial step where we need to control and optimize the various process parameters to synthesize the material as per the requirements for the particular application. For uniform deposition of thin-films solution processed sol-gel spin coating methodology has been followed. It is preferred over the other techniques as deposition speed, deposition temperature, thickness of deposited thin films, deposition time various parameter can be easily controlled.

2.2 *Synthesis*

Sol-gel methodology is employed for the synthesis of CdS based thin films. This methodology consists of three different stages i.e. formation of homogeneous solution, gel formation and precipitation. In this route of synthesis, we can control the reaction mechanism in any of the above mention stages as per the requirement.

2.2.1 *Synthesis of undoped CdS*

In this work a clear solution of 0.3 M concentration of CdS was synthesized by using Precursor 1 and precursor2 which act as the sources of Cd^{2+} and S^{2-} ion in solvent (2-methoxyethanol). Both the precursors were weighed with the help of weighing machine separately. The weight of precursor was taken on the basis of their molar-concentration to prepare 0.3M of 20 ml solution. Precursors were added one by one carefully along with continuous magnetic stirring. Precursors and solvent used in the synthesis process are listed in table 2.1. After the complete dissolution of both the precursors in solvent, Mono- ethanolamine sol-stabilizer was added drop wise to complete the reaction in a controlled manner. A viscous and clear sol-gel was obtained. The prepared sol was aged for 30 minutes.

2.2.2 *Synthesis of Zn doped CdS*

Zn doped CdS solution was also synthesized in the same manner as undoped CdS solution. The weight of precursors added in the solvent was calculated on the basis of 0.3 molar concentration of precursors in 20 ml of the solution. Cadmium-acetate ($\text{Cd}(\text{CH}_3\text{COO})_2 \cdot 2\text{H}_2\text{O}$) source of Cd^{2+} ions and dopant Zinc acetate ($\text{Zn}(\text{CH}_3\text{COO})_2 \cdot 2\text{H}_2\text{O}$) source of Zn^{2+} ions was used. Initially precursor1 was dissolved in solvent through magnetic stirring for about 20 minutes. Secondly

dopant is poured in the same solution and stirred for another 15 min for complete dissolution of both precursor and dopant. Later-on the precursor-2 source of S²⁻ was added in the same solution. Magnetic stirring was continued for about approximately 20 minutes. Sol stabilizer was added at last with the help of dropper and solution was stirred for another 10 minutes until we obtained a viscous solution in the form of sol-gel. Addition of Zincacetate did not affect the colour and homogeneity of the solution as both the precursors and dopant solution were dissolved completely.

Table 2. 1 Represents the chemical used for the synthesis of CdS solution.

Sr.NO	Chemicals used	Molecularweight (g mol ⁻¹)	Purity (In %)	Manufacturer
1	2- Methoxyethanol	76.10	99	LOBA CHEMIE PVT.LTD MUMBAI
2	Cadmium acetate Di- hydrate (Precursor 1) Cd (CH ₃ COO) ₂ .2H ₂ O	266.12	99	LOBA CHEMIE PVT.LTD MUMBAI
3	Thiourea (Precursor2) (NH ₂ CSNH ₂)	76.12	99	LOBA CHEMIE PVT.LTD MUMBAI

4	Zinc acetate di-hydrate Zn $(\text{CH}_3\text{COO})_2 \cdot 2\text{H}_2\text{O}$	219.50	99	LOBA CHEMIE PVT.LTD MUMBAI
---	---	--------	----	----------------------------------

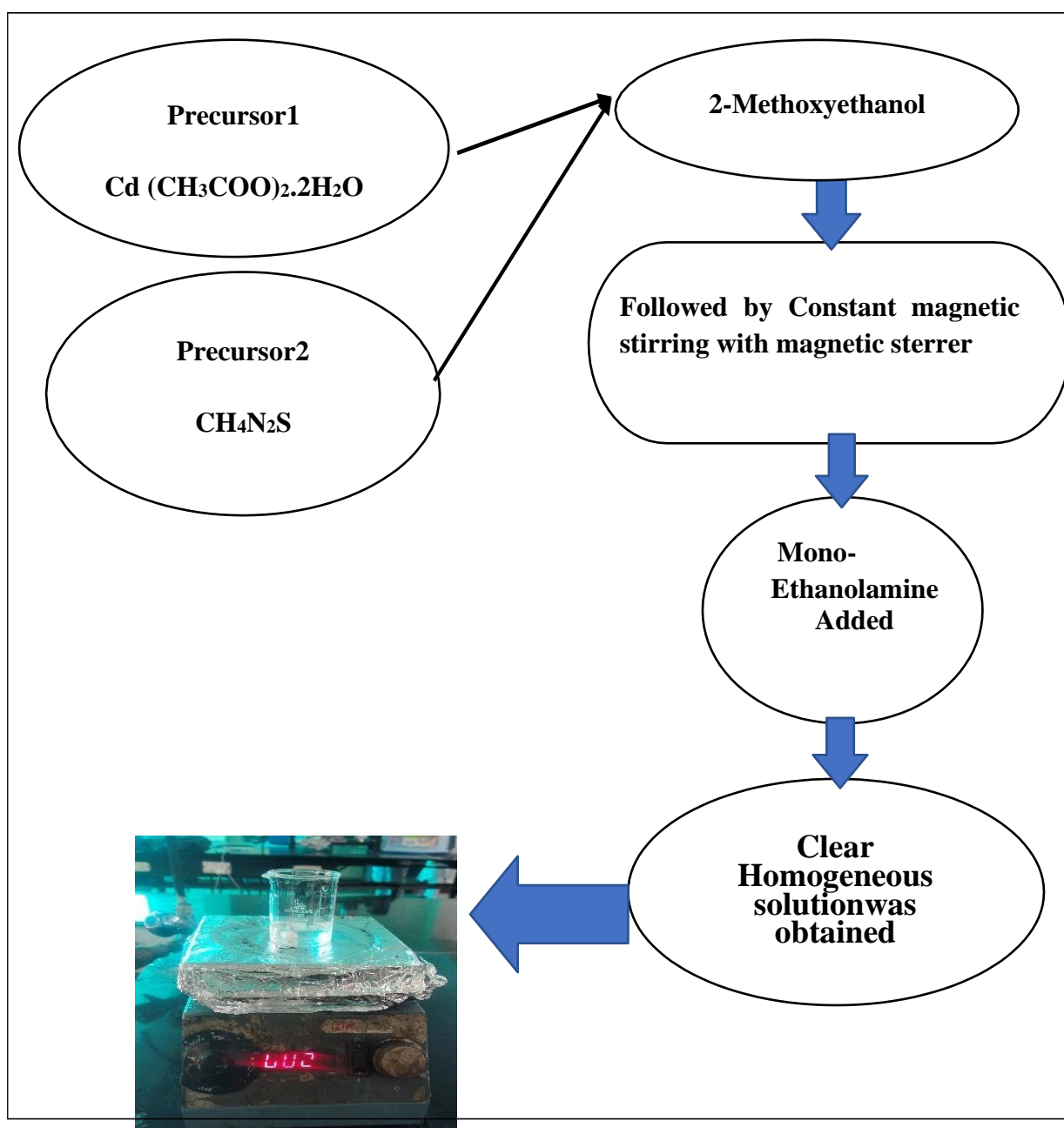


Fig. 2.1 Sol-gel preparation methodology

2.3 *Thin- films fabrication*

Soda lime glass (SLG) of fine quality was used for the deposition of thin-films. With the help of spin coater thin films with uniform thickness were obtained. Thin films were deposited on the glass substrate by repeating the sol-gel spin coating process. In one experimental run, twenty layers were deposited on the substrate. Various steps involved in the thin film deposition process are as follows:

➤ *Cleaning of glass substrate*

Before the deposition of the thin films the glass substrates were thoroughly cleaned with acetone, ethanol and distilled water to remove any type of organic impurities which may degrade the adherence of thin films. Subsequently the substrates were heated on hot plate to remove any type of moisture.

I. Spin Coater

Spin coater (Spin NXG-P1) is programmable a device (shown in Fig.) where various parameters like spin speed, rotation time need to be adjusted. To obtain uniform thin films viscosity of the solution need to be optimum and the material need to be injected at the center of the substrate placed on the rotating disk. It should be noted that to avoid the sprinkling of the material, the revolution rate of the disk should be increased in small steps and not in an abrupt manner. The spin speed and spin time must be high enough to obtain uniform thin films and the solvent should have fast evaporation rate [81].



Fig. 2.2 Represents the Photograph of thin films deposition set-up Spin- coater attached with vacuum pump

➤ *Deposition of thin films*

For the deposition of thin films clinically cleaned glass substrate was placed on the stage and vacuum was created. Vacuum need to be checked carefully otherwise while rotating the substrate may fall off. Two-three drops of sol-gel were poured onto the glass substrate and followed by all set programs in spin coater. Pre-annealing and drying are two compulsory steps that need to be followed before the deposition of next layer. Number of deposited layers can be controlled. Finally, yellowish colour thin films were obtained.

2.4 *Characterization Techniques*

Thin films were prepared at Physics Research Lab, LPU (Phagwara, Punjab) by using the facilities like spin coater, magnetic stirrer, hot plate, muffle-furnace etc. The prepared samples were analysed through various characterization techniques such as XRD, FESEM, UV-VISIBLE spectroscopy, Raman spectroscopy, Photoluminescence spectroscopy, and Electrical characteristics in presence of light and dark.

2.4.1 *UV-Visible Spectroscopy*

Optical properties were studied through UV-Visible spectroscopy. UV- visible spectroscopy is an analytical technique used for the study of chemical compound through the material interaction within UV (200 nm-400 nm) and Visible (400-800 nm) range of electromagnetic spectrum. Material under investigation need to be a chromophore i.e sensitive to UV-Visible range of electromagnetic spectrum. When light falls on the thin films loosely bound outer most shell electrons participates in the electronic transition. These electrons move from valence band to conduction band or to any intermediate state formed due to any intrinsic or extrinsic defects or impurities. Optical properties can be studied through transmission or absorption spectra



Fig. 2.3 Represents the photograph of UV-visible spectrophotometer (UV-1900i)

recorded through SHIMADZU UV- Visible spectrophotometer (shown in Fig. 2.3) in wavelength ranges from 100 nm to 1000 nm. During the interaction of light with thin films different processes of transmission, reflection, absorbance, refraction and scattering of light take place. Every chemical compound shows a strong absorption at a discrete wavelength.

In our work transmission spectra was recorded for all prepared thin films. The transmittance spectra were recorded in the wavelength range of 300-1100 nm. The transmittance data obtained from UV-visible spectroscopy and thickness calculated through cross sectional FESEM were used to calculate the absorption coefficient by using the equation (2.1).

$$\alpha = \frac{1}{d} \ln \left(\frac{100}{T} \right) \quad (2.1)$$

Where “d” represents the thickness of annealed thin films and “T” represents the transmittance. Optical band gap is calculated by plotting $(\alpha hv)^2$ vs hv i.e Tauc plot and the band gap of the CdS thin films were estimated by using Tauc equation (2.2):

$$\alpha hv = B(hv - E_g)^n \quad (2.2)$$

where α stands for absorption coefficient, E_g stands optical band gap, B is a constant, and n depends on mode of optical transition [82]. For the direct band gap allowed transitions, the value of n is 1/2. The Energy gap (E_g) of CdS thin films is determined by linear extrapolation of the linear region of Tauc plot (at $y=0$).

“The energy required for the transition of electrons between maxima of valence band and minima of conduction band is known as energy gap (E_g)”. The variation in E_g may be attributed to the presence of defects (disorder, lattice mismatch or presence of impurities). The extent of variation in the band gap depends on the positioning of defect states in relation to the edges of transition bands. The energy corresponding to the transition between valence or conduction band and any defect state is called Urbach- energy [83]. This is the weak absorption region in absorption spectra where absorbance varies exponentially with respect to energy. The inverse of the slope of linear region of $\ln(\alpha)$ vs hv plot provides the value Urbach-energy (E_u), which allow us to calculate the energy associated with defects or localized state. Minimum value of Urbach energy indicates the lower value of the disorder present in the thin films prepared[84].

2.4.2 X-Ray Diffraction Technique

Identification of obtained phase and planes in a unit cell in crystalline material identified through XRD. Atoms in a crystal are periodically arranged. The scattered light from atoms forms a diffraction pattern due to constructive interference. The diffraction pattern formed by the scattered light gives an information about the various type of atomic arrangement in lattice. In order to produce diffraction pattern atomic spacing between atoms in a lattice should be equal to the wavelength of the radiation used.

Production of X-rays

X rays are produced in cathode ray tube by using Cu as a target cathode material. Highly energetic electrons produced by heating the filament are bombarded on the target material by applying some potential. Bombarded electrons are highly energetic and efficient to dislodge the inner shell electrons of the target. Characteristic X-rays are produced as outer shell electrons move to inner shell to fill the vacancy created due to dislocation of inner electrons. Cu- $K\alpha_1$ x-rays (1.546 \AA) are used to characterize the specimen under investigation. These x-rays have short wavelength and high intensity. These x-rays are collimated and directed on to the specimen to be analyzed. Specimen on the stage rotates at some angle (θ) in the path of collimated x-rays and detector is used to detect diffracted x-rays mounted on an arm rotates at angle (2θ) with respect to the source as shown in Fig.2.4.

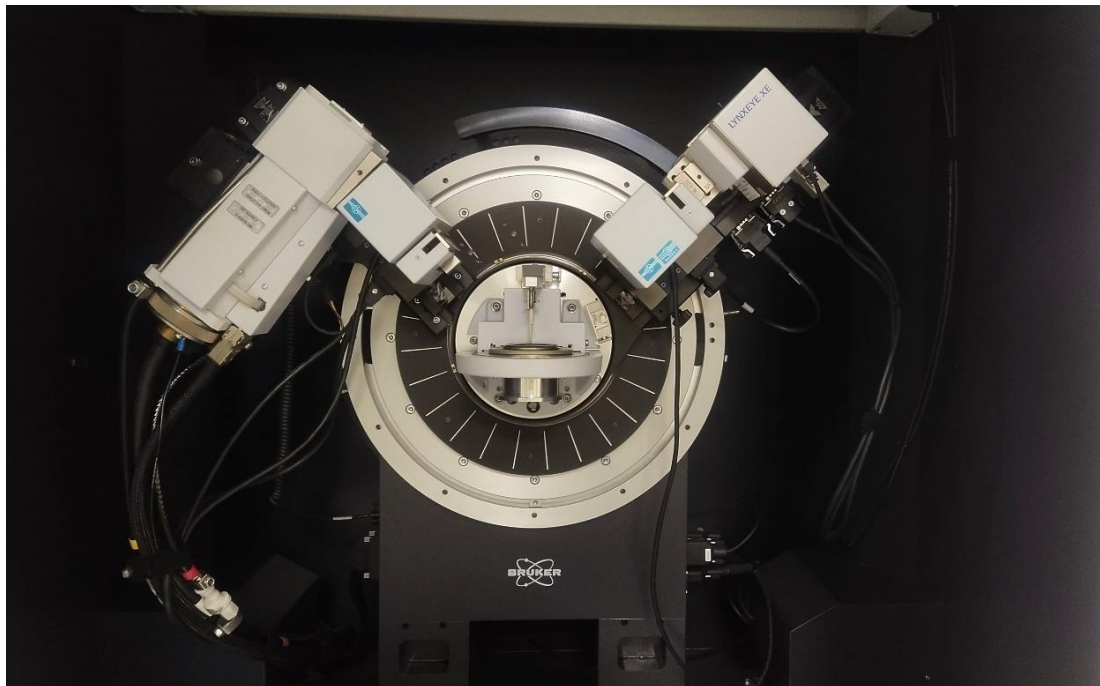


Fig. 2. 4 Photograph of Bruker X-ray diffractometer (AXS D8 ADVANCE A25)

Most commonly samples are characterized in two different modes powder diffraction mode and thin film mode. All crystalline solid materials prepared in the form of pellets, crystals are crushed in to form of fine powder. Peaks and planes identification of whole material can be done by using very small amount of prepared material. Thin film mode is used for the samples contains different number of atomic layers. Diffraction patterns can only be obtained if diffracted rays follow the Bragg's law. Diffraction patterns produced due to constructive interference of reflected x-rays are detected by diffractometer. It provides the data in the form of signals and further these signals are converted in to data in the form of intensity and angle 2θ . Data provided helps to plot a graph which shows the number of counts detected by the detector at a specific angle 2θ . 2θ is the angle between source and detector. Intensity of these peaks depends upon nature of the material as well. For amorphous material no peak can be detected as periodicity is missing while in case of semicrystalline material a broad hump can be obtained but noise level will be high or background effect might be there.

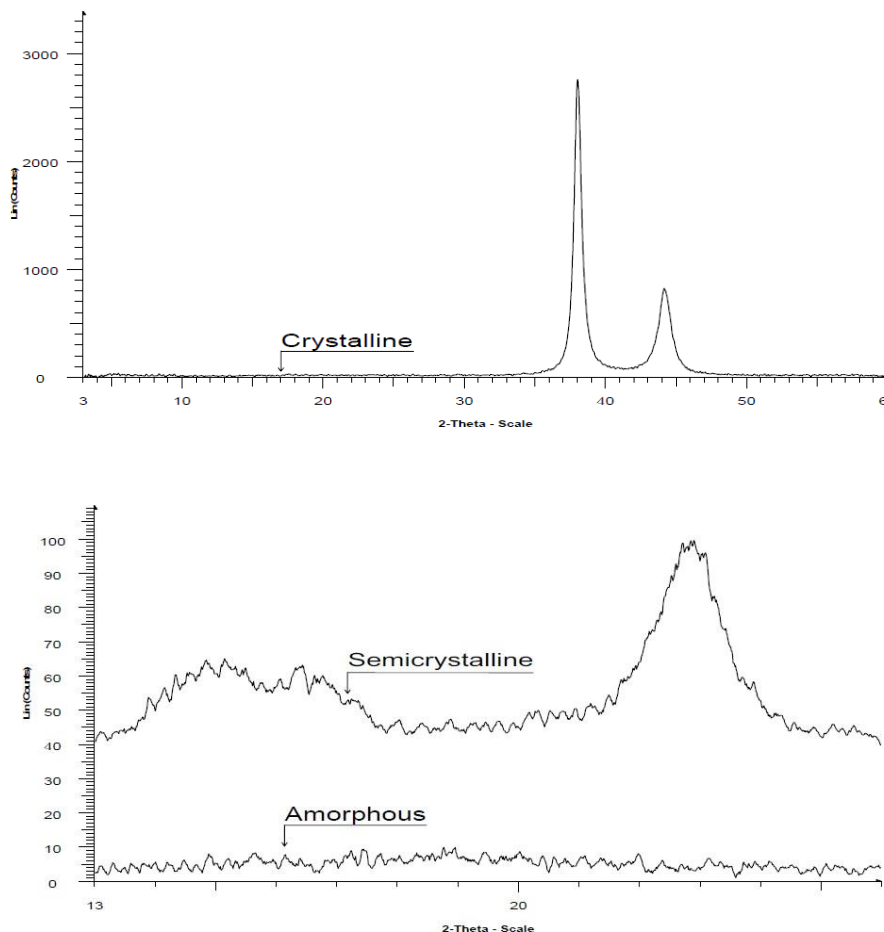


Fig. 2.5 Represents the X-ray diffraction pattern images for crystalline, semicrystalline and amorphous materials [85].

At each position of the obtained peaks unique set of planes exist that can be obtained through standard references available. From these diffraction patterns we can obtain:

1. ***Crystallite size (D)***
2. ***Lattice constants***
3. ***d-spacing between lattice planes***
4. ***Strain***

The crystallite size was calculated by Debye Scherrer formula given by equation (2.3) for various diffraction planes.

$$D = 0.9\lambda/\beta\cos\theta \quad (2.3)$$

Where λ is the wavelength of Cu-K α (1.54Å) radiation, β is full width half maxima (FWHM), θ is the position angle which is half of 2θ . Lattice strain was also calculated by the equation given below:

$$\varepsilon = \beta\cos\theta/4\sin\theta \quad (2.4)$$

Lattice constants a, b and c were calculated by using equation (2.5) for hexagonal phase.

$$\frac{1}{d^2} = \frac{4}{3} \left[\frac{h^2 + hk^2 + k^2}{a^2} \right] + \frac{l^2}{c^2} \quad (2.5)$$

As CdS exist in two phases i.e cubic or wurtzite phase. In our work hexagonal phase was obtained consistently. For hexagonal structure $a = b \neq c$.

2.4.3 Raman spectroscopy

Raman spectroscopy is a non-destructive analytical tool that can be used for the identification of protein structure, chemical compounds and reaction mechanisms. Identification of the compounds is possible through the vibrational modes study observed through Raman spectroscopy. This spectroscopy is based on inelastic scattering of light. When a monochromatic beam of light falls on the material, molecules get excited to a virtual state and come back to ground state through emission of scattered photon. The wavenumber difference

between incident photon and scattered photon is known as Raman shift. Resonant Raman scattering and normal Raman scattering are two distinct forms of Raman scattering. Resonant Raman scattering can be evident when a photon of energy nearly equal or slightly greater than the band gap of material employed. On the other hand, If the energy of the incident photon is not sufficient or less than the band gap of the material, in that case normal Raman scattering will be observed. In later scenario, Transverse optical (TO) modes and multi phonon scattering modes are not observable. In Resonant Raman scattering enhanced electron-phonon interaction results in observation of Longitudinal optical phonon modes (LO), Transverse optical phonon modes (TO) and Surface optical phonon (SOP) modes. Surface phonon modes are observable between LO and TO modes frequency range. The SOP modes are observable for very small sized particles residing on the surface due to increase in grain size of nanostructured material. Strong electron-phonon interaction is represented in terms of intensity of Raman spectra. The observed vibrational modes are represented in terms of intensity and frequency shift. The obtained Raman spectra is sensitive to crystalline structure and defects present with in the molecule. The presence of a particular compound is sensitive to peak position while shape of the peak and shift is corresponding to the defects present.



Fig. 2. 6 Represents the Photograph of Raman spectrophotometer available with laser source of 488 and 532 nm wavelength.

2.4.4 FESEM

Field Emission Scanning Electron Microscopy (JEOL JSM-7610F Plus) was used for the microstructural studies. FESEM has an advantage of being capable to produce high-resolution

microstructural images in the range few nanometres. The specimen under investigation must be conducting. Polymers and semiconductors are made conducting through uniform thin gold coating on it. Highly energetic electron beam produced through the tip of cold the source. Electron beam in microscope is focused on the specimen through electromagnetic lenses in vacuumed column. These lenses help to focus the electron beam towards the specimen. Secondary electrons, back scattered electrons, X-rays and photons emitted due to interaction of electron beam with the specimen. In most of the work secondary electron configuration was used for microstructural study.

2.4.5 Electrical Characterization

Electrical study was carried out through Keithley source meter. I-V characteristics were recorded in two different conditions one is in dark and another in presence of light. White halogen lamp was used as a light source. To enhance the conductivity two Ag electrodes 200 μm apart were deposited on the thin-films. Thin-films were exposed to light for certain period of time and I-V response was recorded at different voltages. Voltage was varied in the range of -5V to +5V. Reproducibility was also checked for 300 cycles at fixed voltage. To verify the applicability of the prepared samples for Photo-sensing devices Photosensitivity, Responsivity, Rise time and recovery time was also calculated prepared devices. The ratio of photocurrent to dark is known as photosensitivity(S).

$$\text{Photosensitivity(S)} = \frac{I_{ph} - I_d}{I_d} \quad (2.6)$$

Where I_{ph} and I_d represents the photocurrent and dark current.

Photocurrent per unit power is defined as Responsivity.

$$\text{Responsivity (R)} = I_{ph}/P \quad (2.7)$$

Power (P) of light falls on the illuminated area was calculated as $P = IA$ watt Where i is intensity of light used and 'A' is defined as total area under illumination.



Chapter -3

Structural and Optical studies of CdS thin-films

3.1 Introduction

In this chapter structural and optical properties of the prepared thin films were studied. During the synthesis optimization of the various process parameters such as effect of the pH level, thermal annealing and molar concentration of the prepared solution was done to improve the structural and optical properties of the prepared thin films for the photodetection application. Reaction rate of the prepared solution depends on the pH level and molar concentration of the prepared solution. All mentioned parameters were found to be responsible to improve the structural and optical properties. Annealing time was also varied to improve the crystallinity of CdS thin films. Initially synthesis was done by varying the annealing temperature and time only. It was observed that cadmium oxide (CdO) was formed majorly along with CdS after annealing in air ambient condition. To avoid the formation of this secondary phase (CdO) pH level of the solution was controlled. The solution of pH-8,10 was used for the synthesis of CdS thin films. The prepared thin films were annealed at temperature 400 °C, 450 °C, 500 °C for 30,60 and 90 minutes. From here we found the best suitable pH level to synthesize the CdS thin films. Later on, to improve the optical and structural properties of synthesized thin films at pH-10 the molar concentration of both the precursors were varied. The prepared thin films with different molar concentration solution i.e. 0.2 M, 0.3 M and 0.4 M were sintered for 180 minutes. Coding of prepared thin films samples were given in table

Table 3- A Represents the composition, annealing temperature and annealing-time and figure coding for the prepared samples of CdS thin films

Name of material of the samples	Molarity/pH values of the solution used	Annealing temperature (° C)	Annealing time (minutes)	Samples coding
CdS	0.3M/(pH-8)	400	30	1a
		450		1b
		500		1c
	0.3M /(pH-8)	400	60	2a
		450		2b
		500		2c

	0.3M/(pH-8)	400 450 500	90	3a 3b 3c
CdS	0.3M /(pH-10)	400 450 500	60	4a 4b 4c
CdS	0.2M /(pH-10) 0.3M/(pH-10) 0.4M/(pH-10)	400	180	5a 5b 5c

3.2 Results and discussion

3.2.1 Thermal annealing effect on structural and optical properties

Structural properties

Fig (3.1) - (3.3) shows the thermal annealing effect on structural properties. CdS thin films were annealed at different temperatures. Annealing at high temperatures results in formation of Cadmium oxide CdO as shown in Fig 3.1. To improve the crystalline quality, CdS thin films were annealed for different times (30 minutes, 60 minutes and 90 minutes) also. Thin films annealed for longer times (60 minutes and 90 minutes) and at higher temperatures (450 °C and 500 °C) result in formation of CdO phase along with the CdS peaks as reported by S.R. Gosavi and M.Dhrani devi et al. [50,58]. No CdO peak was observed for CdS thin films annealed at 400 °C for different annealing times. At the same time improvement in crystalline quality could be observed for the films annealed at 400 °C for longer time. The crystalline quality of the prepared thin films could be improved through annealing at 450 °C for 30 minutes. Thus, formation of CdO phase can be minimized by controlling the annealing temperature and the annealing time as well. A careful analysis of the peak positions reveals that the peaks shift towards the lower angle with increase in temperature and the annealing time. With an increase in the annealing temperature, the size of the crystallites increased from 12 to 34 nm, and the lattice stresses decreased from 1.4 to 0.8.

The surface morphology of CdS thin films annealed at 400°C, 450°C, 500°C for different annealing times is shown in Fig. 3.4. The surface micrographs confirm uniform surface coverage of the substrate with thin films. Thin films annealed at 400 °C (60 min) found to be uniformly deposited on the glass substrate and closely packed crystallites could be seen in micrographs. Fine grain boundaries were observed with rise in annealing temperature. It maybe due to increase in grain size Agglomeration was observed in thin films annealed at 450 and 500 °C for 60 and 90 minutes. Long-time annealing at high temperature (500 °C) lead the overgrowth of white crystal over the surface of CdS thin films which may be oxides. Abdolazadeh Ziabari et al. also reported similar kind of grains growth [86]. The average grain size of the films lies in the range of 15 nm to 70 nm.

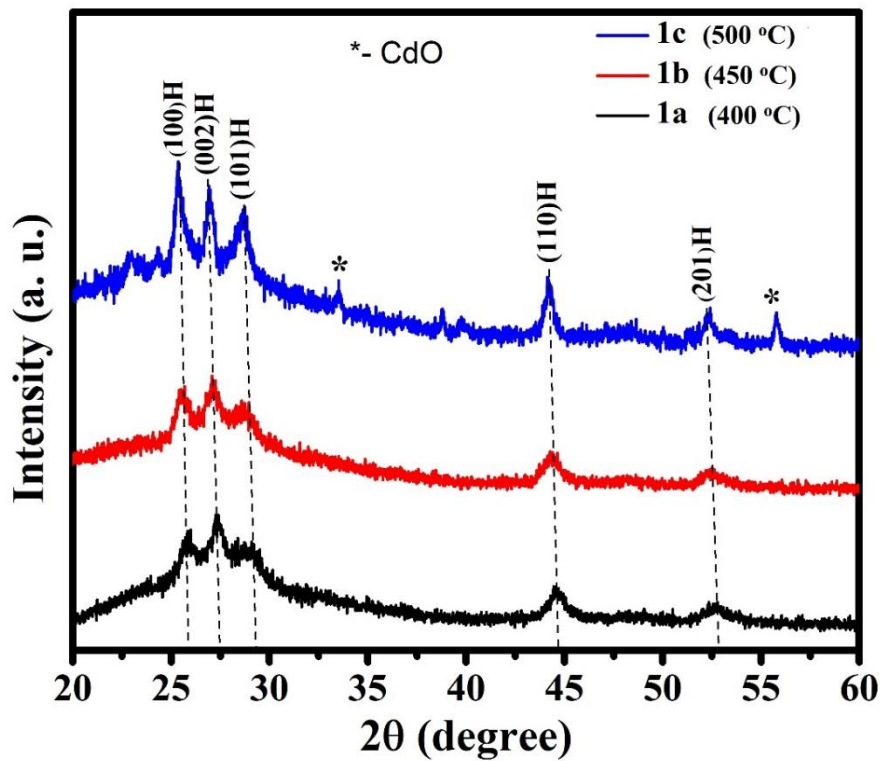


Fig. 3. 1 The above diagram shows the XRD-diffraction patterns of samples coded 1a-1c annealed at different temperatures for 30 minutes with pH-8

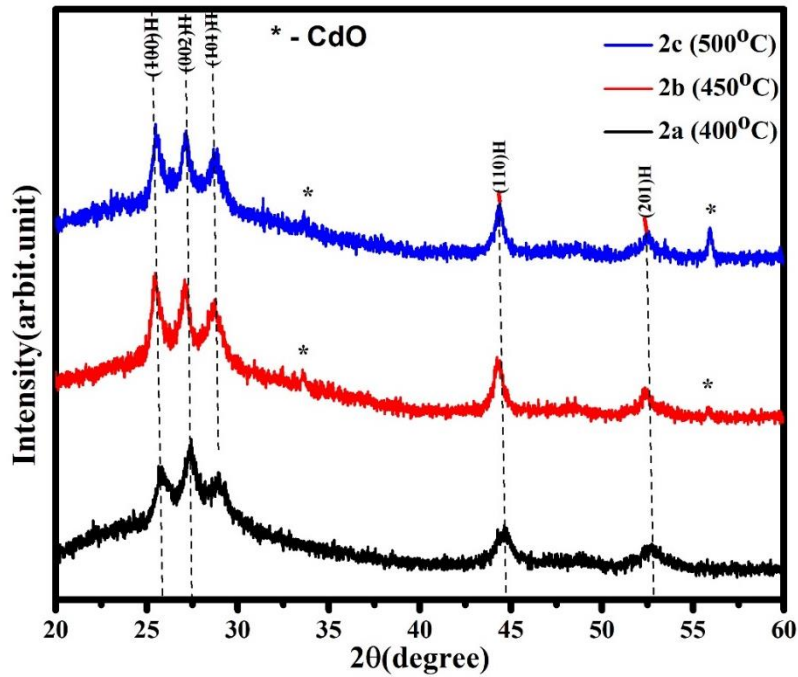


Fig. 3. 2 The above diagram shows the X-ray diffractograms of CdS thin films annealed at different temperatures for 60 minutes with pH-8

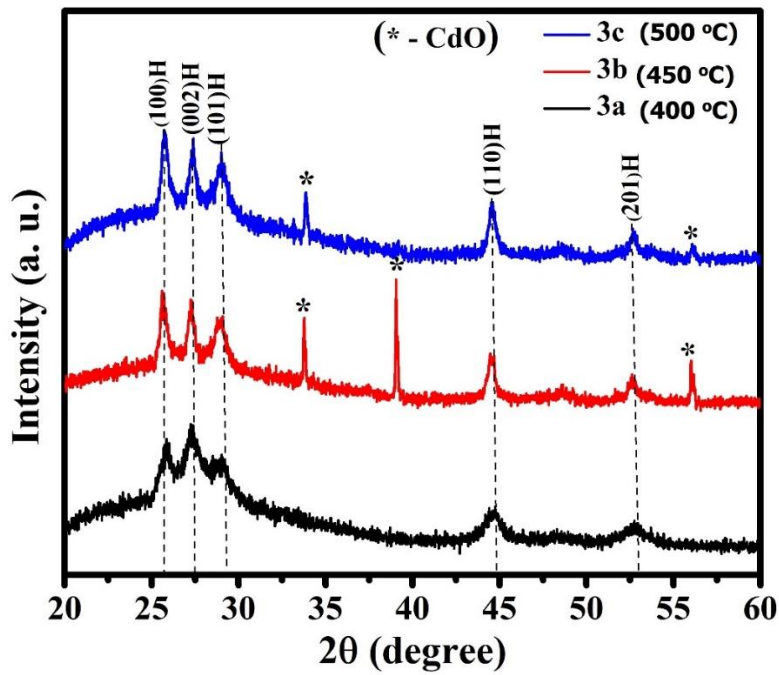


Fig. 3. 3 The above diagram shows the X-ray diffractograms of thin-film samples coded 3a- 3c (Refer table 3-A)

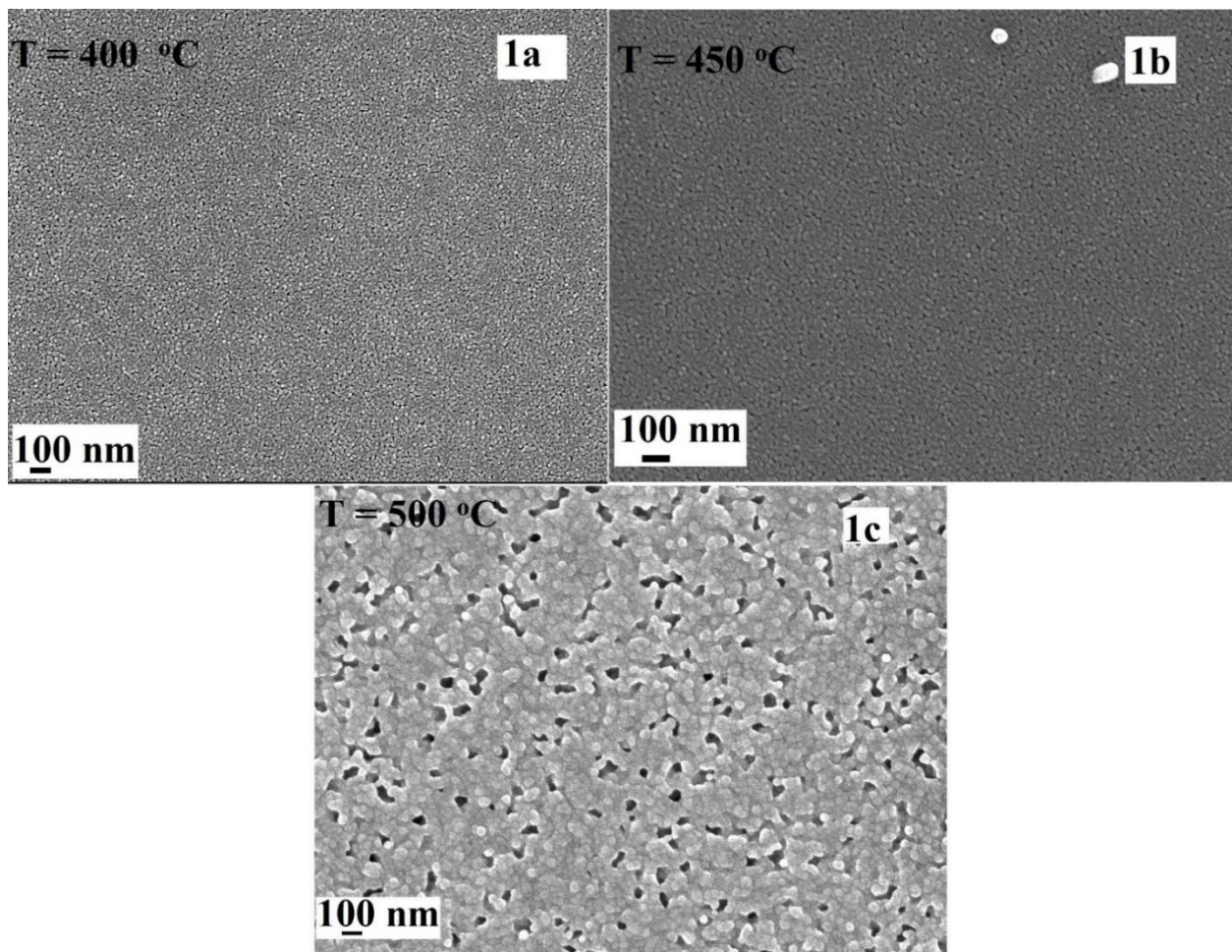


Fig. 3.4 The above diagram shows annealing temperature effect on the surface micrographs for thin film samples coded as 1a-1c

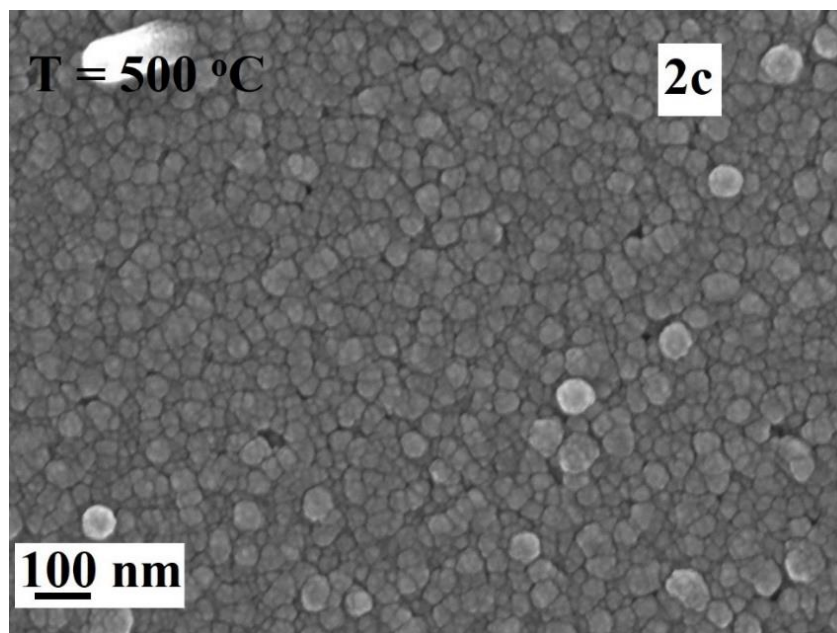
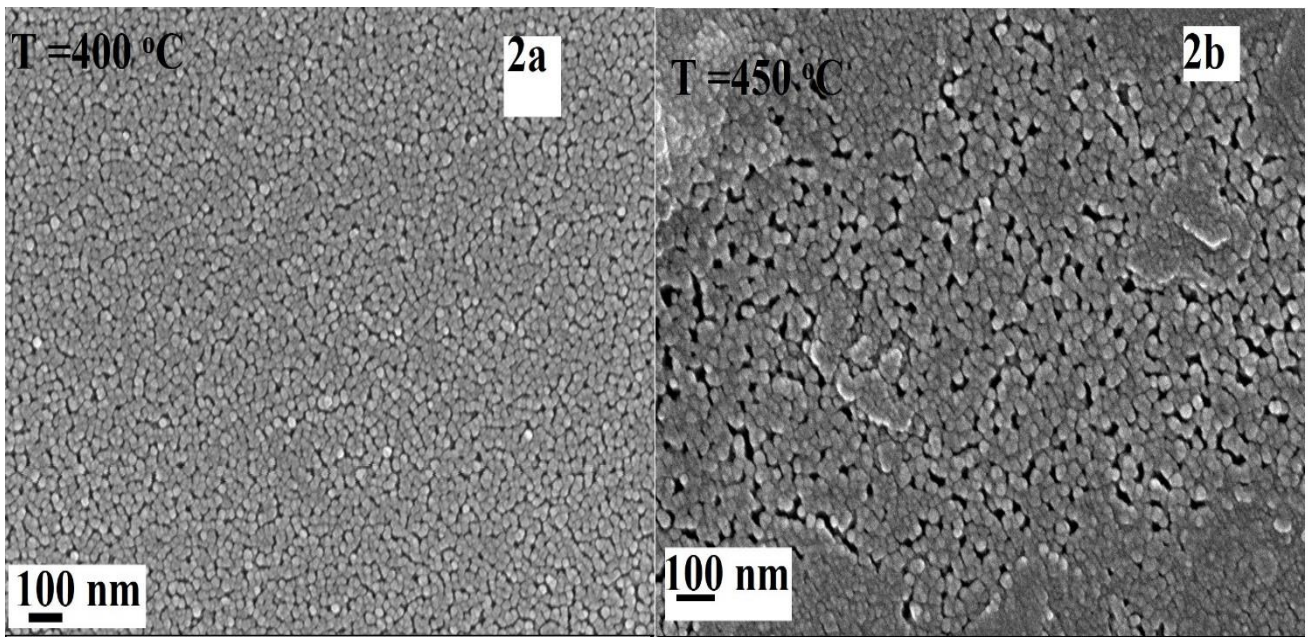


Fig. 3.5 The above diagram shows the surface micrographs for thin films annealed for 60 minutes at different temperatures

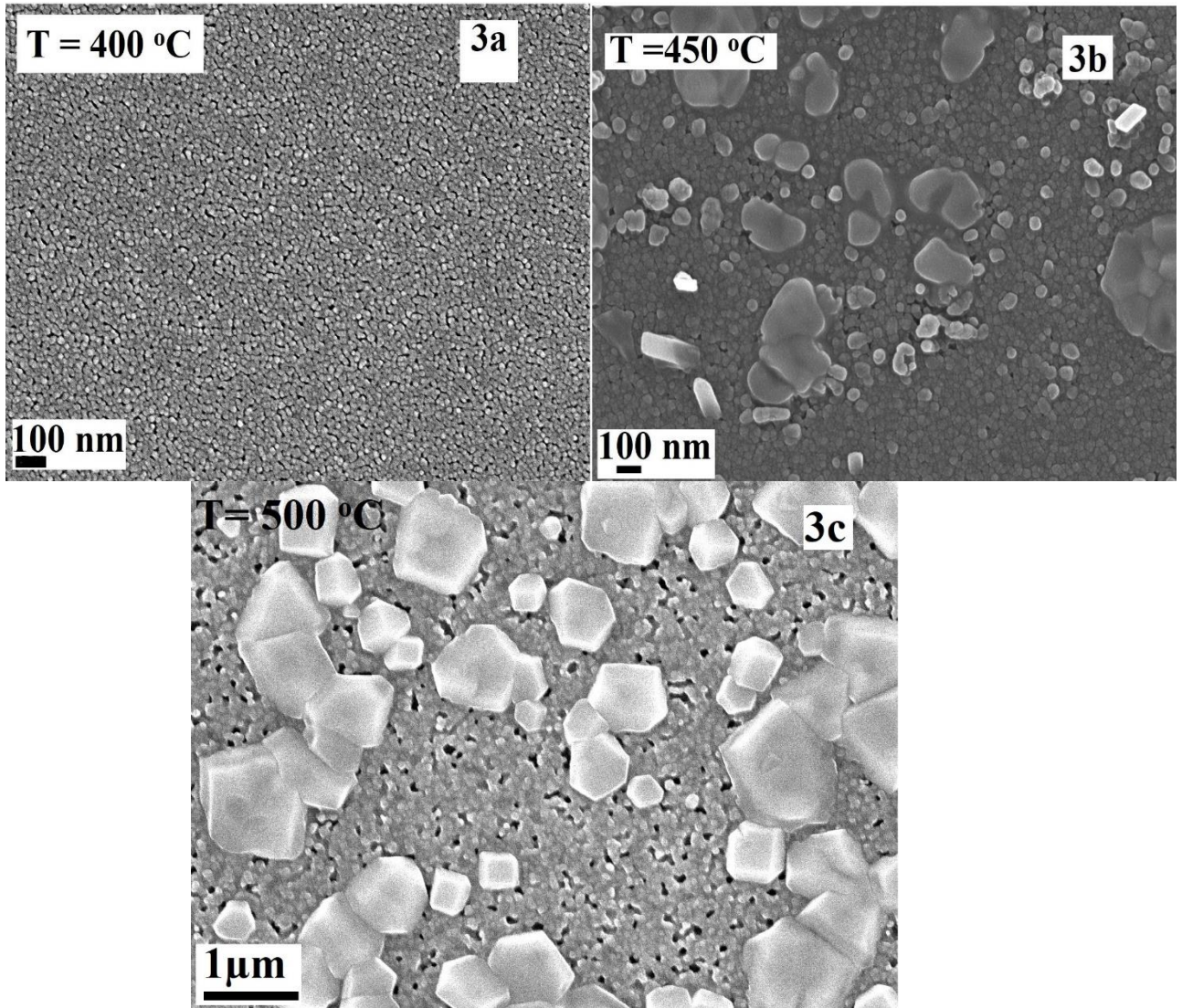


Fig. 3. 6 The above diagram shows the surface micrographs for thin films annealed for 90 minutes at different temperatures

Optical study

The variation of the optical band gap for thin films samples coded as 1a- 3c is illustrated in Table 3- A. It was observed that either annealing temperature or annealing time need to be increased to enhance the optical characteristics. As we can see in Fig. 3.5 transmittance is decreased with increase in annealing temperature. It may be due to improvement in crystallite size or increase in thickness. The optical band-gap has been reduced from 2.44 - 2.38 eV. It was due to the removal of lattice disorder, impurity or strain present in film [60].

A slight increase in optical band gap was observed in thin films annealed at high temperature annealing for 60 minutes and 90 minutes. Similar type observations were reported by Metin et.al [87]. Sulphur evaporation or oxidation might be the responsible for this degradation in optical

properties of CdS thin-films annealed at high temperatures $>400^{\circ}\text{C}$ for long time

The vibrational modes of CdS thin films analyzed by Raman spectroscopy are shown in Fig 3.11. The high intensity peak observed at 301 cm^{-1} corresponds to the fundamental longitudinal optical phonon mode (1LO) of wurtzite-CdS. The other two low intensity peaks observed at 603 cm^{-1} and 904 cm^{-1} correspond to higher order overtones of the fundamental modes 2LO and 3LO respectively. The intensity of higher order modes increases with rise in annealing temperature. The intensity ratio of 2LO and 1LO modes represented by $\gamma = \frac{I_{2LO}}{I_{1LO}}$ also increases with annealing temperature which signifies improvement of crystalline quality of the CdS thin films. The vibrational spectroscopy results are in agreement with the results obtained in x-ray diffraction studies. Surprisingly, vibrational modes of CdO phase peaked at $\sim 265\text{ cm}^{-1}$ and $\sim 390\text{ cm}^{-1}$ were not observed in CdS thin films[74,88]. This may be due to the low penetration depth of 488 nm laser in CdS thin films. The UV-Visible spectrophotometry results show that absorption coefficient of CdS thin films at 488 nm is approximately 10^7 m^{-1} which means most of the light is absorbed near the surface. Thus, it is difficult to retrieve information of impurities lying deep in the thin film by the given laser source.

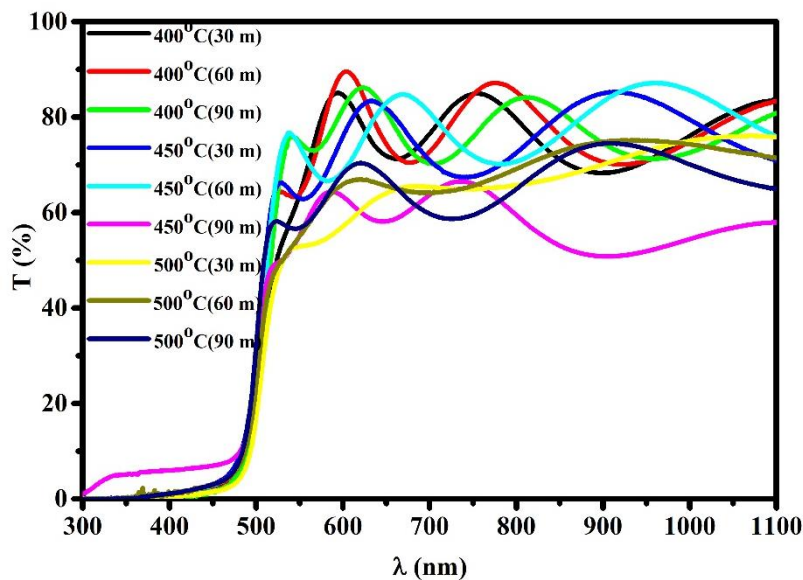


Fig. 3. 7 The above diagram shows the transmission spectra of thin films samples 1a-3c with pH-8 annealed at different temperatures 400°C , 450°C and 500°C .

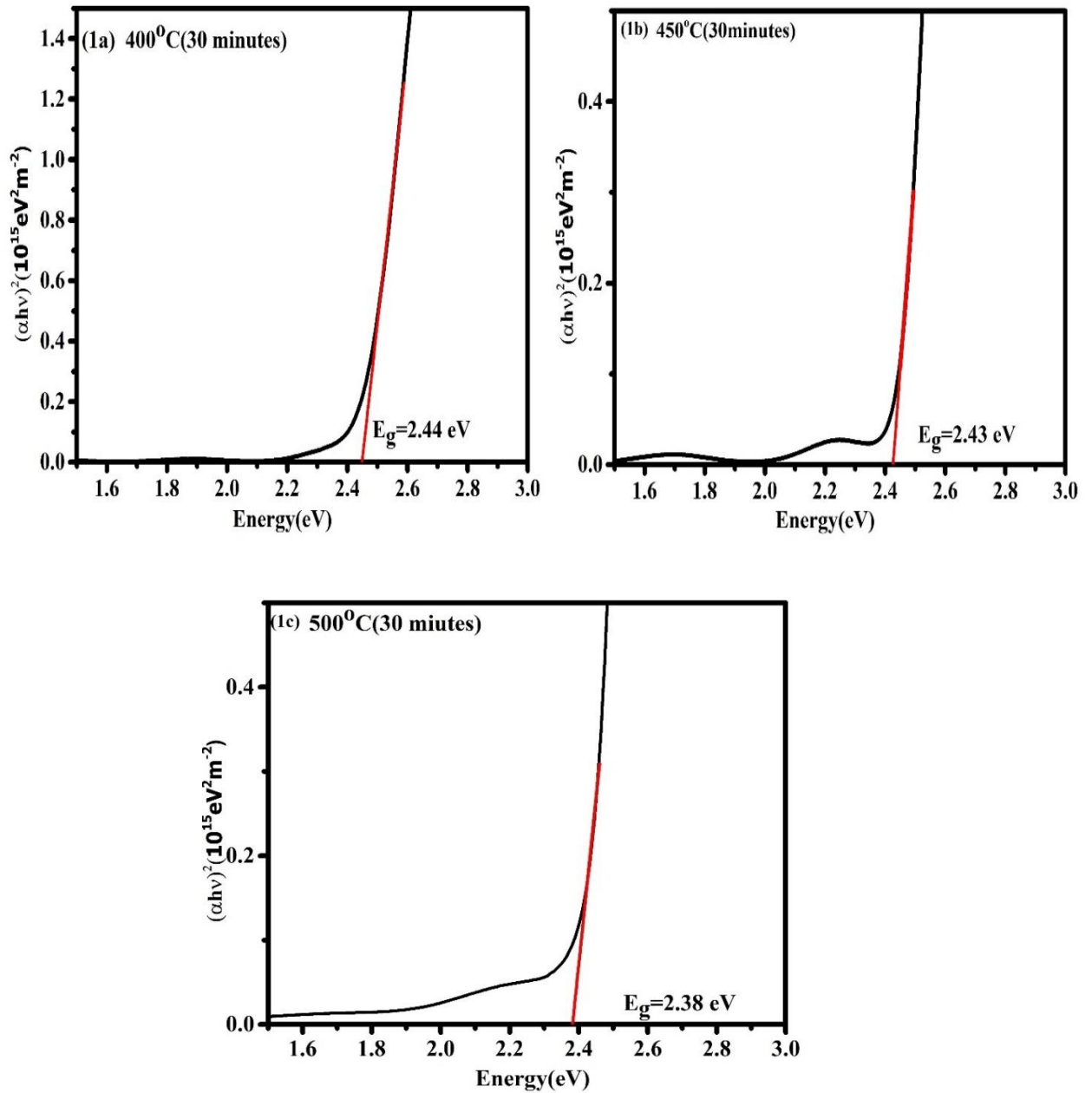


Fig. 3. 8The above diagram shows the Band gap (E_g) of samples 1a-1c.

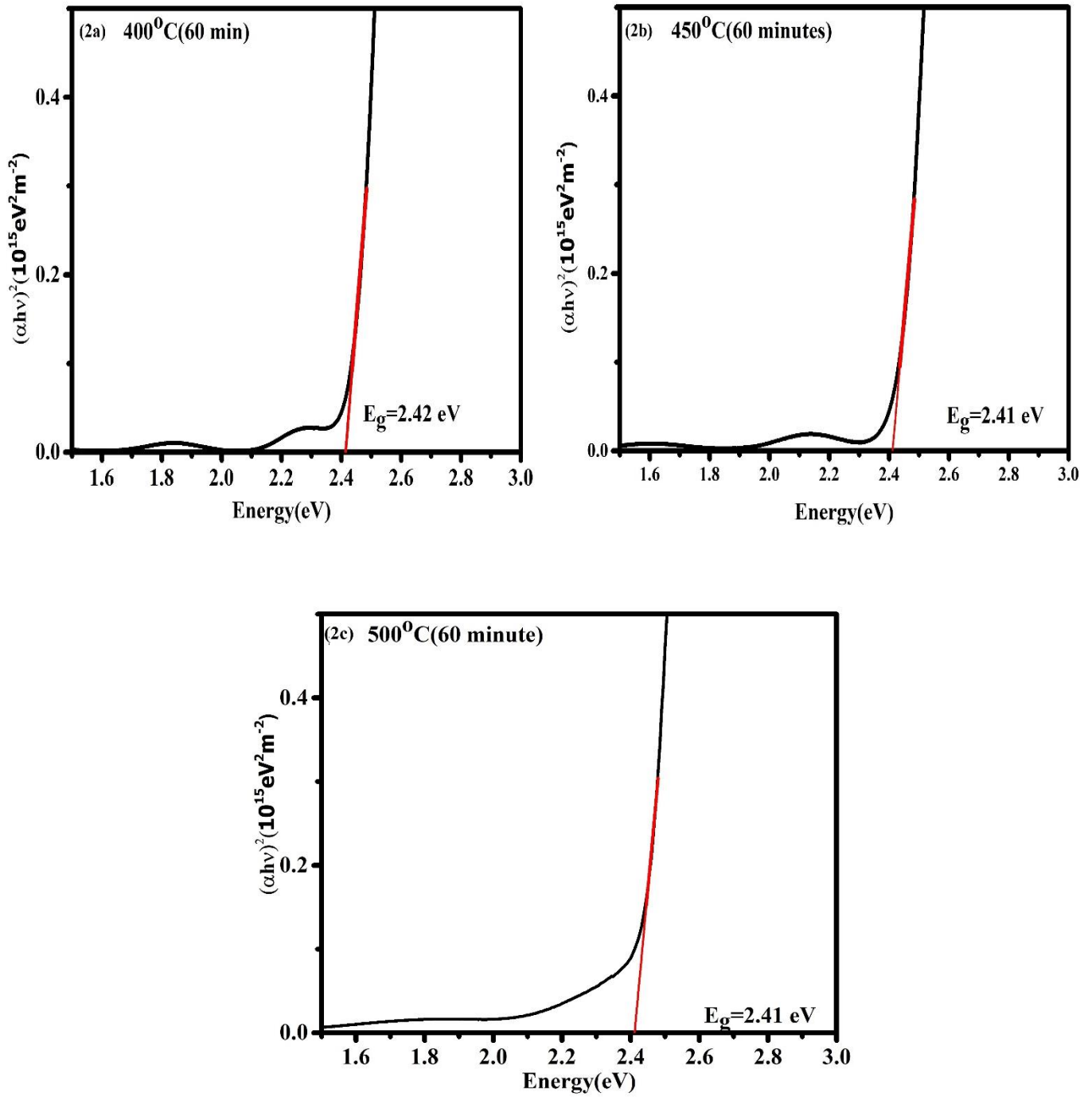


Fig. 3.9 The above diagram shows the band-gap (E_g) of samples 2a-2c.

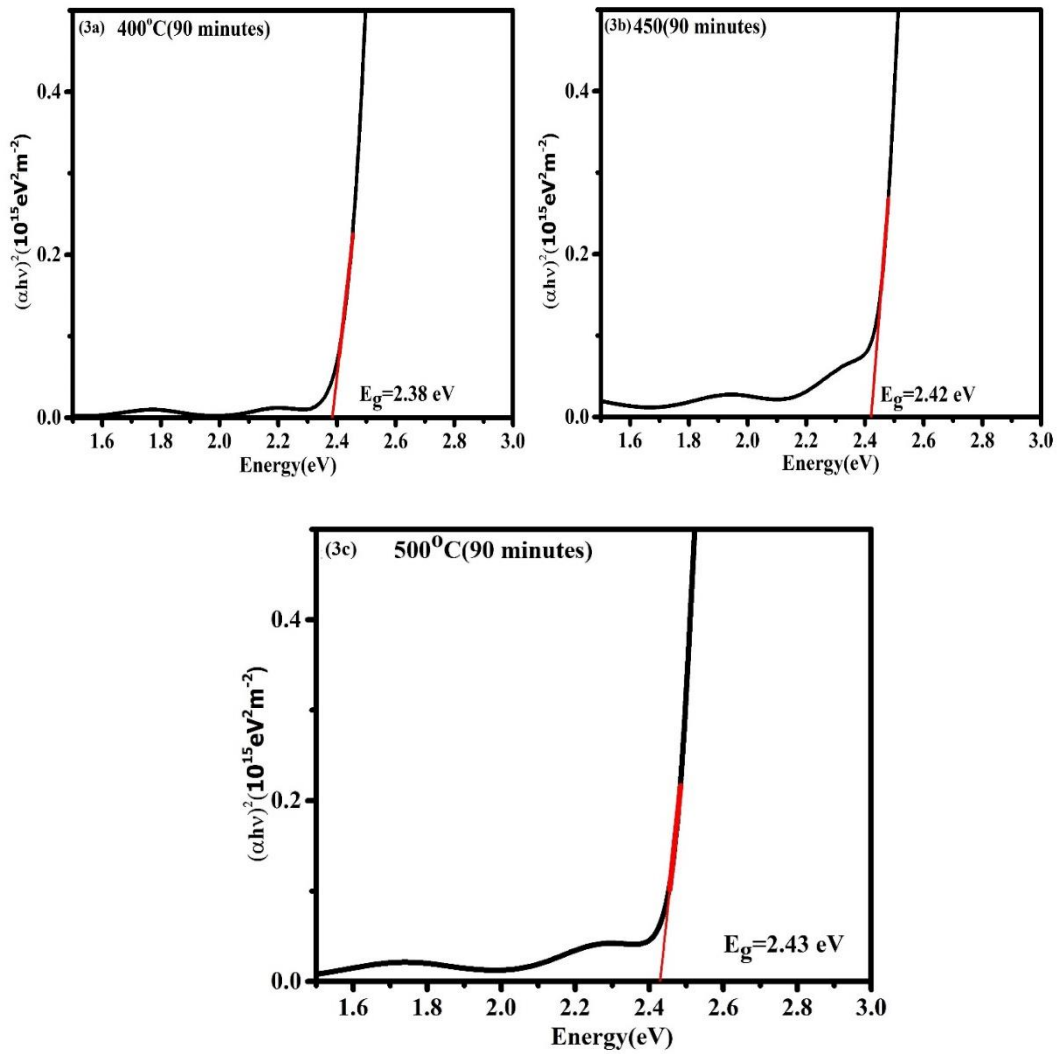


Fig. 3. 10 The above diagram shows the band- gap (E_g) of samples coded as 3a-3c

Table 3- B Shows the Calculated optical band gap for thin films 1a-3c from Tauc-plot

Sample Code	Band gap(E_g) (eV)
1a	2.44
1b	2.43
1c	2.42
2a	2.43
2b	2.41
2c	2.41
3a	2.38
3b	2.42
3c	2.43

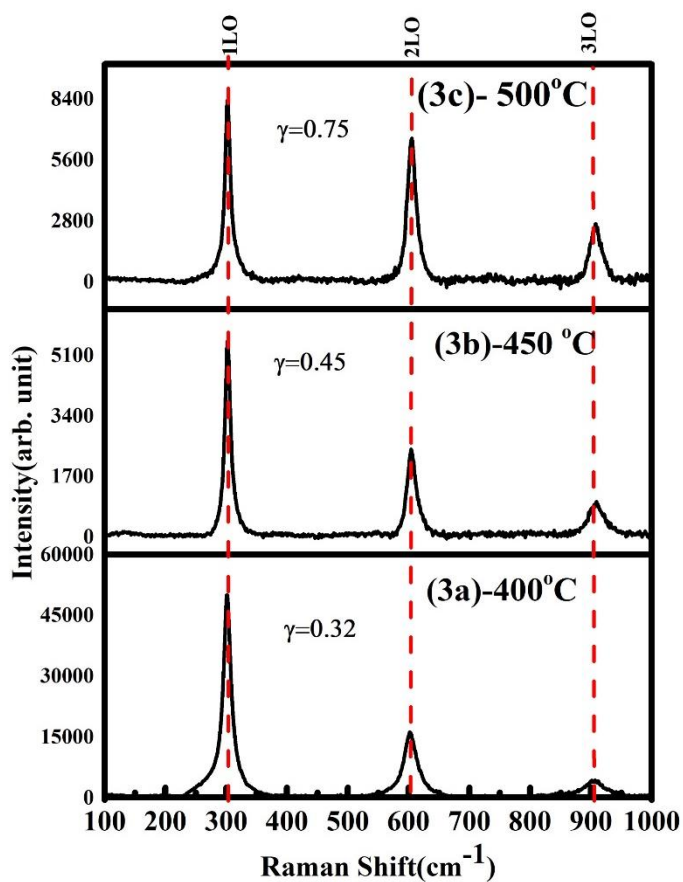
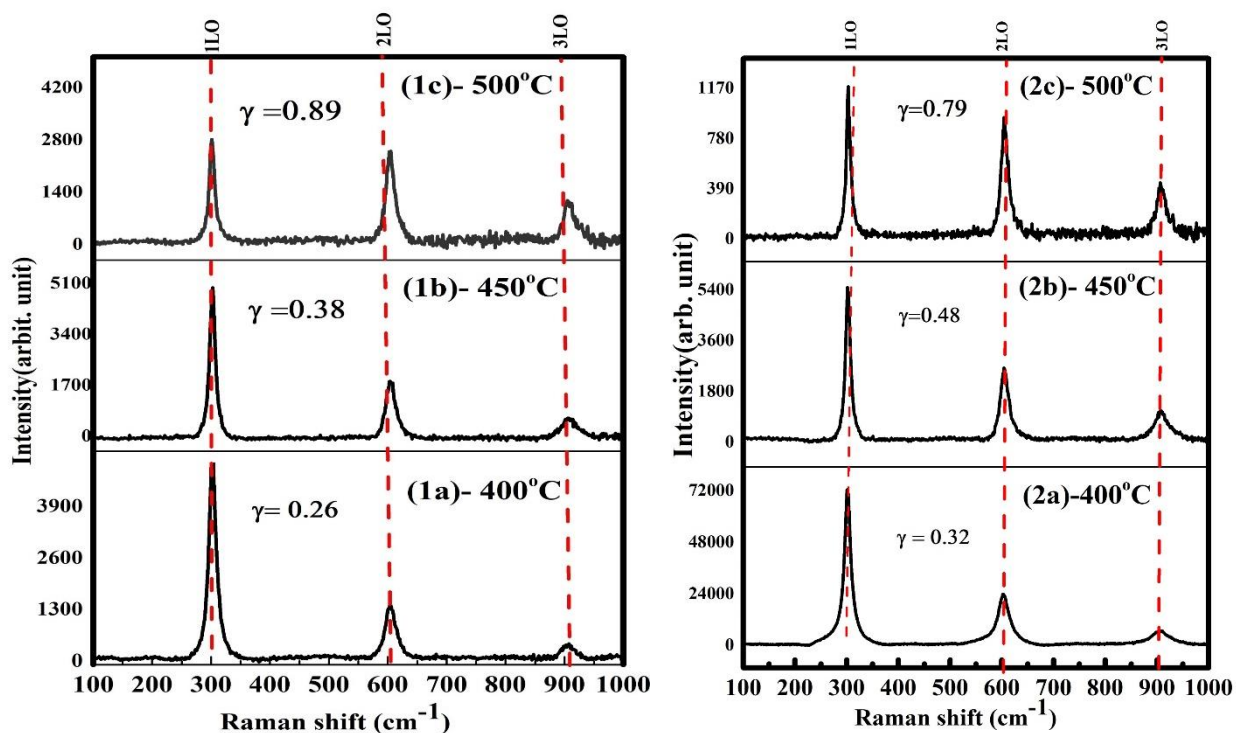


Fig. 3.11 The above diagram represents the observed Longitudinal modes of 1a-1c shows 30 minutes annealed samples, 2a-2c shows 60 minutes annealed samples and 3a-3c shows the LO modes of 90 minutes annealed samples.

3.2.2 *Structural and optical properties of CdS thin films synthesised at pH-10*

Structural study

Fig. 3.10 represents the x-ray diffractograms for thin film samples coded as 4a, 4b and 4c. Wurtzite phase correspond to (100), (002), (101), (110) and (201) planes could be identified. The crystallite growth took place around the (100) plane in all CdS thin films. Peak's intensity has been improved with a rise in annealing temperature and lower angles shift of peaks were also observed. The shift towards lower angles represents the reduction in lattice strain which was confirmed by calculating the FWHM of three major peaks of the wurtzite phase. FWHM is known as peak broadening. It may be due to various reasons such as strain present within the film, lattice mismatch of the substrate and thin films, due to the presence of any defects also. These are some internal causes of peak broadening some external causes such as instrumental error, the excessive slit width of the instrument and different ways of interpretation are also responsible for FWHM. In our work peak broadening due to instrumental error ~ 0.045 is also considered for the appropriate calculation of crystallite size. Phase identification is done by comparing the data with standard reference patterns JCPDS **00-041-1049**. At the same time, X-ray diffractograms represent the formation of cadmium oxide formation observed at high temperatures due to air annealing. The crystallite size increased linearly with temperature and a reduction in lattice strain was also noticed as well. The crystallite size varied from 12.1 nm to 39.1 nm.

W-H plots shown in Fig 3.11 were used to calculate the strain present within the thin films. The slope of the W-H plots represents the strain present within the film and is also helpful to study the type of the strain whether its tensile strain or compressive strain is present. Due to which either expansion or shrinkage in lattice may be caused. In Fig 3.11 (a), (b) and (c) observed value of strain was -0.127, -0.094, -0.051 for the prepared CdS thin films. The obtained values of strain were close in agreement with the strain values tabulated in table 2 calculated by using FWHM and theta values obtained from x-ray diffractogram. The negative value of strain confirms the presence of compressive strain within the films. The strain has been released with an increase in temperature from 400 °C to 500 °C.

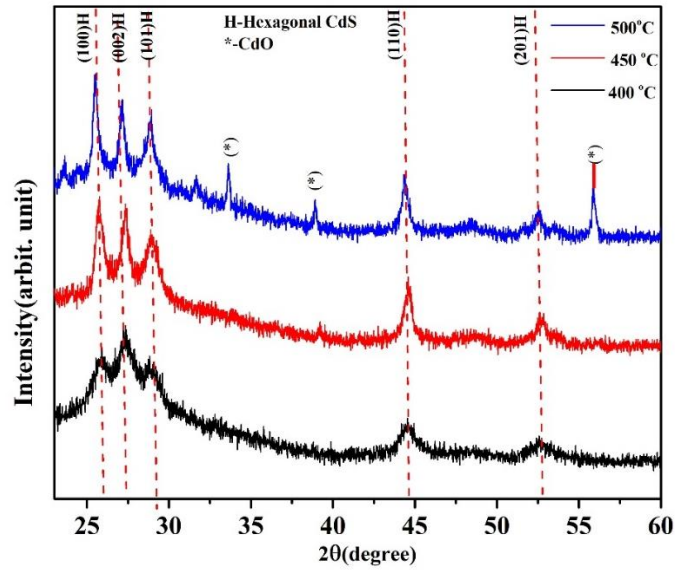


Fig. 3. 12 X-ray diffractograms of thin-film samples 4a-4c annealed for 60 minutes

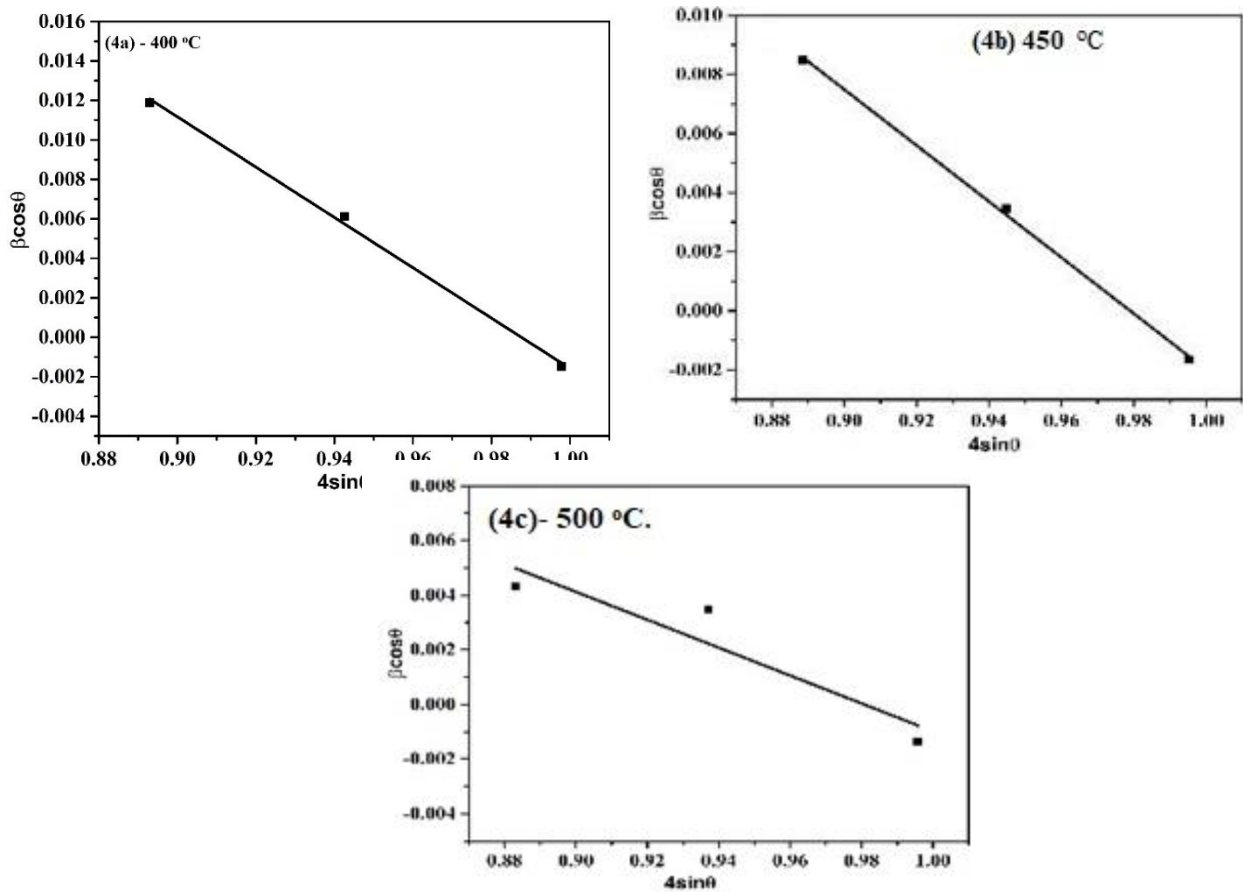


Fig. 3. 13 The above diagrams represent the W-H plots of thin film samples coded as 4a, 4b, 4c annealed for 60 minutes.

Table 3- C Shows the observed values for peak position (2θ), FWHM (β), Crystallite size (D) and Lattice strain

Sample code	Annealing Temperature (°C)	Peak Position (Degree)	FWHM (radian)	Crystallite size (nm)	Lattice strain *10 ⁻¹
4a	400	25.80	0.01177	12.16	1.369
		27.25	0.01177	12.16	1.293
		28.89	0.00408	41.52	0.466
4b	450	25.66	0.00800	17.76	0.962
		27.32	0.00067	21.28	0.771
		28.81	0.00539	26.33	0.596
4c	500	25.51	0.00361	39.36	0.478
		27.11	0.00549	25.96	0.647
		28.83	0.00424	33.75	0.483

Optical study

The Tauc plot $(\alpha hv)^{1/n}$ vs hv as shown in Fig. 3.12(B). The linear region of this Tauc-plot was helpful to find the band gap (E_g). The extrapolation of the linear region of the Tauc plot at $y=0$ gives the value of the optical band gap of prepared thin films. Where value n can be 2 or $1/2$ depending upon the nature of the material used. For direct band gap materials $n=1/2$ and indirect band gap materials $n=2$. From this data of the optical band gap, we can conclude which energy photons are required to excite the electrons from the valence band to the conduction

band. From Fig. 3.12(B) we could see that the optical band gap initially increased with a rise in temperature 400-450 °C but with a further rise in temperature up to 500°C optical band gap decreased to 2.41 eV. This type of oscillating behaviour of optical band gap was earlier reported by H.Metinet al.[87] . Maximum decrease in transmission was observed at 500 °C. The decrease in band gap at 500 °C may be due to the presence of impurities, which act as shallow traps in CdS thinfilms annealed in the air as reported by Gutiérrez Lazos et al.[88].

Every energy state has vibrational as well as rotational levels. Along with the band-to-band transitions, vibrational level transitions are also there. Raman spectroscopy plays an important role to study the vibrational modes of a material [89,90]. The vibrational mode study was carried out through laser source with an excitation wavelength of 488nm (as shown in Fig. 3.13). For the prepared thin films Longitudinal optical phonon modes were observed. Fundamental optical phonon mode (1LO) was obtained at 302 cm^{-1} . Second and third-order overtones (2 LO and 3LO) were also seen in Raman spectra at frequency 604 cm^{-1} and 905 cm^{-1} . The ratio of 2LO/1LO also increased, which confirms the increase of multiple phonon scattering due to improved crystalline quality with rise in annealing temperature [91]. The slight shift of peaks towards the lower frequency side was found for CdS thin films annealed at 500°C as compared to 400°C annealed thin films which mean the release of compressive strain in thin films. Similar kind of results could be concluded from XRD also.

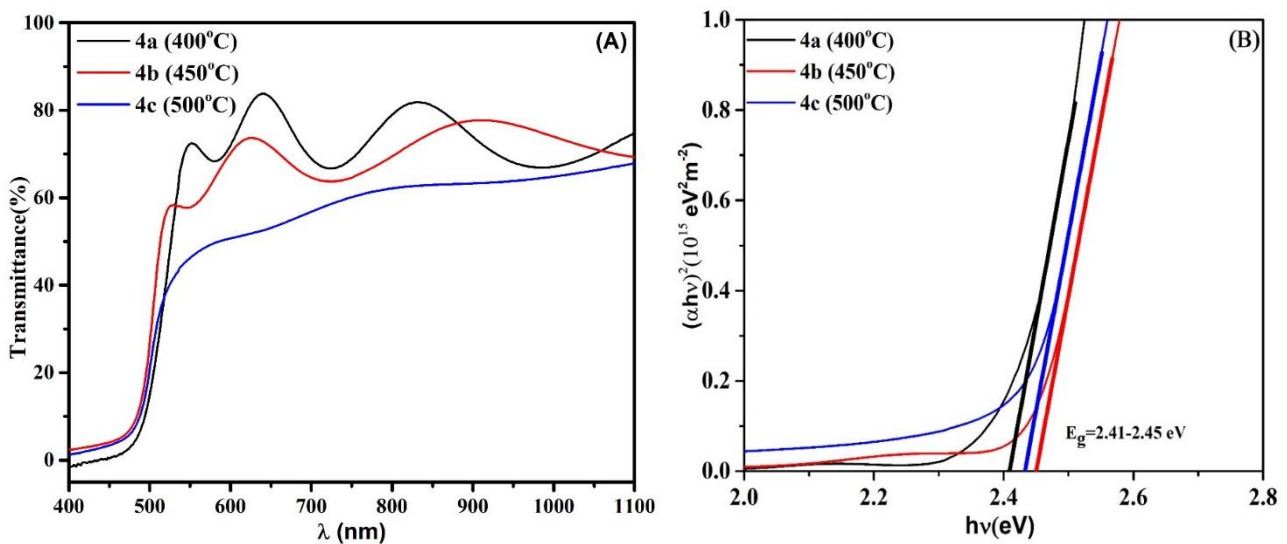


Fig. 3. 14 The above diagram shows the observed (A) transmittance spectra and (B) TAUC-plot for thin films samples 4a-4c annealed for 60 minutes.

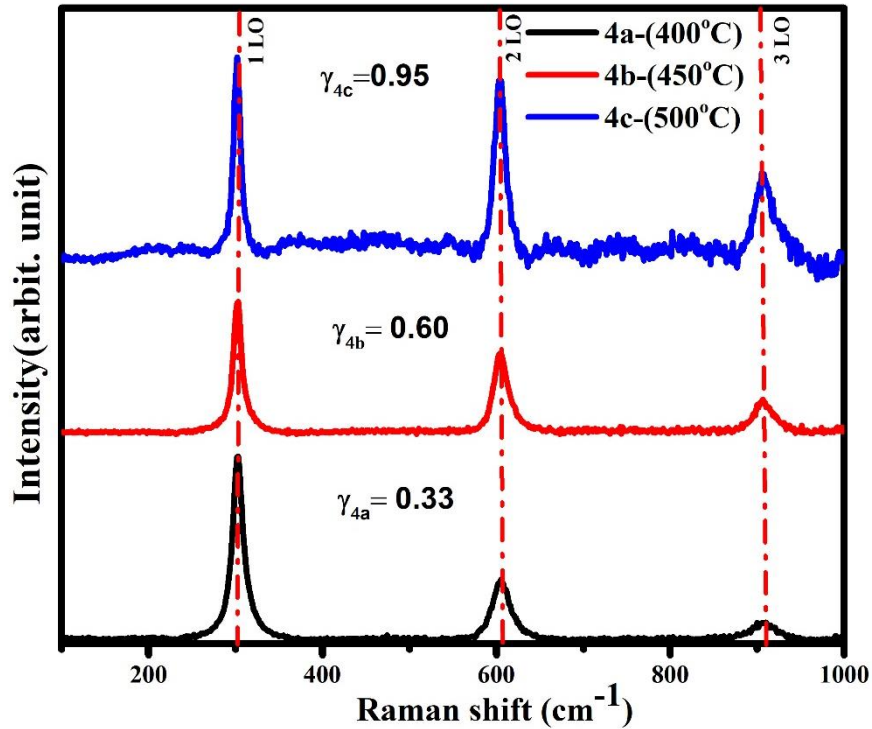


Fig. 3. 15 The above diagram represents the Raman spectra of thin film samples coded as 4a-4c annealed for 60 minutes with pH-10.

3.2.3 Study the Molar concentration effect on structural and optical properties of thin films

Structural study

Fig. 3.14 The above diagram shows the X-ray diffractograms of CdS thin films prepared with different molar concentrations (0.2 M – 0.4 M) annealed at 400 °C for 180 minutes with pH-10 represents the XRD patterns of annealed thin film samples 5a-5c. Five diffraction peaks at 25.70°, 27.28°, 28.71°, 44.38° and 52.53° which were depicted correspond to (100), (002), (101), (110) and (201) planes. All obtained peaks revealed the purely hexagonal phase of annealed CdS thin films. The peak corresponds to (002) plane is found to be dominant peak as compare to the other peaks. The FWHM's value correspond to (002) plane for all three samples of CdS thin films were used in Scherrer formula given in equation (2.1) to calculate the crystallite size. The observed peak broadening of XRD diffraction patterns was due to variation in crystallite, strain present between substrate and thin film as well as due to instrumental error [83][84]. W-H plots (Fig 3. 15) were also plotted to calculate the micro strain present and crystallite size of prepared thin films more precisely. Calculations were done by assuming that the synthesised material is homogeneous in nature. From the obtained results it could be seen

that CdS thin films prepared from 0.3M concentrated solution has minimum value of FWHM and maximum crystallite size. While Crystallinity degradation was observed for the CdS thin films synthesized from the solution with higher molar concentration (0.4M). It may be due to induced strain or interstitial defects as number charge carrier increases with increase in molarity of the solution. These results are in accordance with by M. D. Devi et al [58,92]. The value of strain present in CdS thin films were obtained from the W-H plots. It could be noticed that the CdS thin films synthesized from 0.3 M concentrated solution have tensile strain while those synthesized from solution with 0.4 M concentration have compressive strain. Dislocation density (δ) was also helpful to confirm the trend of imperfections with increase in molar concentration of solution used to prepared the CdS thin films.

$$\delta = 1/D^2$$

Dislocation density initially decreased from 0.0025 to 0.0008 with rise in molar concentration from 0.2 to 0.3 M of the solution. while imperfections have been increased to 0.0023 for CdS thin films prepared from 0.4 M concentrated solution. Thus, it can be concluded that increased concentration of the sol may be a cause of lattice distortion and reduction of crystallite size.

Fig. 3.16 illustrates the microstructural characteristics of thin films samples labeled as 5a-5c. The Images exhibit the uniform dispersion of particles over the glass substrate. The reduction in grain boundaries was observed for the thin-films prepared from 0.3 M and 0.4 M concentration. Grain size was increased. The black pin holes may be due to shrinkage of the thin films after annealing. The particles were found in the range of 100 nm. In addition to the above scanning electron micrographs cross-sectional FESEM were also taken to determine the thickness of the thin films shown in right-hand side of Fig. 3.16. It has been observed that initially thickness increased for thin films prepared from 0.3 M solution. More increase in molarity (i.e 0.3 to 0.4M) thickness of thin films decreased. Thickness of thin films was 638nm (0.2 M solution), 670nm (0.3 M solution) and 573 nm (0.4 M solution)[84].

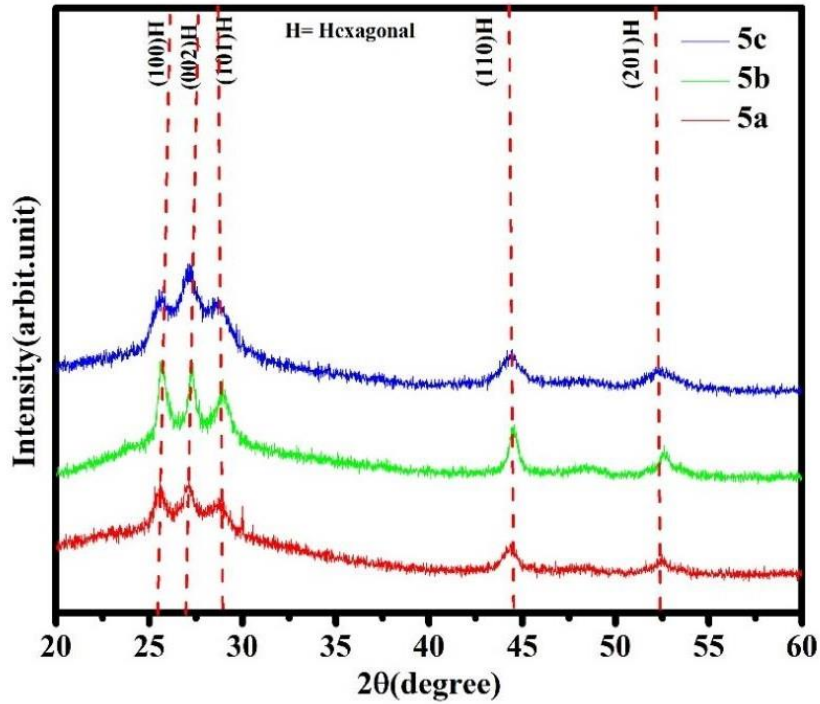
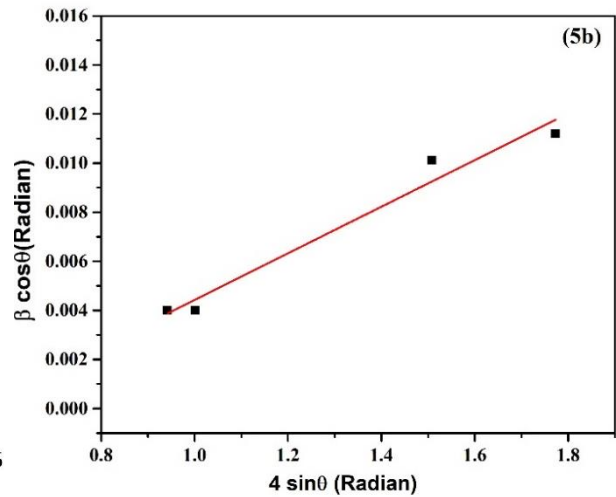
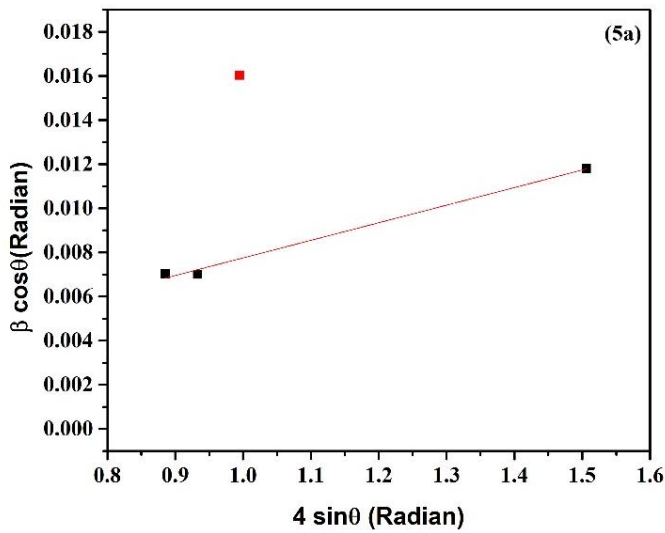


Fig. 3.16 The above diagram shows the X-ray diffractograms of CdS thin-films prepared with (5a) 0.2M, (5b)) 0.3M, and (5c) 0.4 M molar concentrated sol and annealed at 400°C for 180 minutes.



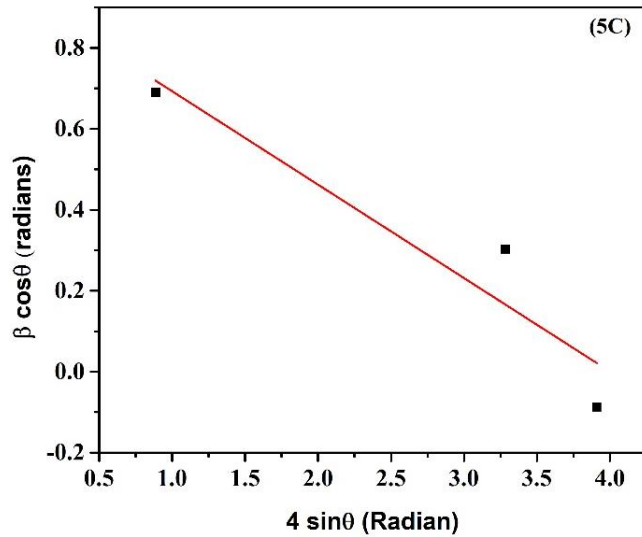


Fig. 3. 17 The above diagram represents the W-H plots of thin film samples prepared by varying the molar concentration of the sol where (5a) 0.2M, (5b) 0.3M, (5c)0.4M

Table 3- D Shows the Peak position (2θ), FWHM(β), Crystallite size (D) and the value of lattice strain.

Sample code	Concentration(M)	Peak Position (Degree)	FWHM (Radian)	Crystallite Size (D) (nm)		Lattice Strain ($\times 10^{-2}$)
				Scherrer Formula	W-H Plot	
5a	0.2	26.99	0.00721	19.76	22.35	0.79
5b	0.3	27.24	0.00412	34.61	49.5	0.94
5c	0.4	27.07	0.00927	20.50	13.84	-0.23

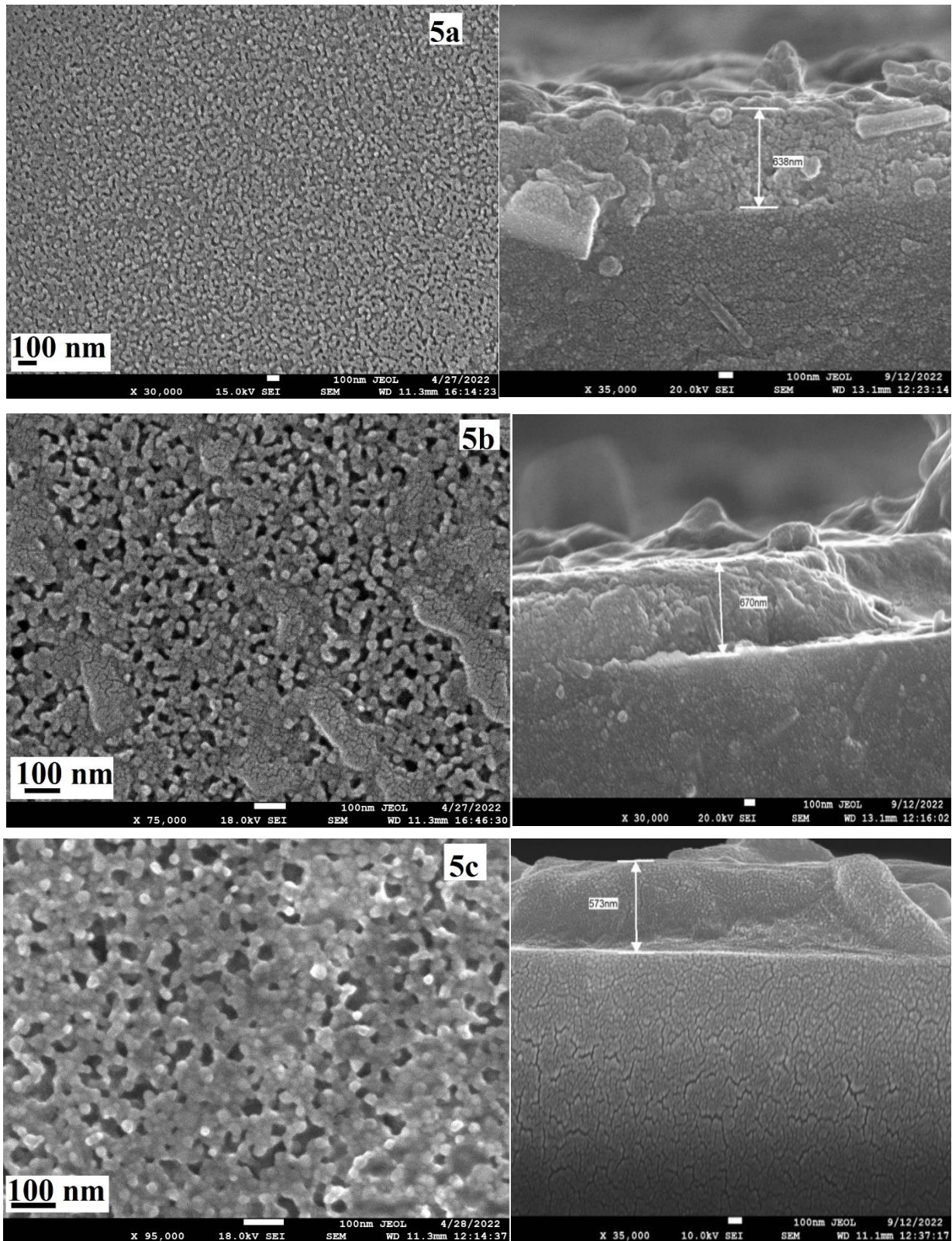


Fig. 3. 18 The above diagram shows the surface micrographs and thickness for CdS thin- films having different molar concentration of precursors

Optical study

Fig. 3.17 represents transmission spectra of thin films prepared with different molar concentration of the sol used. Transmittance varied from 83% to 73% in the visible region of electromagnetic spectrum. The number of interference fringes also increased with increase of molarity which means thickness of the thin films increase with respect to the molarity (provided number of CdS layers are same). The shift of absorption edge towards the higher wavelength could be seen for the films prepared with 0.3 and 0.4 molar concentration of the solution as compared to 0.2M. Thickness of thin films were observed through Cross-sectional FESEM. The optical band gap evaluated is comparable with the energy gap of CdS in bulk ~ 2.41 eV. Optical band gap is lessened for CdS thin films (400 °C) with rise in molarity except thin films prepared from 0.3M solution. while absorption edge in **Fig. 3.18** is sharpened (i.e. shifted towards higher wavelength) with rise in molarity means transmittance also declined. No such change in optical band gap found on varying the molarity from 0.2 M to 0.3 M. E_g reduced from 2.43 to 2.41 eV for 0.4M prepared CdS thin films. This may be due to formation of any localized state within the forbidden band gap due to annealing as reported by [60,67,93,94]. The minimum calculated value of E_u is 84.6 meV for 0.3 M CdS thin films confirms the minimum disorder presence. The good crystalline quality with crystallite size of 34.61 nm and minimum FWHM 0.00412 radian from XRD confirms 0.3M as the best suitable molarity for the prepared samples under optimum conditions.

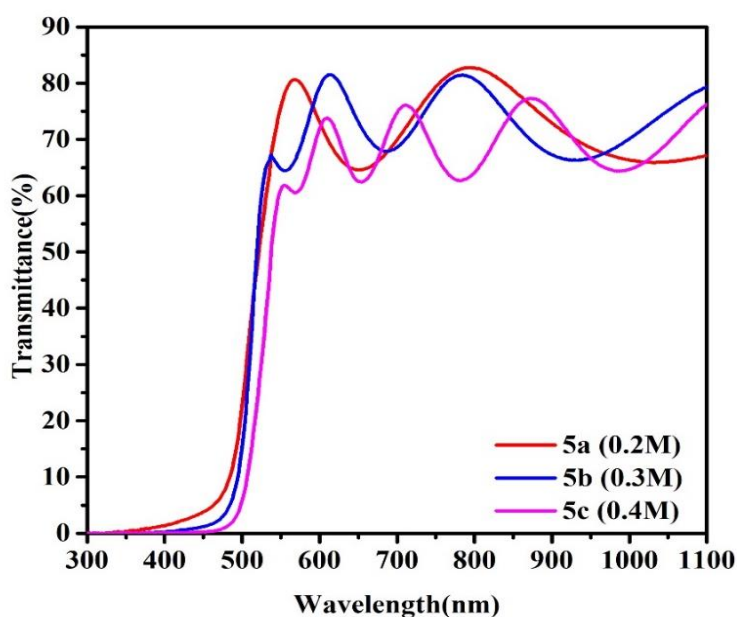


Fig 3. 19 The above diagram shows the transmittance of thin films samples 5a,5b and 5c prepared by varying the molar concentration of the solution

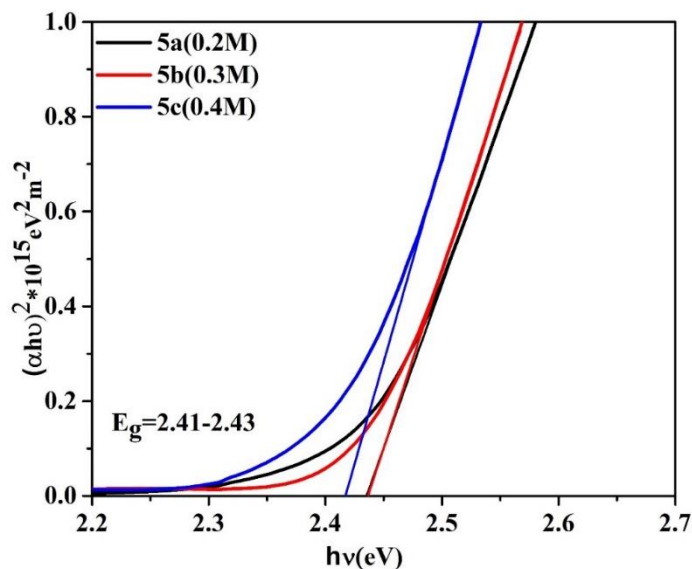


Fig. 3. 20 The above diagram represents the calculated optical band gap of thin-films samples coded 5a,5b and 5c with different molar concentration of the solution

3.2.4 Structural and optical studies of thin-films deposited on flexible (PET) substrate

Structural study

Polyethylene terephthalate (PET) was used as flexible substrate. The diffraction pattern observed for prepared thin film sample-7a shown in Fig 3.19. The prepared samples were annealed at 300 °C for 120 minutes to improve the crystalline quality so that phase identification become possible. Three peaks correspond to (002), (110) and (201) planes were observed. The observed peaks were corresponding to hexagonal phase of CdS. **Fig 3.20** shows the micrographs of CdS thin-films deposited on flexible substrate. Dense thin films were uniformly deposited on the substrate. The particle size was found in the range of nano meters.

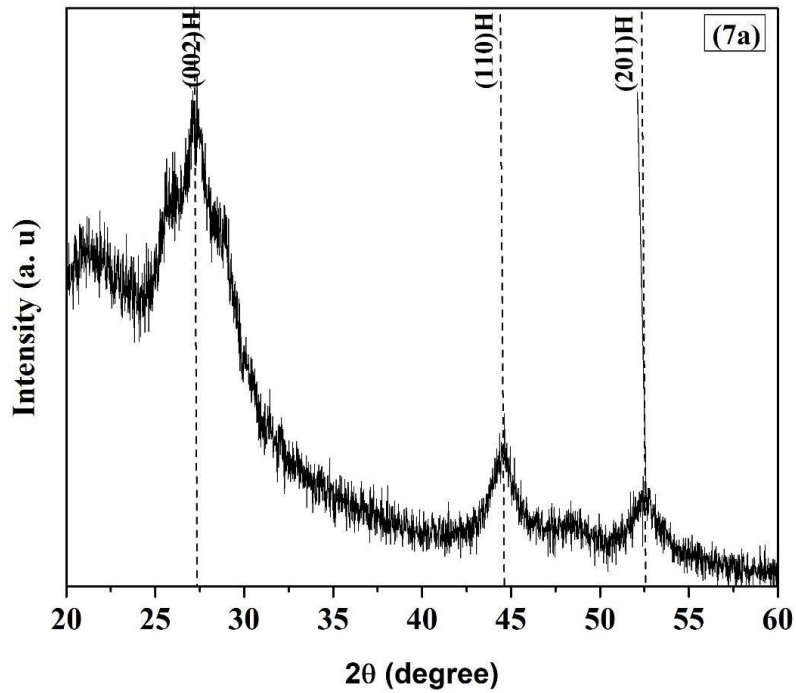


Fig. 3. 21 The above diagram shows the diffraction patterns of thin-films deposited on PET.

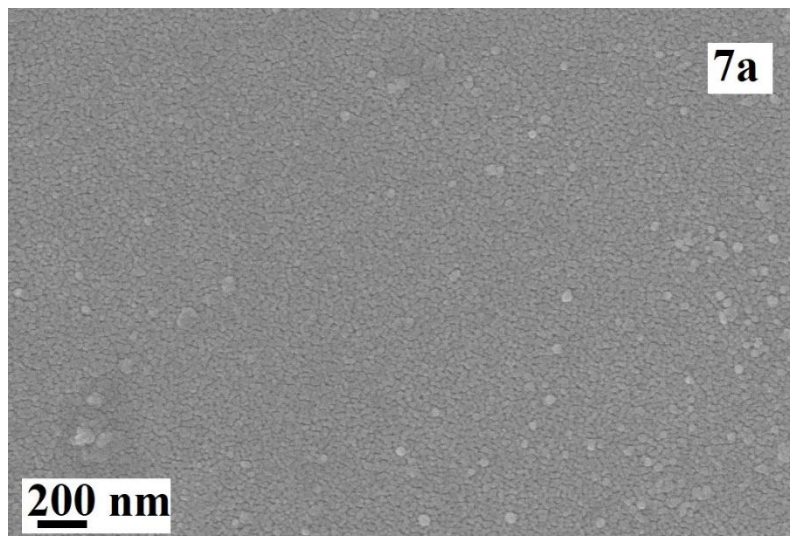


Fig. 3. 22 Surface morphology of CdS thin-films deposited on PET

Optical study

Fig 3.21 - Fig. 3.22 represents the transmittance curve and calculated optical band gap graphs for thin films deposited on PET substrate. Due to multiple reflection of light through number of layers deposited broad interference fringes were observed in transmittance graph (Fig. 3.21). Transmittance has been observed 75% between 580 - 900 nm wavelength range. The transmittance falls around 520 ± 5 nm. This fall in transmittance due to absorbance of light. Absorption coefficient was calculated through equation (2.1) which is 10^{-11} cm^{-1} . The

absorption is low as compared to thin films deposited on the glass substrate. This decay in absorption may be due to lattice mismatch between PET and CdS thin films. The calculated optical band was 2.44 eV. The observed band gap was almost within the range of data observed for thin films deposited on the glass substrate as well as with previous reported literature.

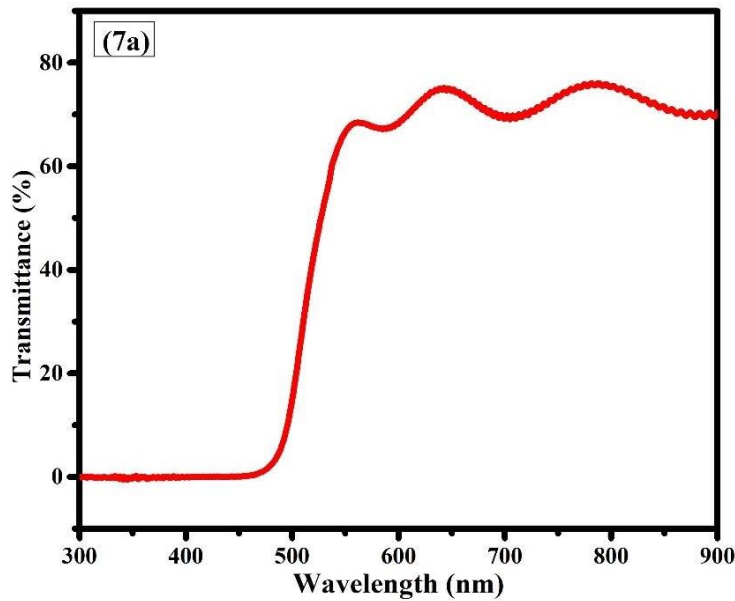


Fig 3. 23 The above diagram shows the transmittance graph of CdS thin films deposited on flexible substrate prepared with 0.3 Molar concentrated solution.

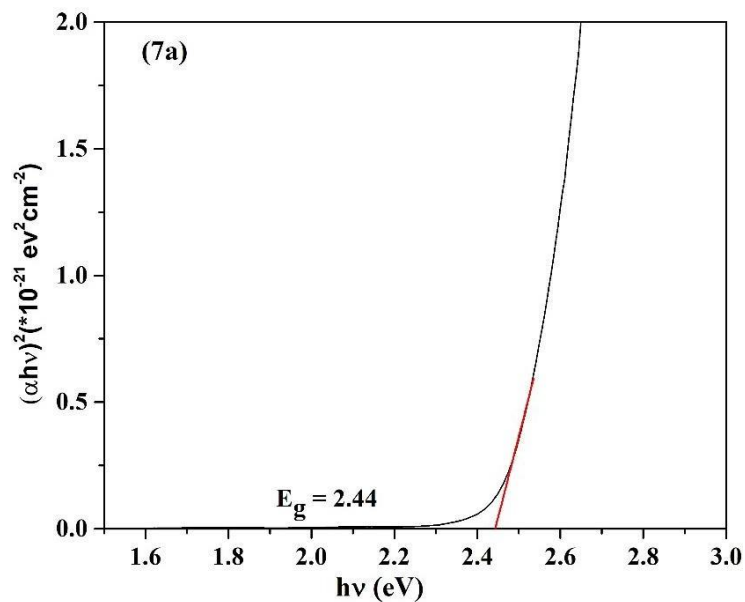


Fig. 3. 24 The above diagram shows the optical band gap of CdS thin-films deposited on flexible substrate prepared with 0.3 Molar concentrated solution.

3.3 Summary

The work presented in this chapter is based on the optimization of the process parameters for the prepared CdS thin films. From the results and discussion, it could be concluded that

- *Annealing at high temperature for long time introduced CdO along with CdS Which increased with increase in annealing temperature and time. Thus, controlled thermal annealing is required to avoid the formation of oxides and to improve the crystalline quality of the prepared thin films.*
- *Annealing at 400 °C was considered as best suitable annealing temperature.*
- *Annealing time (30 minutes, 60 minutes and 90 minutes) also varied to improve the crystallinity at certain temperature. Thus, it could be observed synthesis at low temperature is also possible by increasing the annealing time.*
- *Excess of precursor's concentration introduced the defects and lattice deformation in lattice to avoid that 0.3 M concentrated solution was considered as best suitable for the fabrication of CdS thin films.*
- *Thin films were synthesised on PET substrate also having good structural and optical properties comparable with results obtained for thin films on glass substrate which further need to be optimized.*



Chapter -4

Structural and optical studies of Zn: CdS thin films

4.1 Introduction

In this chapter investigates the influence of Zn-dopant concentration on both structural and optical characteristics of prepared CdS thin films. Thin-films were deposited on Soda lime glass (SLG) substrate and Polyethylene Terephthalate (PET) substrate as well. The various parameters used and the sample coding of prepared thin films is shown in Table 4-A. Dopant is an external impurity that is added to create some defects in the lattice. The position of the defect state may be in an intermediate of the forbidden gap, towards the valence band, or below the conduction band depends on the concentration of dopant added. The addition of a dopant may vary the optoelectronic properties of prepared thin films. This work has been performed to improve the optical, structural, and electrical behavior of CdS thin films for photonic device application. Pb, Cu, Sr, Sn, Zn, etc are some well-known dopants that can be used as their ionic radii is comparable with Cd⁺². In our work, we tried to improve various properties of CdS thin films by introducing Zn⁺² ions as a dopant within the CdS lattice. For that purpose, Zinc acetate has been used as a source of Zn⁺² ions. Three different solutions of Cd_xZn_{1-x}S with different dopant concentrations were prepared. Where x was varied as 1%, 2%, and 3% as per the weight percentage of precursor 1 (Cadmium acetate dihydrate). Dopant concentration is varied to analyze its effect on the optoelectronic properties of the prepared thin films. Prepared thin films were annealed at 400 °C to improve their structural and electrical properties. There is a possibility of various type of defects formation such as interstitial defects, substitutional defects, and anti-site defects, etc. The tuning in properties of the material depends upon the type as well as on the position of defects formed. It can be deep-level and shallow-level defects or any localized state can be formed within the bandgap. If the defects will be introduced within the valence or conduction band are called deep-level defects called traps. On the other hand, if defects are formed on the surface of the material means most of the charge carriers are residing on the surface than the volume in that case shallow defects would be present.

Table 4- A The table below represents the pH-values, annealing temperature and annealing time and sample coding for the prepared samples of Zn: CdS thin films deposited on SLG and PET

Name of the samples	Zn content	pH- values	Molarity of solution (Molar)	Annealing temperature (° C)	Annealing time (minutes)
6a	0.01	10	0.3M	400	120
6b	0.03				
6c	0.05				
7b	0.03	10	0.3M	300	120

4.2 Results and discussion

4. 2.1 Structural and optical studies of Zn:CdS thin-films fabricated on SLG

Structural properties

Phase identification doped thin-films is done through X-ray diffractograms. CdS thin films were characterized in thin film mode where angle 2θ is varied from the range $20^\circ - 70^\circ$. The interference patterns of x-rays were obtained at an angle 25.58° , 27.02° , 28.62° corresponding to (100), (002), and (101) planes. The peak corresponding to the plane (002) is the dominant peak. The obtained peak position (JCPDS:00-006-314) confirms the hexagonal phase of prepared CdS thin films. The hexagonal phase of CdS is considered the stable phase. The increase in intensity and shift in peak positions was observed in X-ray diffraction patterns with an increase in dopant concentration. The increase in intensity and reduction in FWHM reflects the improvement in crystallite size. As a result, the stress between the thin films and the substrate is reduced. X-ray diffractograms were also used to calculate the different parameters such as FWHM, crystallite size, strain, d-spacing, and lattice constants. For hexagonal structure, $a = b \neq c$ and the angle between edges represented by α, β, γ where $\alpha = \beta = 90^\circ$ while the angle $\gamma = 120^\circ$. 'd' spacing between the planes was calculated by using Bragg's law equation (1) given below

$$2d \sin\theta = n\lambda \quad (1)$$

Where $n=1$ represents the order of reflections, λ is known as the wavelength of X-rays (1.54

θ used, θ is half of the value of angle corresponding to peak position (2θ), by putting all values d spacing between planes can be calculated.

Lattice constants were calculated by using equation (2)

$$\frac{1}{d^2} = \frac{4(h^2 + k^2 + hk)}{3a^2} + \frac{l^2}{c^2} \quad (2)$$

Calculated values are shown in Table (1) for different concentrations of dopant added to the solution Zn doped CdS thin films were found to be closely packed. The calculated c/a ratio ~ 1.42 is found to be very close to the standard value of the ideal hexagonal structure (1.62) on comparing with JCPDS card number 00-006-314. NO additional peak of ZnS or ZnO was observed in Fig. 4.1 which confirms that Zn has occupied some space within the lattice. Thus, it may be responsible for the creation of interstitial or substitutional defects. The formation of these defect states directly influences the optical properties of the compound.

Table 4- B Represents the d -spacing between different Plane orientations for Zn: CdS thinfilms.

Sample Code	d (100) (Å)	d (002) (Å)	d (101) (Å)
6a	3.493	3.294	3.137
6b	3.503	3.279	3.121
6c	3.471	3.277	3.118

Table 4- C Lattice parameter of Zn: CdS thin films

Sample code	c (002)	a (100)	c/a
6a	6.588	4.033	1.632
6b	6.558	4.044	1.621
6c	6.554	4.007	1.633

Table 4- D Represents the 2θ , FWHM, Crystallite size(D), dislocation density(δ)

Samplecode	(h k l)	2θ (Degree)	FWHM (Radian)	Crystallitesize (nm)	Dislocation density (δ)
6a	(002)	27.08	0.0176	8.84	0.0127
6b	(002)	27.02	0.0141	11.11	0.0081
6c	(002)	27.15	0.0198	7.85	0.0162

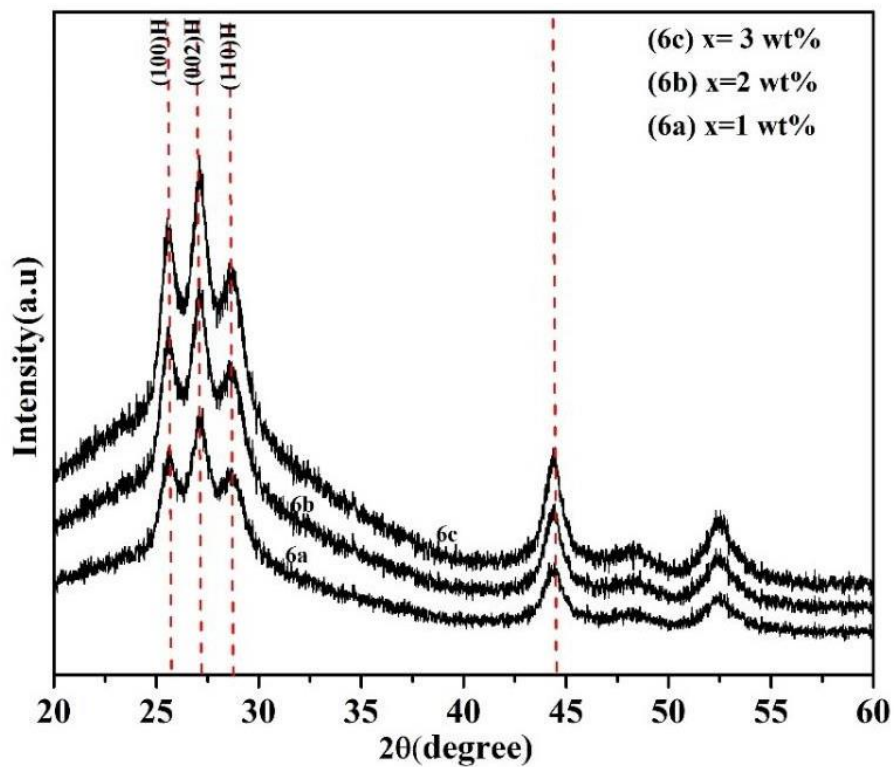


Fig. 4. 1 The above graph represents the X-ray diffractograms of Zn: CdS thin films coded as 6a, 6b and 6c prepared by varying the dopant concentration

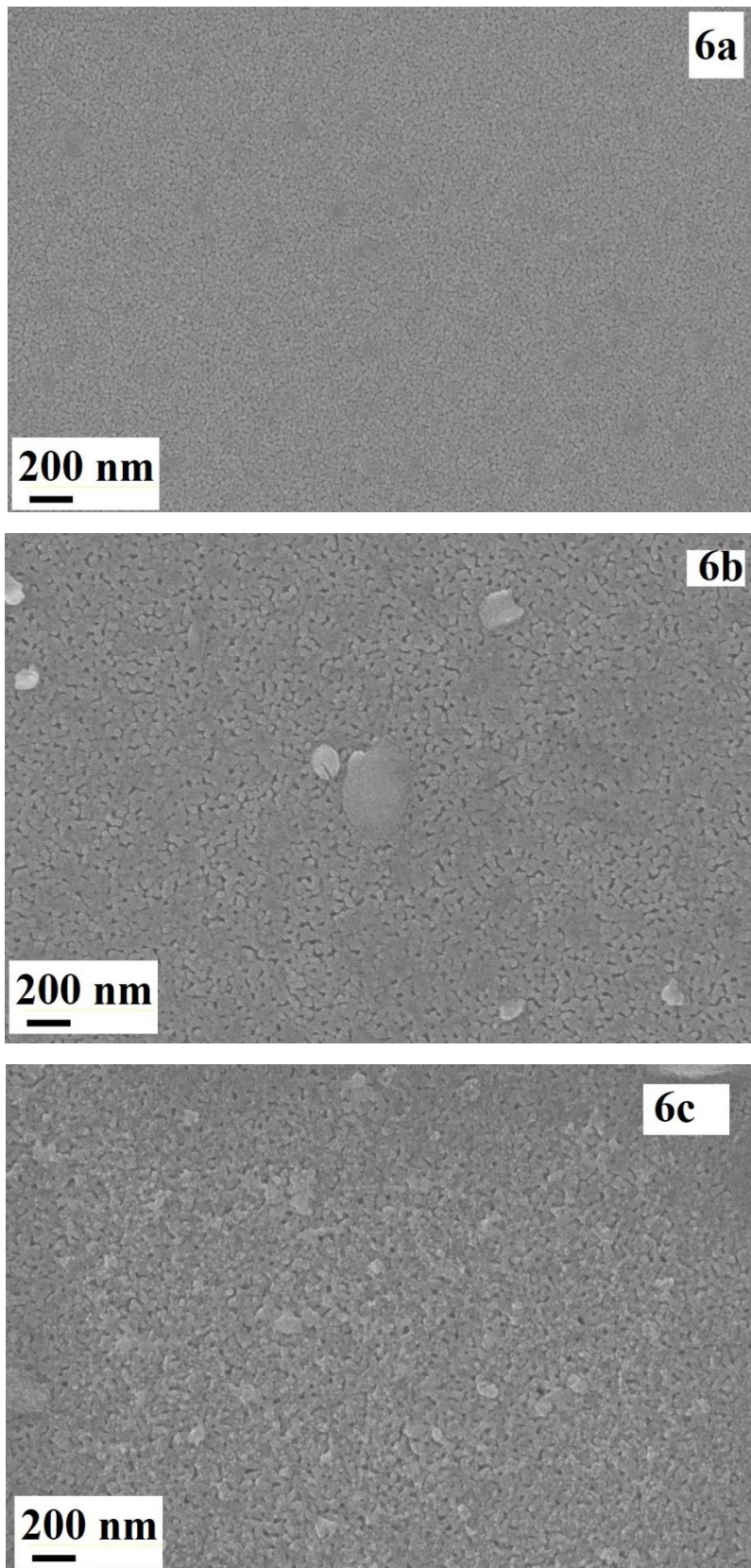


Fig. 4. 2 Represents the Surface micrographs of Zn: CdS thin films prepared with different concentrations(6a) Zn=0.01, (6b) Zn= 0.03 and (6c) Zn= 0.05 of dopant and annealed at 400°C

Optical Properties

Optical studies help us to find out the active region of the active material. Every material which is applicable for photonic devices must have some wavelength range in the electromagnetic spectrum in which it can be optically active (i.e shows some absorption). The linear region where transmittance suddenly falls is known as the absorption region or optical active region of the material. As shown in Fig. 4.3 transmittance of the Zn doped CdS thin films falls around 520 ± 10 nm. The absorption edge has been shifted towards the lower wavelength with an increase in Zn^{+2} ion content. A nice interference pattern in Fig. 5.2 was observed due to the occurrence of constructive interference between reflected light from different layers of the thin films. These interference patterns also confirm the uniformity of the different layers of the prepared thin films. The absorption coefficient of the prepared thin films was calculated by using equation (3)

$$\alpha = \frac{1}{d} \ln\left(\frac{100}{T}\right) \quad (3)$$

Where ‘d’ represents the thickness of thin films and ‘T’ is known as transmittance. The thickness of the thin films was calculated with the help of cross-sectional FESEM. The optical band gap of prepared thin films (coded 7b) was calculated through extrapolation of the linear region of the Tauc plot $(\alpha hv)^n$ vs hv . Where $n=1/2$ for direct band gap. It has been observed that the optical band gap varied from 2.39 eV- 2.41 eV. Non-linear behaviour was observed in the optical band gap of Zn: CdS thin films. The obtained band gap was close to the band gap of CdS bulk. This variation in the optical band gap may be occurred due to the formation of interstitial or substitutional defects formation by Zn^{+2} within the host-lattice. Zn-doped thin film sample code 6b was found to be best suitable for the photodetection application. The increase in Zn^{+2} ion’s concentration also reduces the crystallite size and increases the resistance of prepared thin films [95,96]. The obtained results are good in agreement with the earlier reported literature from other research groups [51]

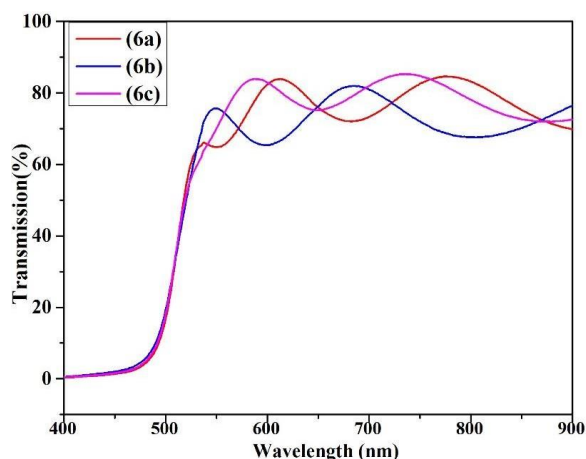


Fig. 4.3 Represents the transmittance of $CdxZn_{1-x}S$ thin films (where 6a, 6b and 6c corresponds to $x=0.01, 0.03, 0.05$)

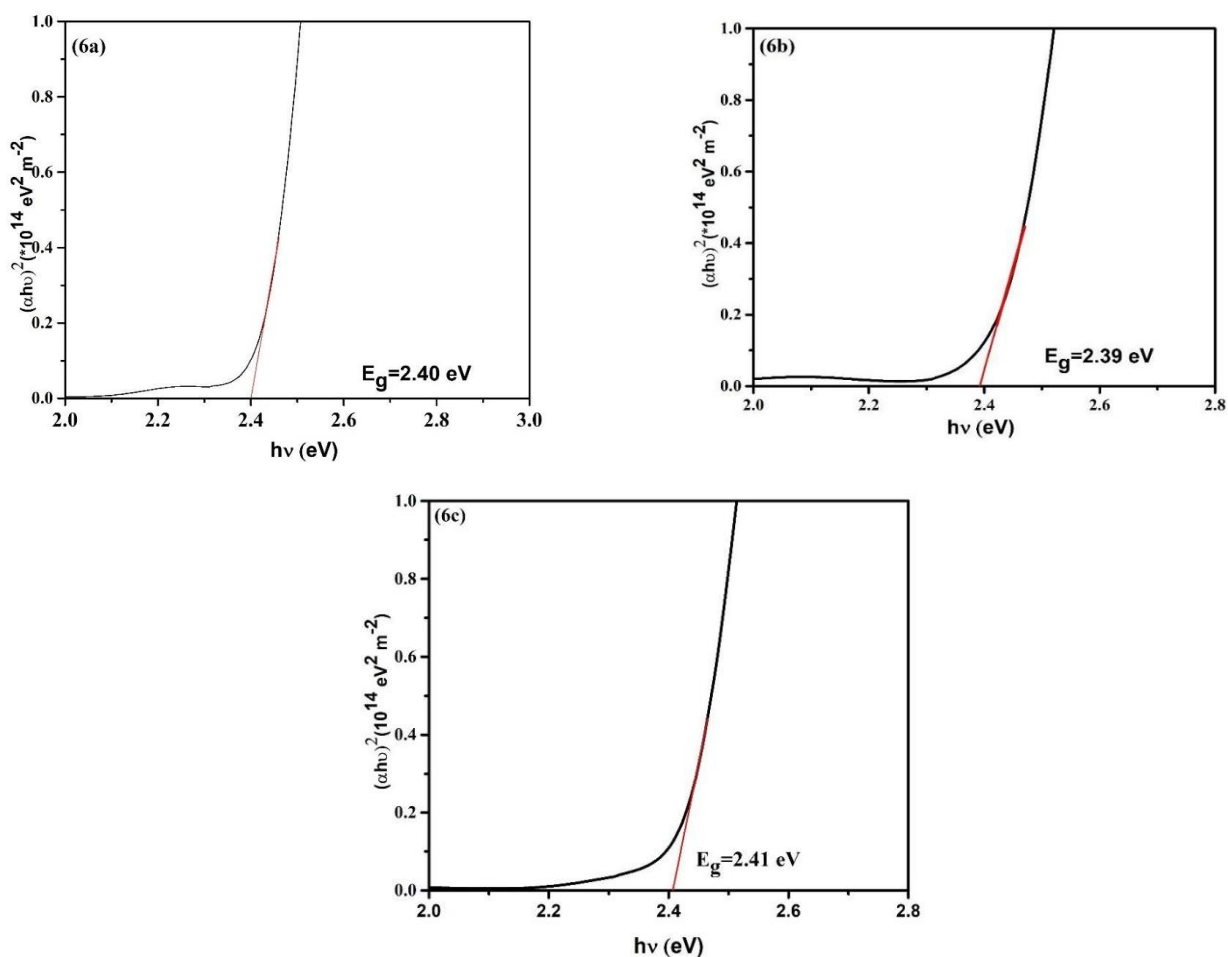
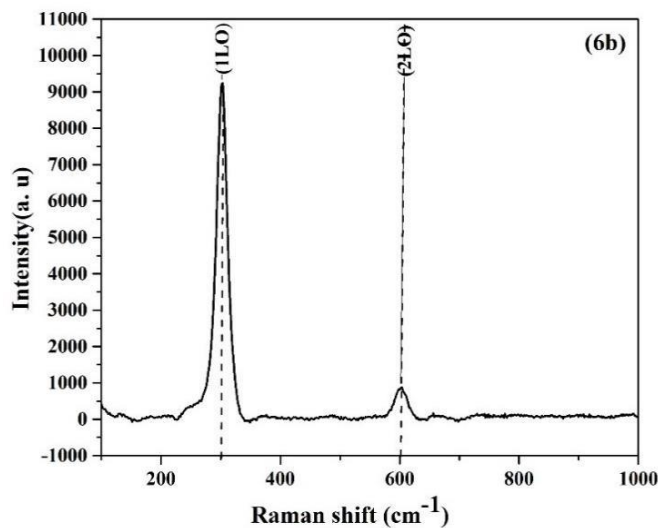
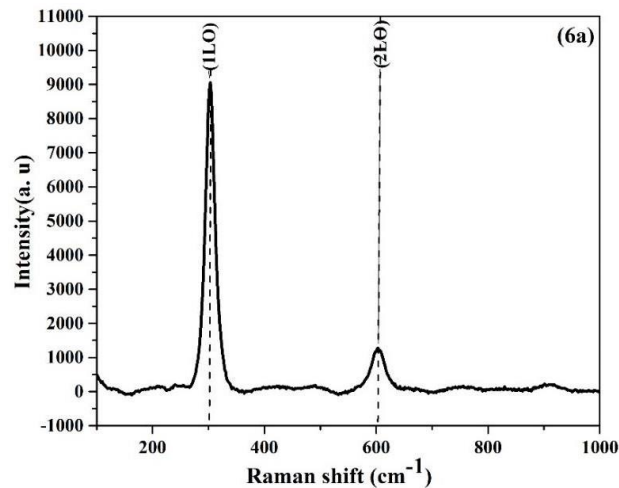


Fig. 4. 4 Optical band gap of $CdxZn_{1-x}S$ (where 6a, 6b and 6c corresponds to $x = 0.01, 0.03, 0.05$) thin films annealed at $400^{\circ}C$

Raman spectroscopy

Raman spectroscopy has been used for the vibrational modes study. Raman spectra shown in Fig.4.5 has been recorded at wavelength 488nm for undoped and Zn-doped CdS thin films. Longitudinal optical phonon modes could be seen at 303 cm^{-1} and 601 cm^{-1} . The observed vibrational modes are known as first order and second order longitudinal optical phonons. No additional peak corresponding to ZnS was observed. This indicates that Zn^{+2} ions occupied some space within the host lattice without creating any distortion. The observed 1LO peak has been shifted towards lower wavenumber side from 303.112 cm^{-1} to 303.059 cm^{-1} which may be due to a change in bond lengths. Peak intensity has been increased for 1% and 2% Zn:CdS thin films while a slight decrease in intensities has been noticed for 3% Zn:CdS thin films. The increase in intensities of Raman peaks confirms the improvement in crystallite size. The obtained results also support the Xrd data. Thus, the noticeable blue shift and slight asymmetrical broadening in peaks may be due to structural disorders or substitutional defect formation due to the addition of dopant [97].



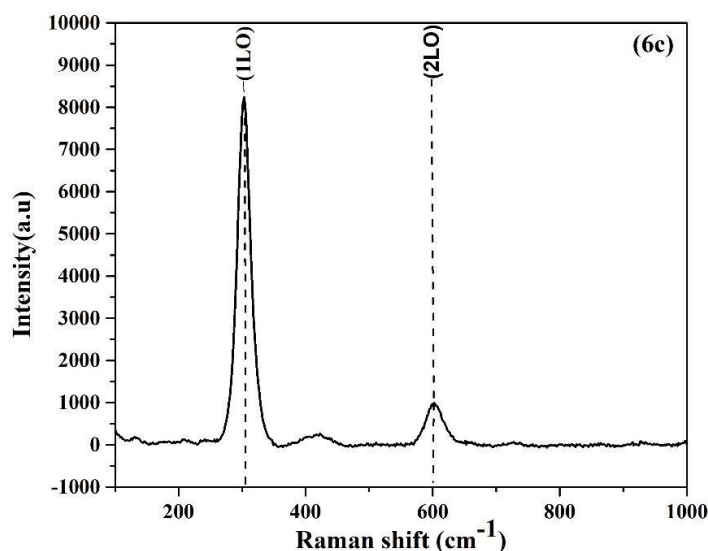


Fig. 4. 5 The above graphs 6a,6b and 6c represents the optical phonon modes of Zn: CdS thin films.

4.2.2 Structural and optical properties of Zn: CdS thin films deposited on flexible substrate

Fig. 4.6 represents the X-ray diffractogram of $Cd_xZn_{1-x}S$ for $x=0.03$ thin films deposited on PET. The best suitable concentration for doping has been optimized through the results obtained for Zn: CdS thin films deposited on SLG (soda lime glass). The diffraction peaks have been observed at 25.80° , 27.24° , 44.44° , and 52.68° . The obtained peaks correspond to (100), (002), (110) and (201) planes confirming the hexagonal phase of thin-films. The obtained peaks were broadened and shifted towards the higher angle side. It may be due to the strain present between the substrate and thin films deposited or within the thin films. The presence of compressive strain was confirmed in prepared thin films through W-H plots (Fig. 4.7). Thus, shrinkage in films took place which might be due to shrinkage in the polymer used. The obtained hexagonal phase is a stable phase of CdS. The crystallite size has been calculated from the Scherrer formula. The average crystallite size calculated for Zn: CdS thin film on PET was 6.10 nm.

The surface micrographs for the sample coded as 7b (deposited on PET) were also recorded. Which helps to analyze the surface morphology of prepared thin film samples. The uniform deposition of thin films over the substrate was observed surface micrographs shown in Fig 4.8. Irregular grain boundaries and cracks were observed for the thin film sample coded as 7b. It may be due the shrinkage of PET substrate. This may also cause the strain in thin films. Reduced

grain size and cracks would also affect the photodetection properties of thin films as free charge carrier would not be able to travel long path length at lower value of potential applied.

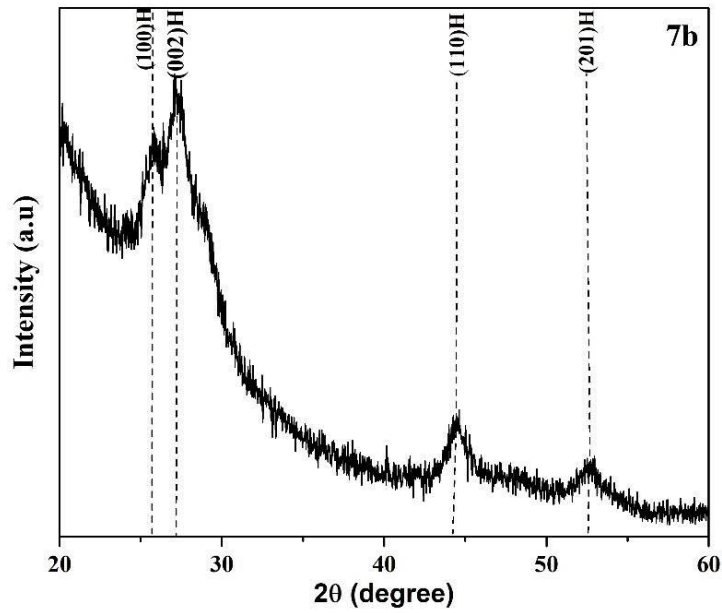


Fig.4. 6 The above graph represents the X-Ray diffraction pattern for $Cd_xZn_{1-x}S$ (where $x=0.03$) thin film deposited on PET

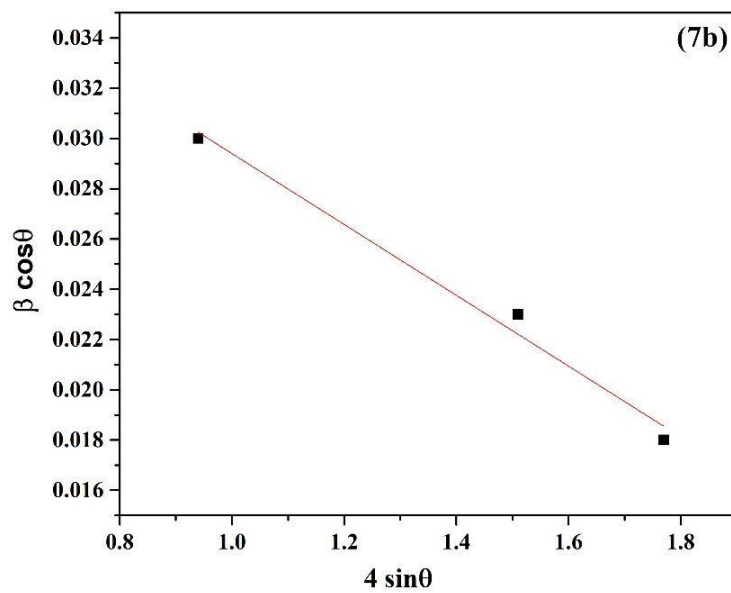


Fig. 4. 7 The above graph represents the W-H plot for thin film sample coded as 7b deposited on PET

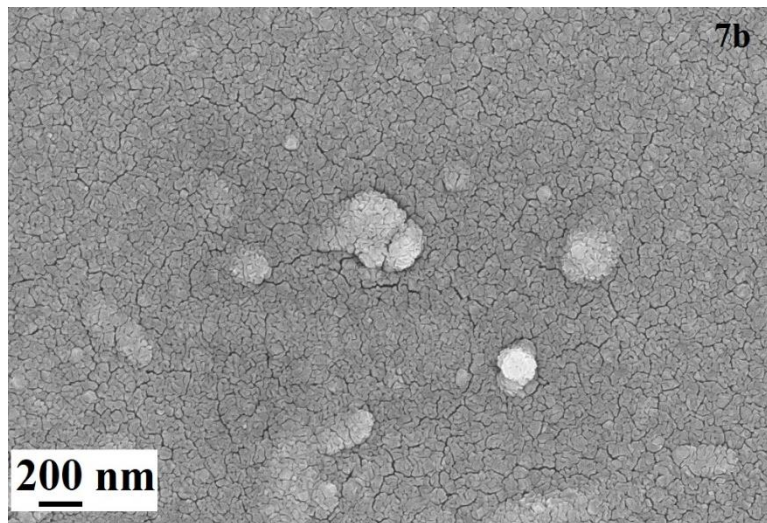


Fig. 4. 8 Represents the Surface micrograph of $Cd_xZn_{1-x}S$ (where $x=0.03$) thin films deposited on PET

Optical study

Fig.4.9 shows the transmittance curve for Zn: CdS thin-films deposited on the PET substrate. Transmittance of curve shows broad interference fringes which are formed due to constructive interference of reflected light through the different layers of the prepared thin films. The obtained transmittance curve shows the 75% of transmittance in visible range of the electromagnetic spectrum and sharp absorption curve could be observed near about 526 ± 5 nm. The absorption coefficient and optical band gap of prepared thin films was calculated by using equation (3) and Tauc equation $E_g = (\alpha h\nu)^{1/2}$. The calculated optical band gap was 2.45 eV (shown in Fig. 4.10). The obtained value of optical band gap was slightly higher than the optical band gap of Zn: CdS thin films deposited on glass substrate. This increase in band gap was due to reduction in crystallite size of prepared thin films and strain introduced due to shrinkage of PET during the annealing. The obtained results were consistent with surface morphology also.

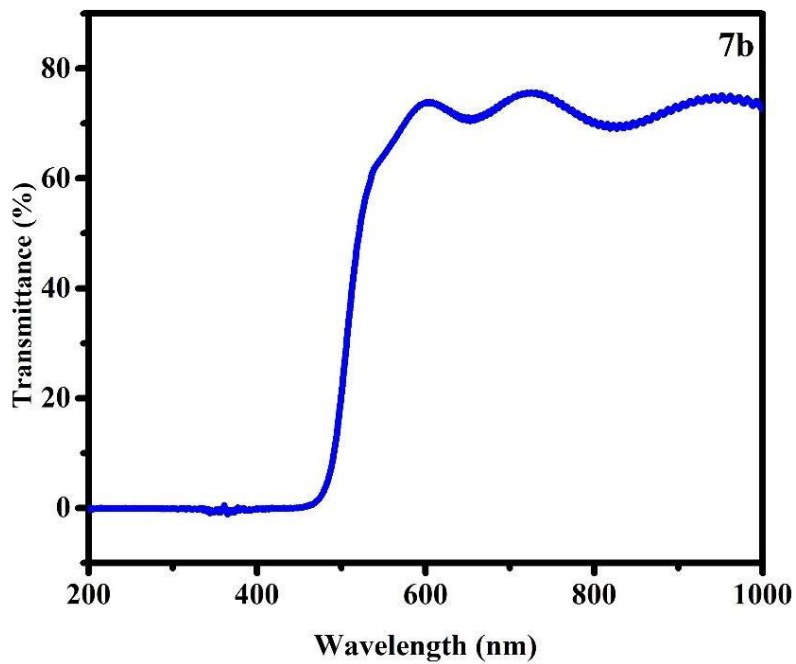


Fig. 4. 9 Represents the transmittance curve for $Cd_xZn_{1-x}S$ (where $x = 0.03$) thin films deposited on PET

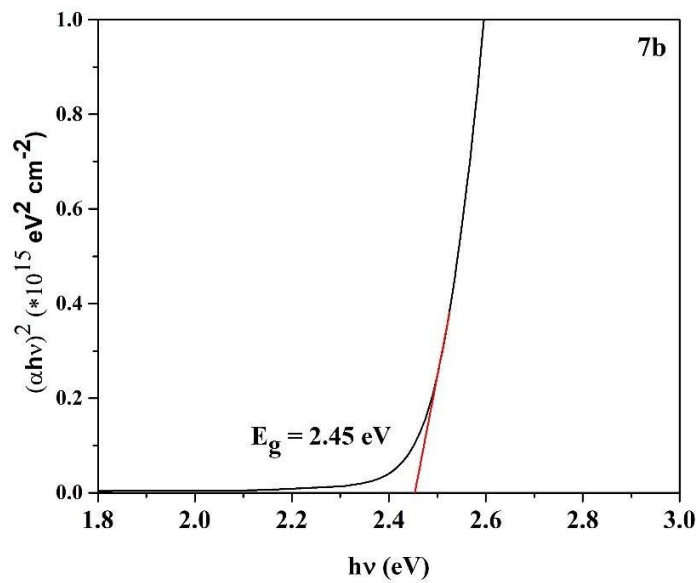


Fig. 4. 10 The above graph represents the Optical band gap of $Cd_xZn_{1-x}S$ (where $x=0.03$) thin films deposited on PET



Chapter-5

*Electrical study and Photoconductivity of CdS
and Zn:CdS thin films*

5.1 *Introduction*

This chapter is based on Electrical study of thin films deposited on glass and PET substrate. The best suitable samples analysed through structural and optical studies were preferred for the electrical study. The I-V properties of undoped thin films on glass substrate were represented in graphs 4a, 4b and 4c. Thin film's samples coded as 4a-4c were annealed at different temperatures 400°C, 450 °C and 500 °C for 60 minutes. I-V properties of Zn: CdS thin films were analyzed to study the effect of dopant concentration on photoconductivity as shown in graphs 6a, 6b and 6c. Dopant concentration was varied from 1%-3%. The molarity and pH level of the prepared solution was kept constant as optimized for undoped CdS thin films. CdS thin-films (undoped) annealed 450 °C has shown maximum electrical conductivity. The photocurrent has been reduced for thin films annealed at 500 °C due to formation of CdO. Thus, the formation of CdO initiated influence the electrical properties of thin films. The formation of CdO was initiated at 450 °C also as shown in *Fig. 3. 2*. Thus, to avoid the formation of oxides doped thin films were annealed at 400 °C for two hours. Long- time annealing also helpful to enhance the structural and electrical properties of prepared thinfilms. Next efforts had been done to synthesise thin films on flexible substrate PET to study their electrical behaviour. Maximum annealing temperature that can be used for PET is 300 °C. The obtained results are discussed in this chapter. Both doped and undoped thin films were prepared with 0.3 molar concentrated solution (pH-10). The variation of current was noticed by varying the applied voltage from -5 V to +5V across the conducting electrodes placed at 200 cm apart.

5.2 *Results and discussion*

The I-V characteristics of prepared CdS and Zn: CdS thin films under illumination and dark conditions shown in Fig. 5.1 -5.3. It has been observed that the current increased rapidly under illumination conditions (white light) for sample 4b (i.e. annealed at 450 °C). The photocurrent was varied from 10^1 - 10^3 nano amperes range for undoped thin films. The maximum current was found to be 1204 nA for the sample 4b. It may be due to reduction of lattice disorders and improvements in crystallite size of the prepared thin films annealed at different temperatures. But the photocurrent reduced for the sample 4c (i.e. annealed at 500 °C), which may be due incorporation of oxygen atoms on the surface of CdS thin film annealed in air. During the annealing at high temperature, the formation of CdO was also observed. This defect state may be introduced within the energy gap region. The formation of a defect state affects the electrical

conductivity as free charge carriers may be trapped within this defect state for a long time. On the other-hand value of dark current (I_d) was found to be very small (as shown in table.5-A) as compared to photocurrent which was 0.02 nA. This small current was due to the absorption of oxygen molecules on the surface of CdS thin film during the annealing in air. Under dark conditions, these oxygen molecules trap the holes and reduce the recombination rate of electrons and holes. Due to this reason small number free charge carrier can avail the conductivity. While under the illumination conditions holes generated neutralize these oxygen ions and the process of desorption followed. This process of absorption of oxygen ions on the surface of thin films was responsible for the small value of dark current [98].

Photocurrent was also enhanced by varying the Zn dopant concentration. Zn: Cds thinfilms prepared with different Zn-concentrations were named as 6a,6b and 6c. The obtained values of photocurrent and dark current are tabulated in table 5 B. Photodetection capability of a device is detected through its photosensitivity and responsivity. The maximum photosensitivity i.e. ratio of photocurrent to dark current was observed for the sample 6b and responsivity was also found very high for the same sample. The value observed for photosensitivity and responsivity was 21400 and 0.13A/W which is also very high as compareto previous reported literature (tabulated in table 5-D).

Fig 5.5- Fig. 5.6 represents the I-V characteristics of thin-films deposited on the flexible (PET) substrate. The prepared thin-films were annealed at 300 °C. The Photocurrent was noticedby using two different light intensities i.e. 0.58 mw/cm⁻² and 4.09 mw/cm⁻². It has been observed that photocurrent enhanced four times as compare to current observed for low intensity. Which confirms that thin films deposited on the flexible substrate were photosensitive. The maximum value of photosensitivity was obtained 1453 for sample 7a which is undoped sample, while for Zn: CdS thin-films on PET sensitivity was decreased to 35.11. The presence of high density of defect states per unit volume might be responsible for this reduction in photocurrent. Annealing at low temperature and presence of oxygen in polymer structure which released in lattice during the annealing may also cause of decrease in photocurrent and low sensitivity of thin films deposited on PET [99,100]. Thus, addition of Zn introduced more lattice defects which drastically reduced the photoconductivity of thin films. Thus, the photodetection properties of thin films deposited on PET substrate can be improved by increasing the annealing-time or increasing the intensity of light used.

5.3 *Photoconductivity*

Reproducibility of prepared thin films of undoped as well as doped were also checked through

photoconductivity. Thin films were illuminated for 30 sec. When light is turned on time taken by the device to increase the current from 10 -90 % is known as its response time and after 30 sec when light gets off time taken by the device to reduce the current from 90-10 % is known as its recovery time. Response time of Zn: CdS thin-films were also reduced 43% as compare to CdS thin films. Fig 5.2, 5.6 and 5.9 represents the photoconductivity of thin films deposited on glass and PET substrate. Minimum response time i.e. 0.68 sec was observed for sample 6b (deposited on glass substrate).

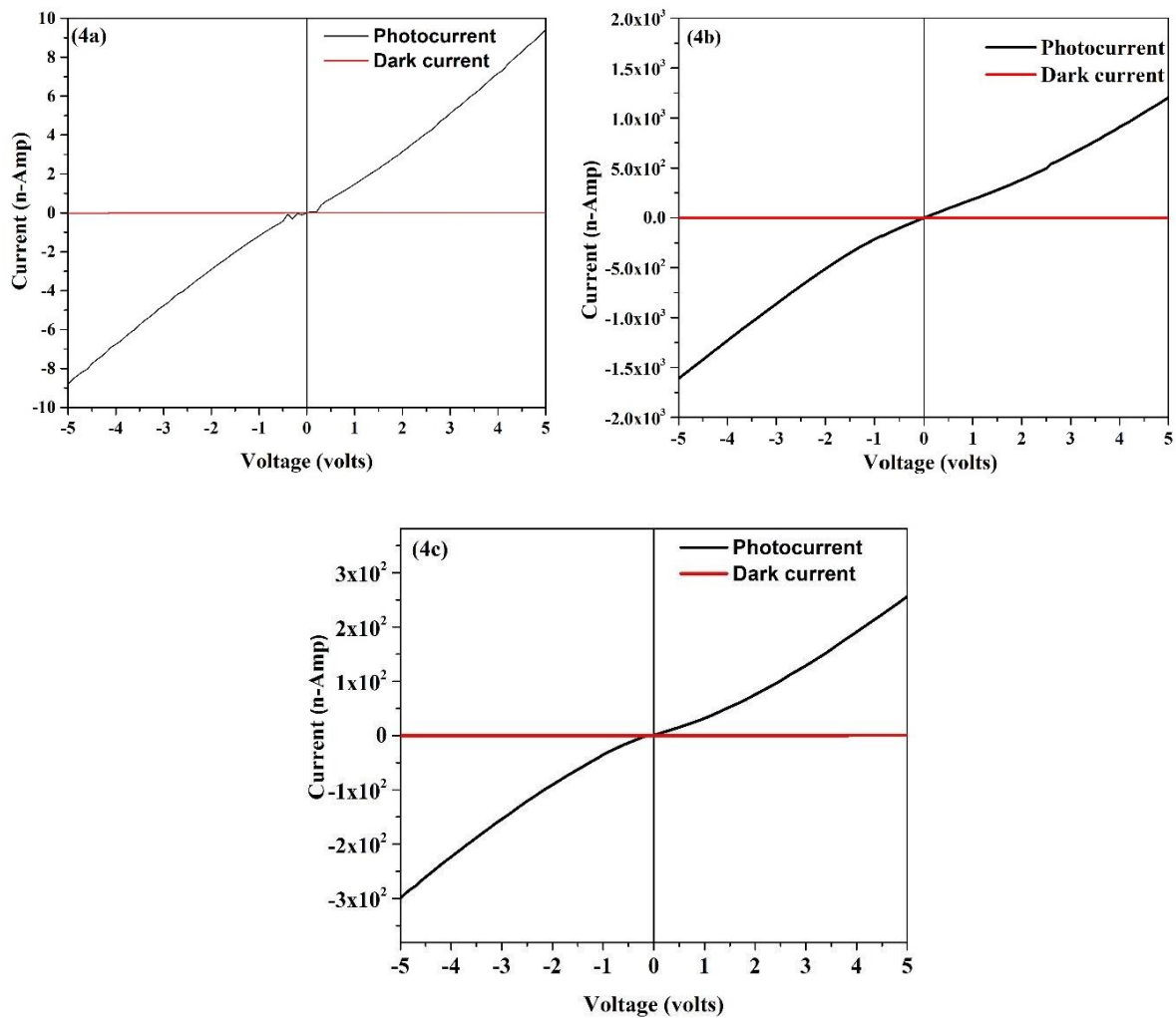


Fig. 5. 1 Represents the I-V characteristics of thin films samples annealed for 60 minutes where (4a) 400°C, (4b) 450 °C and (4c) 500 °C.

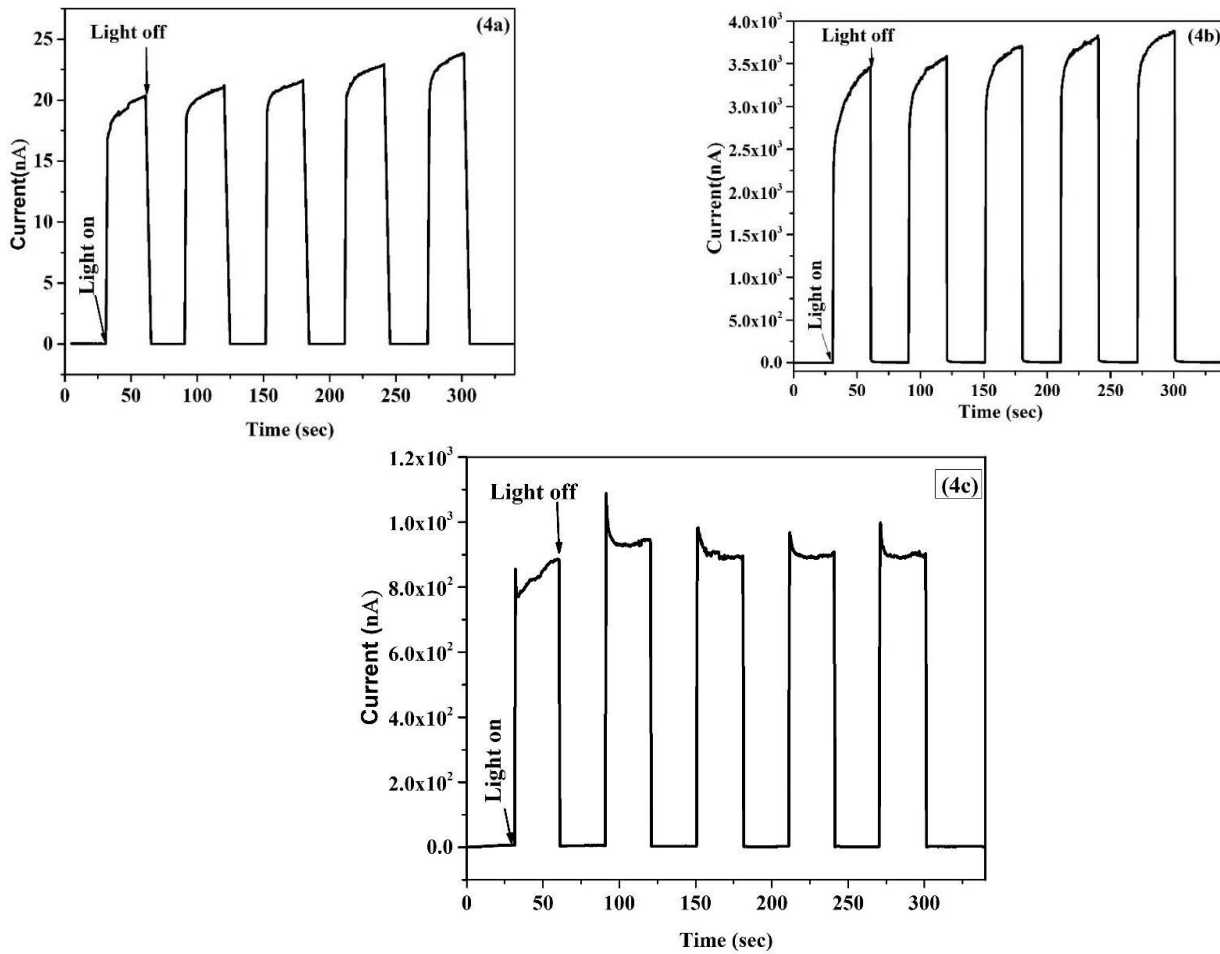


Fig. 5. 2 Represents the Photoconductivity of thin films samples coded as 4a, 4b and 4c annealed at 400 °C, 450 °C and 500 °C.

Table 5- A

Represents the photocurrent, dark current, rise time and decay time for CdS thin -films coded as 4a,4b and 4c

Sample code	Annealing temperature (oC)	Photocurrent (nano-Amp)	Dark current (n-Amp)	Photo-sensitivity (I_{ph}/I_d)	Rise time (sec)	Decay time (sec)
4a	400	9.42	0.02	589	1.20	3.89
4b	450	1204	0.79	1524	1.15	0.24
4c	500	256	0.22	1163	0.36	0.40

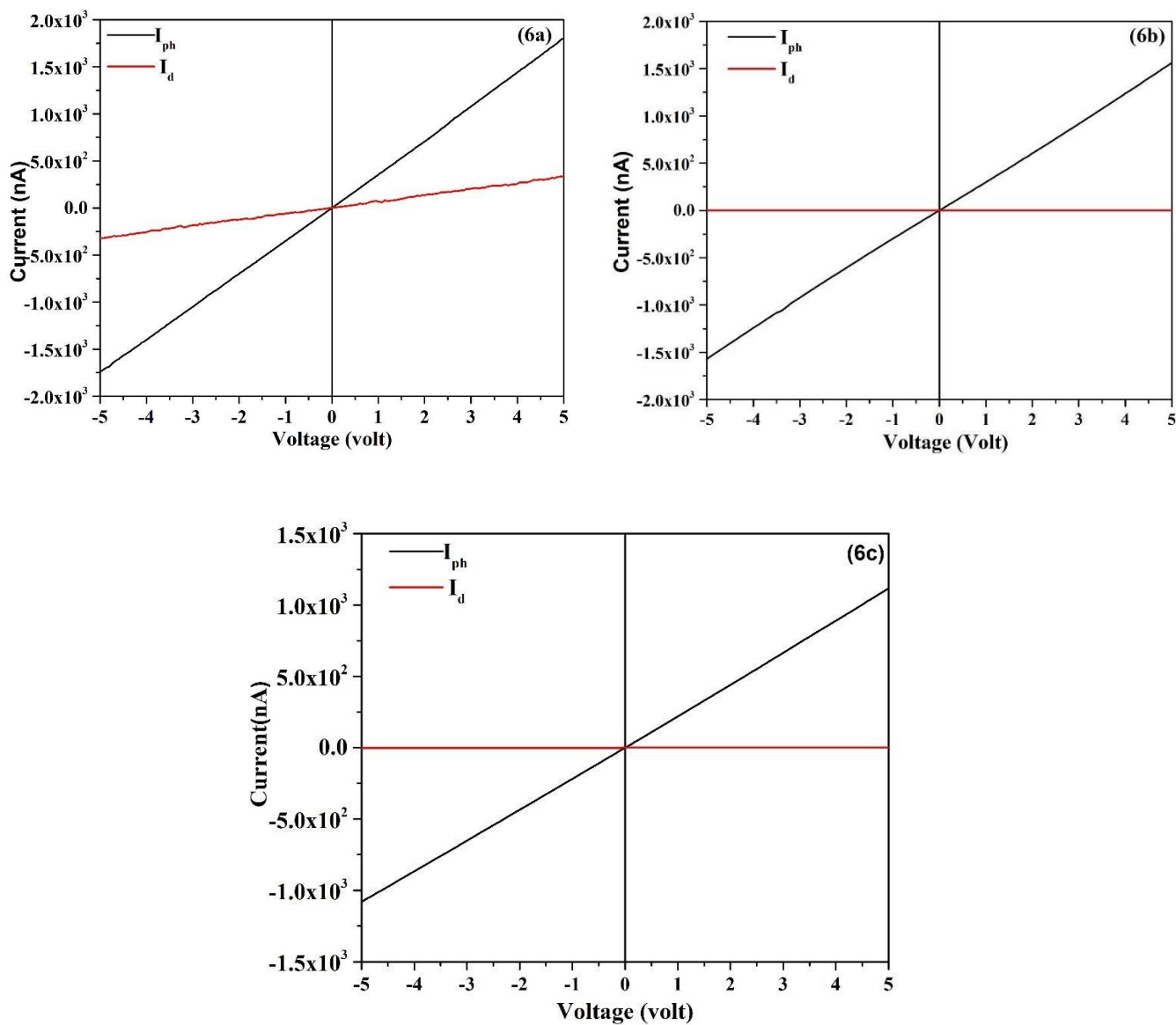


Fig.5. 3 Represents the I-V characteristics of $Cd_xZn_{1-x}S$ where 6a,6b and 6c are the graphs of thin films prepared with different concentration of Zn i.e. $x=0.01,0.03$ and 0.05

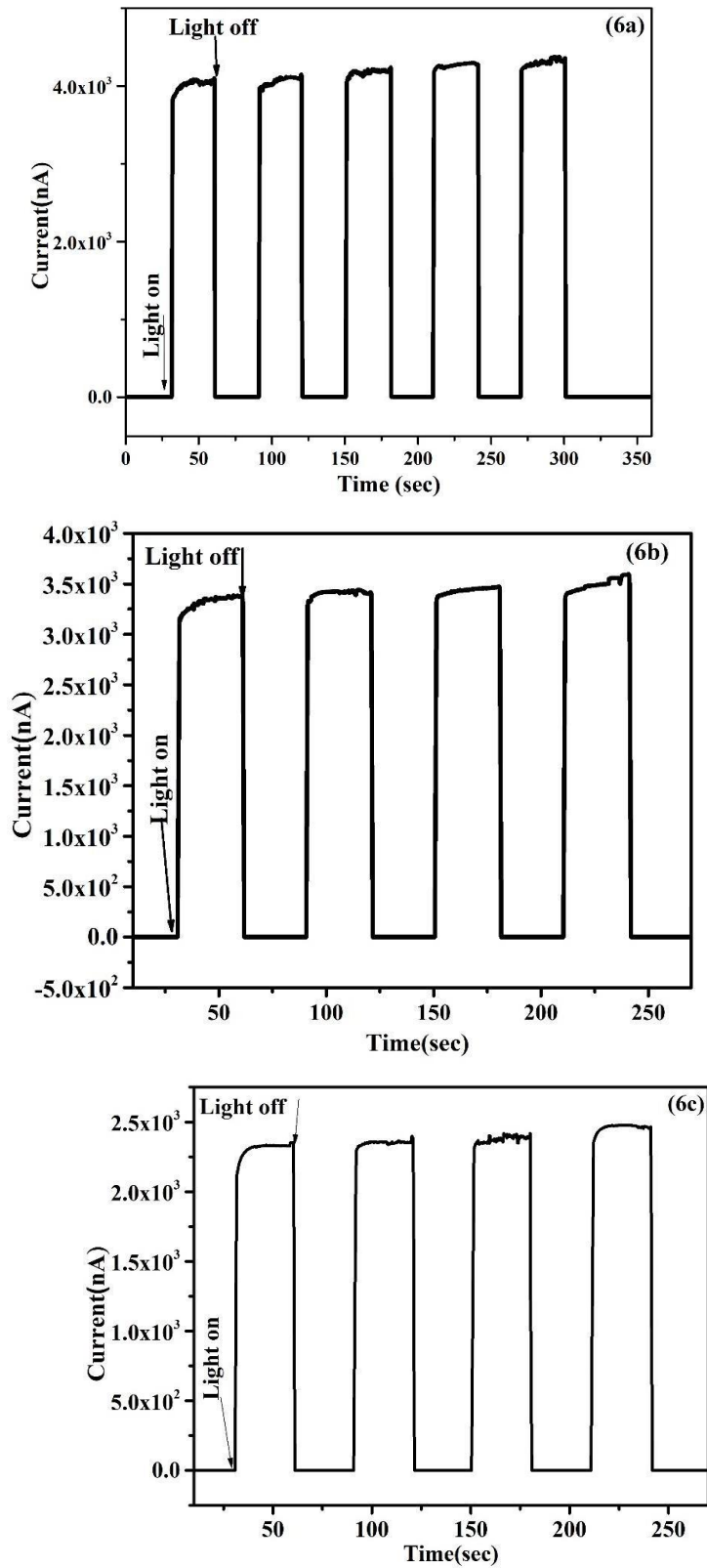


Fig. 5. 4 Represents the Photoconductivity of $Cd_xZn_{1-x}S$ where 6a,6b and 6c are the graphs of thin films prepared by varying concentration of Zn i.e. $x=1\%$, 2% and 3% and prepared thin films were annealed at $400\text{ }^\circ\text{C}$.

Table 5- B

Represents the Photocurrent, dark current, Photosensitivity, Responsivity, response time and recovery time for Zn doped CdS thin films coded as 6a, 6b and 6c.

Sample Name	Photocurrent (nA)	Dark current (nA)	Sensitivity I_{ph}/I_d	Responsivity (A/W)	Response time (sec)	Recovery time (sec)
6a	1806.85	0.328	$5.507 \cdot 10^3$	0.12	0.69	0.48
6b	1562.34	0.073	$2.14 \cdot 10^4$	0.13	0.77	0.68
6c	1117.30	0.170	$6.57 \cdot 10^3$	0.09	1.321	0.68

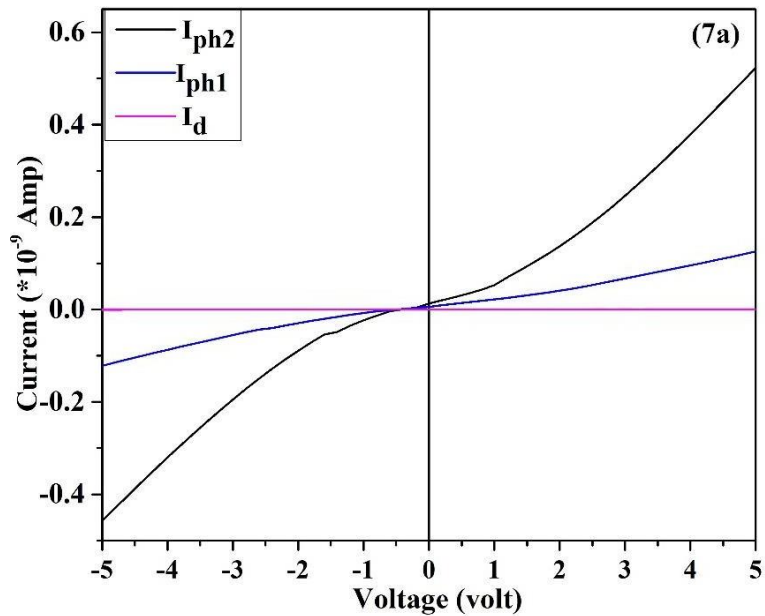


Fig 5. 5 Represents the I-V characteristics of CdS thin films deposited on PET annealed at 300 °C

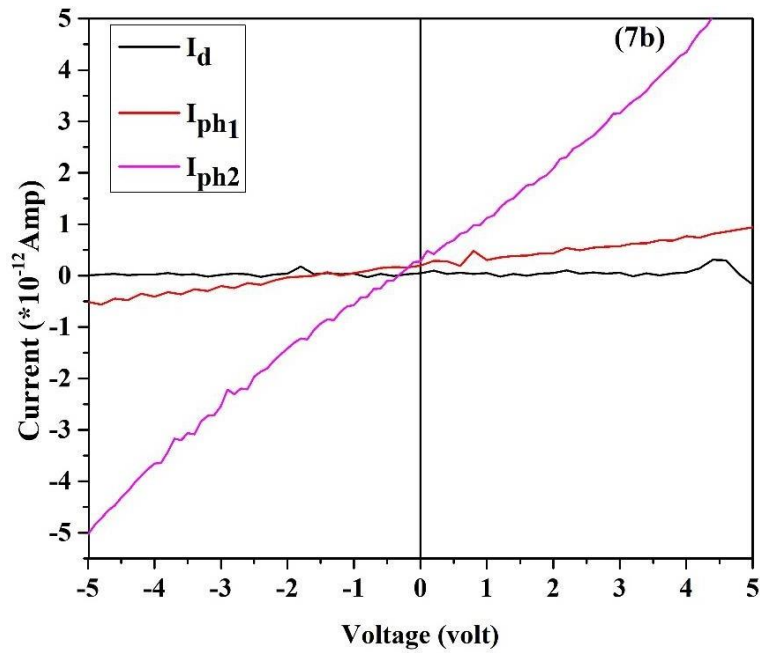


Fig. 5.6 Represents the I-V characteristics of $Cd_xZn_{1-x}S$ ($x=2\%$) thin films deposited on PET.

Table 5- C

Represents the calculated values of Photocurrent, dark current, sensitivity, response time and recovery time for maximum intensity for thin films coded as- 7a and 7b deposited on PET substrate.

SampleName (.PET)	Photocurrent (pA)	Dark current (pA)	Sensitivity I_{ph}/I_d	Response time (sec)	Recoverytime (sec)
7a	523.52	0.36	1453	4	5
7b	5.79	0.17	35.09	3.25	6

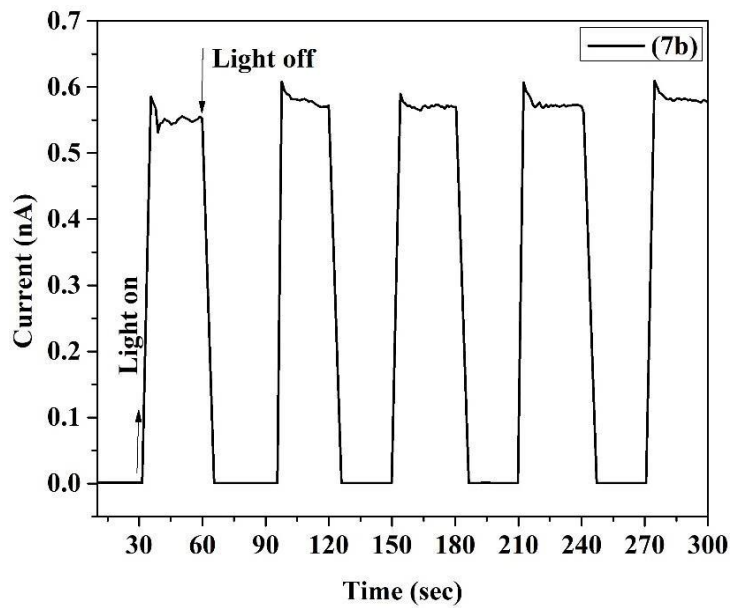
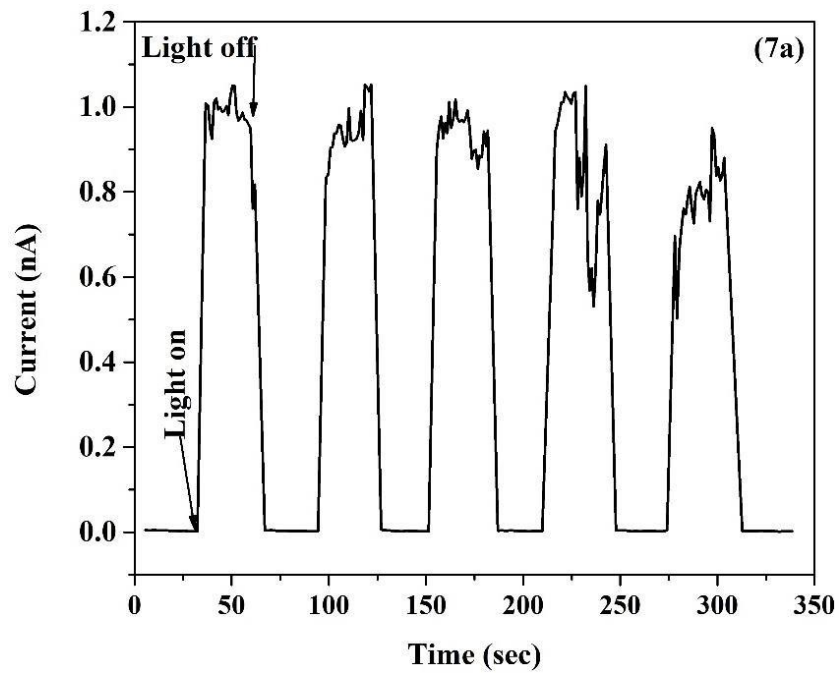


Fig. 5. 7 Represents the Photoconductivity of CdS and Cd_xZn_{1-x}S (where $x=0.03$) thin films on PET substrate.

Table 5- D Represents the Previous work reported

Methodology	Power(Watt)	Sensitivity(%)	Responsivity (A/W)	Risetime (sec)	Falltime	Ref
CBD	200	99.72	-	-	-	[101]
Vacuum Thermal Evaporation	-	222	-	1.81	10.52	[102]
HCBD	32	9.5×10^3	3.48×10^{-3}	1.22	3.46	[103]
SPRAY PYROLYSIS	1.3×10^{-3}	10^6	0.38	1.4×10^{-3}	1.4×10^{-3}	[104]
MCBD	-	5400	0.65	9×10^{-3}	11×10^{-3}	[92]
CBD	-	10^4	0.51	-	-	[83]
MCBD	30	952	0.37	10^{-2}	10^{-2}	[105]
SPRAY PYROLYSIS	-	-	0.37	0.21s	0.24 s	[106]
Sol-gel spin coated	0.011×10^{-3}	2.14×10^6	0.13	0.77	0.68	This work



Chapter-6

Summary and conclusion

6.1 Summary

Annealing temperature and annealing time both parameters were optimized initially. It has been observed that not only annealing temperature, in fact annealing time also an important parameter that need to be controlled to improve structural and optical properties of CdS thin films. Polycrystalline CdS thin films prepared by sol-gel driven spin coating were uniformly deposited with good adherence on the glass substrate. The transmission of the annealed CdS thin films is more than 60 % in the visible range. The direct optical band gap decreased from 2.44 -2.38 eV. Raman spectroscopy and XRD measurements show the wurtzite phase of CdS. The crystalline quality of CdS thin films is improved with rise in temperature and annealing time as well. But annealing for longer times and at higher temperatures lead to the formation of CdO phase in the CdS thin films. The formation of CdO phase can be minimized by controlled thermal treatment in the air ambiance. As a result, we could see agglomeration in FESEM at 500 °C (90 minutes) and larger grain size creates the voids in the lattice which also degrade the optical properties of CdS thin films.

The formation of Cadmium oxide was controlled by increasing the pH level of the synthesized solution (pH-10). Thin films with improved structural and optical properties could be obtained through annealing at 400 °C, 450 °C and 500 °C for 60 minutes. Wurtzite phased CdS thin films corresponding to (100), (002), and (110) planes, were synthesized. Annealing of prepared CdS thin films affected the structural, optical, and electrical properties of prepared thin films. Crystallite size improved gradually and reduced the strain as well. The crystallite size varied in the range of 12.1 nm - 39.3 nm. It was noticed that the optical band gap and photocurrent decreased to 2.41 eV and 0.25 μ A in the high-temperature range of 500 °C. It was due to defect (CdO) formation. From the results obtained, it can be concluded that CdS thin films are suitable to work as photosensor in the visible range of spectra and their photoelectrical properties can be enhanced further by adding a suitable impurity.

CdS thin films prepared with 0.3 Molar concentrated solution was found to be better than as compare to 0.2 M and 0.4 M concentrated solution. The vibrational modes in Raman spectra and the values of 2θ obtained from XRD confirms the formation of wurtzite CdS. The optical band gap was varied from 2.41-2.43 eV. Morphological study shows the spherical shaped crystallite formation and agglomeration has been observed with rise in precursor concentrations (0.3 M and 0.4 M). First and second order LO phonon modes found at 303 cm^{-1} and 602 cm^{-1} . The increases in intensity of higher order overtones (2LO) in Raman spectra confirms the increase in crystallite size as could be seen for 0.3M annealed CdS thin films but decrease in

Raman peak intensity seen for 0.4M annealed CdS thin films which may be due to lattice distortion or defect state which was confirmed from increased FWHM (0.00927 radian). The crystallite size calculated from Debye Scherrer formula lie in the range 19.76- 34.61 nm. It has been observed that thin films prepared with 0.3 M solution has the maximum crystallite size 34.61 nm and also have less value of Urbach energy ~84.6 meV. Furthermore, it can be concluded that variation in precursor's concentration is crucial parameter that affects the thickness, lattice disorders, optical energy gap, grain size of the thin films prepared. From the obtained electrical results, it could be concluded that CdS thin films synthesized with 0.3M concentrated solution is best suitable candidate for photodetector applications in visible range of electromagnetic spectrum.

For the further enhancement in optoelectronic properties Zn:CdS thin films were synthesised. Thin films were prepared with different concentration of Zn content added. The incorporation of Zn has reduced the disorder by occupying some vacant or interstitial sites within the lattice. Lattice shrinkage was also observed. Optical band gap varied from 2.431 eV to 2.447 which was also very close to optical band gap of bulk CdS. Photodetection properties of the Zn:CdS thin films were found to be improved. Photocurrent has been increased in Zn doped CdS thin films as compare to CdS thin films. Responsivity is found to be maximum 0.13 A/W for Zn doped CdS thin films sample coded as 6b. The obtained results showed that addition of Zn as dopant was helpful to improve the photoconductivity of prepared thin films which makes it suitable photonic devices.

To enhance the application of CdS and Zn:CdS thin films were also synthesised at Polythene terephthalate (PET) substrate. Structural optical and electrical properties were studied. The optical band gap of CdS and Zn: CdS (Zn =0.03) thin films were 2.44 and 2.45 eV. The diffraction peaks obtained in Xrd and Raman spectroscopy confirmed the hexagonal phase of prepared thin films. In Xrd broad dominant peak corresponding to (002) plane was obtained. The crystallite size was in the range of nano- meters. Electrical properties of CdS thin films deposited on PET was comparable with thin films deposited on the glass substrate. Unfortunately, the photoconductivity of Zn: CdS thin films synthesised on PET were drastically reduced. The photoconductivity of Zn doped thin films might be reduced due to the presence compressive strain. The shrinkage of PET substrate might be the cause of this strain. FESEM results confirmed the uniform deposition of the thin films over the substrate.

6.2 Conclusion

Highly sensitive and reproducible CdS and Zn: CdS thin films could be synthesised in this

journey of more than 3 years. Thin films were synthesised through simple sol-gel spin coating methodology. The cost for the fabrication of thin films was very low and no special conditions were required through the synthesis process. The whole work was done at the room temperature. The obtained results were improved as compare to previous reported literature. From the work presented here it could be concluded that structural, optical and electrical properties of CdS thin films could be improved by increasing the pH level of the solution, molarity and through the controlled annealing. Maintaining the pH level means controlling the reaction rate. Thus, by increasing the reaction rate we can reduce the structural defects and electrical properties can also be enhanced at the low temperature. In this way, we could also avoid the formation of Cadmium-oxide impurity phase which reduced the various properties of prepared CdS thin films. Further addition of dopant was helpful to improve photodetection abilities of the prepared Zn: CdS thin films. The effect of substrate was also studied. Thin films deposited on PET could also be used for optoelectronic devices. But as the shrinkage of PET and annealing at low temperature both parameters were found to be responsible for reducing optoelectronic properties of the Zn:CdS thin films. As we could see that structural quality of thin films improved at high temperatures for thin deposited on the glass substrate.

6.3 Future scope

As our thin film elements have shown good photo-sensing characteristics both on glass and PET substrate. So, more research investigations are required in future for the thin films deposited on flexible substrate such as PET. These thin films element might be used for the industrial purposes and in fiber optic communication. Also, the structural, optical and photo-sensing properties can be enhanced by using various type of dopants.

References

- [1] W.A. Chee, Introductory Chapter: Photodetectors, (2018) 3–8. <https://doi.org/10.5772/intechopen.82045>.
- [2] W.W. Gärtner, Depletion-layer photoeffects in semiconductors, *Phys. Rev.* 116 (1959) 84–87. <https://doi.org/10.1103/PhysRev.116.84>.
- [3] R.P. Riesz, High speed semiconductor photodiodes, *Rev. Sci. Instrum.* 33 (1962) 994–998. <https://doi.org/10.1063/1.1718049>.
- [4] L.R. Canfield, 6. Photodiode Detectors, in: *Exp. Methods Phys. Sci.*, Elsevier, 1998: pp. 117–138.
- [5] X. Wei, F.-G. Yan, C. Shen, Q.-S. Lv, K.-Y. Wang, Photodetectors based on junctions of two-dimensional transition metal dichalcogenides, *Chinese Phys. B.* 26 (2017) 38504.
- [6] J. Jose, A. Ravindran, K.K. Nair, A Review On ZnO Hetrojunction Photodetector For UV Application, *ICTACT J. Microelectron.* 2 (2017) 300–304.
- [7] K.H. Park, K. Jang, S.U. Son, Synthesis, optical properties, and self-assembly of ultrathin hexagonal In₂S₃ nanoplates, *Angew. Chemie - Int. Ed.* 45 (2006) 4608–4612. <https://doi.org/10.1002/anie.200601031>.
- [8] F. González-Posada, R. Songmuang, M. Den Hertog, E. Monroy, Room-temperature photodetection dynamics of single GaN nanowires, *Nano Lett.* 12 (2012) 172–176. <https://doi.org/10.1021/nl2032684>.
- [9] Z. Wang, M. Safdar, C. Jiang, J. He, High-performance UV-visible-NIR broad spectral photodetectors based on one-dimensional In₂Te₃ nanostructures, *Nano Lett.* 12 (2012) 4715–4721. <https://doi.org/10.1021/nl302142g>.
- [10] J. Svensson, N. Anttu, N. Vainorius, B.M. Borg, L.E. Wernersson, Diameter-dependent photocurrent in InAsSb nanowire infrared photodetectors, *Nano Lett.* 13 (2013) 1380–1385. <https://doi.org/10.1021/nl303751d>.

- [11] Y. Li, H. Wei, H. Wang, H. Tang, Voltammetric analysis of single nanobubble formation on Ag and Ag@MoS₂ nanoelectrodes, *J. Phys. Chem. C* 125 (2021) 3073–3080. <https://doi.org/10.1021/acs.jpcc.0c10928>.
- [12] L. Jia, W. Zheng, *PhotoniX Vacuum-ultraviolet photodetectors*, (2020) 1–25.
- [13] F.P. García De Arquer, A. Armin, P. Meredith, E.H. Sargent, Solution-processed semiconductors for next-generation photodetectors, *Nat. Rev. Mater.* 2 (2017) 1–16. <https://doi.org/10.1038/natrevmats.2016.100>.
- [14] J. Hu, Y. Shi, Z. Zhang, R. Zhi, S. Yang, B. Zou, Recent progress of infrared photodetectors based on lead chalcogenide colloidal quantum dots, *Chinese Phys. B* 28 (2019). <https://doi.org/10.1088/1674-1056/28/2/020701>.
- [15] D. Zheng, H. Fang, M. Long, F. Wu, P. Wang, F. Gong, X. Wu, J.C. Ho, L. Liao, W. Hu, High-Performance Near-Infrared Photodetectors Based on p-Type SnX (X = S, Se) Nanowires Grown via Chemical Vapor Deposition, *ACS Nano* 12 (2018) 7239–7245. <https://doi.org/10.1021/acsnano.8b03291>.
- [16] M.R. Gao, Y.F. Xu, J. Jiang, S.H. Yu, Nanostructured metal chalcogenides: Synthesis, modification, and applications in energy conversion and storage devices, *Chem. Soc. Rev.* 42 (2013) 2986–3017. <https://doi.org/10.1039/c2cs35310e>.
- [17] T. Zhai, X. Fang, L. Li, Y. Bando, D. Golberg, One-dimensional CdS nanostructures: Synthesis, properties, and applications, *Nanoscale* 2 (2010) 168–187. <https://doi.org/10.1039/b9nr00415g>.
- [18] X. Fang, T. Zhai, U.K. Gautam, L. Li, L. Wu, Y. Bando, D. Golberg, ZnS nanostructures: From synthesis to applications, *Prog. Mater. Sci.* 56 (2011) 175–287. <https://doi.org/10.1016/j.pmatsci.2010.10.001>.
- [19] Y. Zhang, J. Cai, T. Ji, Q. Wu, Y. Xu, X. Wang, T. Sun, L. Yang, Z. Hu, Superionic conductor-mediated growth of ternary ZnCdS nanorods over a

- wide composition range, *Nano Res.* 8 (2015) 584–591. <https://doi.org/10.1007/s12274-015-0708-z>.
- [20] C.H. Lai, M.Y. Lu, L.J. Chen, Metal sulfide nanostructures: Synthesis, properties and applications in energy conversion and storage, *J. Mater. Chem.* 22 (2012) 19–30. <https://doi.org/10.1039/c1jm13879k>.
- [21] T. Sinha, L. Verma, A. Khare, Variations in photovoltaic parameters of CdTe/CdS thin film solar cells by changing the substrate for the deposition of CdS window layer, *Appl. Phys. A Mater. Sci. Process.* 126 (2020) 1–14. <https://doi.org/10.1007/s00339-020-04058-4>.
- [22] Y. Yusoff, P. Chelvanathan, Q. Huda, M. Akhtaruzzaman, M.M. Alam, Z.A. Al-Othman, N. Amin, High quality CdS thin film growth by avoiding anomalies in chemical bath deposition for large area thin film solar cell application, *J. Nanosci. Nanotechnol.* 15 (2015) 9240–9245. <https://doi.org/10.1166/jnn.2015.11414>.
- [23] A. Owens, *Semiconductor materials and radiation detection*, (2005) 143–150. <https://doi.org/10.1107/S0909049505033339>.
- [24] I.P. Korneva, K.P. Kornev, M. Ostafin, B. Nogaj, Photodetectors based on heterojunctions of metal - Chalcogenide vitreous semiconductors, *J. Optoelectron. Adv. Mater.* 8 (2006) 808–810.
- [25] C. Scales, P. Berini, S. Member, Thin-Film Schottky Barrier Photodetector Models, *IEEE J. Quantum Electron.* 46 (2010) 633–643. <https://doi.org/10.1109/JQE.2010.2046720>.
- [26] R. Frank, *Structural Analysis, A Companion to Cogn. Sci.* 2 (2008) 450–462. <https://doi.org/10.1002/9781405164535.ch35>.
- [27] L. Saravanan, A. Pandurangan, R. Jayavel, Synthesis and luminescence enhancement of Cerium doped CdS nanoparticles, *Mater. Lett.* 66 (2012) 343–345. <http://dx.doi.org/10.1016/j.matlet.2011.09.006>.
- [28] N.S. Roshima, S.S. Kumar, A.U. Maheswari, M. Sivakumar, Study on vacancy related defects of CdS nanoparticles by heat treatment, *J. Nano*

- Res. 18–19 (2012) 53–61.
<https://doi.org/10.4028/www.scientific.net/JNanoR.18-19.53>.
- [29] B.Y. Zhang, T. Liu, B. Meng, X. Li, G. Liang, X. Hu, Q.J. Wang, Broadband high photoresponse from pure monolayer graphene photodetector, *Nat. Commun.* 4 (2013) 1–11.
<https://doi.org/10.1038/ncomms2830>.
- [30] M. Tan, C. Hu, Y. Lan, J. Khan, H. Deng, X. Yang, P. Wang, X. Yu, J. Lai, H. Song, 2D Lead Dihalides for High-Performance Ultraviolet Photodetectors and their Detection Mechanism, 1702024 (2017) 1–8.
- [31] M.A. Alvi, Z.H. Khan, Synthesis and characterization of nanoparticle thin films of $a-(\text{PbSe})_{100-x}\text{Cdx}$ lead chalcogenides, *Nanoscale Res. Lett.* 8 (2013) 1–10. <https://doi.org/10.1186/1556-276x-8-148>.
- [32] W. Zhou, Y. Peng, Y. Yin, Y. Zhou, Y. Zhang, D. Tang, Broad spectral response photodetector based on individual tin-doped CdS nanowire, *AIP Adv.* 4 (2014). <https://doi.org/10.1063/1.4897521>.
- [33] M. Muthusamy, S. Muthukumaran, M. Ashokkumar, Composition dependent optical, structural and photoluminescence behaviour of CdS:Al thin films by chemical bath deposition method, *Ceram. Int.* 40 (2014) 10657–10666. <https://doi.org/10.1016/j.ceramint.2014.03.050>.
- [34] M. Husham, Z. Hassan, A.M. Selman, Synthesis and characterization of nanocrystalline CdS thin films for highly photosensitive self-powered photodetector, *EPJ Appl. Phys.* 74 (2016) 1–8.
<https://doi.org/10.1051/epjap/2016150414>.
- [35] S.G. Pandya, PREPARATION AND CHARACTERIZATION OF CADMIUM SULPHIDE Available Online at <http://www.recentscientific.com> PREPARATION AND CHARACTERIZATION OF CADMIUM SULPHIDE NANOCRYSTALLINE THIN FILM GROWN BY CHEMICAL METHOD, *Int. J. Recent Sci. Res.* 7 (2016) 14887–14890.

- [36] W. Zhao, L. Liu, M. Xu, X. Wang, T. Zhang, Y. Wang, Z. Zhang, S. Qin, Z. Liu, Single CdS Nanorod for High Responsivity UV–Visible Photodetector, *Adv. Opt. Mater.* 5 (2017) 1–7. <https://doi.org/10.1002/adom.201700159>.
- [37] J. Suganthi, M. Elangovan, S. Johnsonjeyakumar, Preparation And Characterization Study Of Cadmium Sulphide Doped Zinc Thin Films By Thermal Evaporation Technique, *Int. J. Mater. Sci.* 12 (2017).
- [38] T. Bishop, M. Lutheran, S.E. Microscope, Preparation And characterization Study Of Cadmium Sulphide, 12 (2017) 1–12.
- [39] Z. Makhdoumi-Kakhaki, A.A. Youzbashi, P. Sangpour, N. Naderi, The comparison of optical and photodetector properties of Zn, Al and Sn doped and undoped CdS thin films via chemical bath deposition, *J. Mater. Sci. Mater. Electron.* 28 (2017) 13727–13739. <https://doi.org/10.1007/s10854-017-7217-7>.
- [40] X. Wang, C. Liu, C. Wang, Preparation and Photoluminescence Properties of RE-Doped GaN Film by Sol-Gel Method, 680 (2016) 515–519. <https://doi.org/10.4028/www.scientific.net/KEM.680.515>.
- [41] C.Y. Fong, S.S. Ng, N.F. Mohd Amin, F.K. Yam, Z. Hassan, Sol-gel-derived gallium nitride thin films for ultraviolet photodetection, *Microelectron. Int.* 36 (2019) 8–13. <https://doi.org/10.1108/MI-12-2017-0074>.
- [42] J. Wang, Y. Chang, L. Huang, K. Jin, W. Tian, Designing CdS / Se heterojunction as high-performance self-powered UV-visible broadband photodetector Designing CdS / Se heterojunction as high-performance self-powered UV-visible broadband photodetector, 076106 (2018). <https://doi.org/10.1063/1.5042549>.
- [43] Z. Lou, G. Shen, Flexible Photodetectors Based on 1D Inorganic Nanostructures, (2016) 1–19. <https://doi.org/10.1002/advs.201500287>.
- [44] D.J. Late, A. Bhat, C.S. Rout, Photo Sensor Based on 2D Materials, in:

- Fundam. Sens. Appl. 2D Mater., Elsevier, 2019: pp. 465–479.
<https://doi.org/10.1016/B978-0-08-102577-2.00013-0>.
- [45] P. Wang, Q. Bao, W. Hu, Infrared photodetectors, in: 2D Mater. Photonic Optoelectron. Appl., Elsevier, 2019: pp. 105–115.
<https://doi.org/10.1016/B978-0-08-102637-3.00004-8>.
- [46] S. Yip, L. Shen, J.C. Ho, Recent advances in flexible photodetectors based on 1D nanostructures Recent advances in flexible photodetectors based on 1D nanostructures, (2019). <https://doi.org/10.1088/1674-4926/40/11/111602>.
- [47] N.I. Najm, H.K. Hassun, B.K.H. Al-Maiyaly, B.H. Hussein, A.H. Shaban, Highly selective CdS:Ag heterojunction for photodetector applications, AIP Conf. Proc. 2123 (2019). <https://doi.org/10.1063/1.5116958>.
- [48] P. Roy, S.K. Srivastava, A new approach towards the growth of cadmium sulphide thin film by CBD method and its characterization, Mater. Chem. Phys. 95 (2006) 235–241.
<https://doi.org/10.1016/j.matchemphys.2005.06.010>.
- [49] N.T. Shelke, S.C. Karle, B.R. Karche, Photoresponse properties of CdSe thin film photodetector, J. Mater. Sci. Mater. Electron. 31 (2020) 15061–15069. <https://doi.org/10.1007/s10854-020-04069-0>.
- [50] S.R. Gosavi, C.P. Nikam, A.R. Shelke, A.M. Patil, S.W. Ryu, J.S. Bhat, N.G. Deshpande, Chemical synthesis of porous web-structured CdS thin films for photosensor applications, Mater. Chem. Phys. 160 (2015) 244–250. <https://doi.org/10.1016/j.matchemphys.2015.04.031>.
- [51] S. V. Borse, S.D. Chavhan, R. Sharma, Growth, structural and optical properties of Cd_{1-x}Zn_xS alloy thin films grown by solution growth technique (SGT), J. Alloys Compd. 436 (2007) 407–414.
<https://doi.org/10.1016/j.jallcom.2006.11.009>.
- [52] R. Elilarassi, S. Maheshwari, G. Chandrasekaran, Structural and optical characterization of CdS nanoparticles synthesized using a simple chemical

- reaction route, *Optoelectron. Adv. Mater. Rapid Commun.* 4 (2010) 309–312.
- [53] F. Liu, Y. Lai, J. Liu, B. Wang, S. Kuang, Z. Zhang, J. Li, Y. Liu, Characterization of chemical bath deposited CdS thin films at different deposition temperature, *J. Alloys Compd.* 493 (2010) 305–308. <https://doi.org/10.1016/j.jallcom.2009.12.088>.
- [54] C. Letters, S. Prabakar, N. Suryanarayanan, D. Kathirvel, *Electrical and Photoconduction Studies on Chemical Bath*, 6 (2009) 577–581.
- [55] G. Bakiyaraj, N. Gopalakrishnan, R. Dhanasekaran, Influences of thermal annealing on the structural, optical and electrical properties of nanostructured cadmium sulphide thin films, *Chalcogenide Lett.* 8 (2011) 419–426.
- [56] I. Rathinamala, A. Azhagu Parvathi, J. Pandiarajan, N. Jeyakumaran, N. Prithivikumaran, Influence of annealing temperature on structural and optical properties of CdS thin films prepared by sol-gel spin coating method, *Proc. Int. Conf. "Advanced Nanomater. Emerg. Eng. Technol. ICANMEET 2013.* (2013) 713–717. <https://doi.org/10.1109/ICANMEET.2013.6609396>.
- [57] P. Samarasekara, B.M.M.B. Basnayaka, S. Dehipawala, Photocurrent enhancement of spin coated CdS thin films by adding Cu, *ArXiv.* (2017) 1–12.
- [58] M.D. Devi, A.V. Juliet, K. Hari Prasad, T. Alshahrani, A.M. Alshehri, M. Shkir, S. AIFaify, An effect of precursor concentrations on the photodetection capabilities of CdS thin films for high-efficiency visible-light photodetector applications, *Appl. Phys. A Mater. Sci. Process.* 126 (2020) 1–11. <https://doi.org/10.1007/s00339-020-04067-3>.
- [59] M. Shaban, M. Mustafa, H. Hamdy, Morphological and Optical Study of Sol-Gel SpinCoated Nanostructured CdSThin Films, 7 (2015) 19–22. <https://doi.org/10.9790/4861-07611922>.

- [60] F.Y.A.-S. F. Y. Al-Shaikley, Electrical and Optical Properties Dependence on Annealing Temperature for CdS Thin Films, *Indian J. Appl. Res.* 3 (2011) 544–548. <https://doi.org/10.15373/2249555x/may2013/176>.
- [61] C. Doroody, K.S. Rahman, H.N. Rosly, M.N. Harif, M. Isah, Y.B. Kar, S.K. Tiong, N. Amin, A comparative study of CdS thin films grown on ultra-thin glass substrates by RF magnetron sputtering and chemical bath deposition, *Mater. Sci. Semicond. Process.* 133 (2021) 105935. <https://doi.org/10.1016/j.mssp.2021.105935>.
- [62] A.I. Oliva, O. Solís-Canto, R. Castro-Rodríguez, P. Quintana, Formation of the band gap of CdS thin films growth by different techniques, *Mod. Phys. Lett. B.* 15 (2001) 671–674. <https://doi.org/10.1142/S0217984901002269>.
- [63] N.K. Ponon, D.J.R. Appleby, E. Arac, P.J. King, S. Ganti, K.S.K. Kwa, A. O'Neill, Effect of deposition conditions and post deposition anneal on reactively sputtered titanium nitride thin films, *Thin Solid Films.* 578 (2015) 31–37. <https://doi.org/10.1016/j.tsf.2015.02.009>.
- [64] L.S. Ravangave, R.B. Mahewar, Effect of Annealing on Optical Properties of CdS Thin Films International organization of Scientific Research, *IOSR J. Eng.* 05 (2015) 6–8.
- [65] S.S. Shaikh, M. Shkir, E.U. Masumdar, Facile fabrication and characterization of modified spray deposited cadmium sulphide thin films, *Phys. B Condens. Matter.* 571 (2019) 64–70. <https://doi.org/10.1016/j.physb.2019.06.051>.
- [66] S.M.A. Al-dujayli, Characterization of CdS Thin Films Grown by Spray Pyrolysis Deposition Using Different S / Cd Ratios, 6 (2012) 409–417.
- [67] J. Podder, Effect of molar concentration on the optical and surface properties of CdS Thin film EFFECT OF MOLAR CONCENTRATION ON THE OPTICAL AND SURFACE, (2014).
- [68] J. Xing, C. Zhao, E. Guo, F. Yang, High-performance ultraviolet photodetector based on polycrystalline SrTiO₃ thin film, *IEEE Sens. J.* 12

- (2012) 2561–2564. <https://doi.org/10.1109/JSEN.2012.2196429>.
- [69] Z. Liu, G. Chen, B. Liang, G. Yu, H. Huang, D. Chen, G. Shen, Fabrication of high-quality ZnTe nanowires toward high-performance rigid/flexible visible-light photodetectors, *Opt. Express.* 21 (2013) 7799. <https://doi.org/10.1364/oe.21.007799>.
- [70] M. Thambidurai, N. Muthukumarasamy, D. Velauthapillai, N. Murugan, S. Agilan, S. Vasantha, R. Balasundaraprabhu, Nanocrystalline CdS thin films prepared by sol-gel spin coating, *Int. J. Mater. Res.* 102 (2011) 584–586. <https://doi.org/10.3139/146.110505>.
- [71] C.P. Nikam, S.R. Gosavi, Characterization of nanocrystalline CdS thin films deposited on FTO by CBD for photosensor applications, 5 (2014) 267–272.
- [72] M. Reddy, Properties of CdS Chemically Deposited thin films on the Effect of Ammonia Concentration, *IOSR J. Appl. Phys.* 4 (2013) 01–07. <https://doi.org/10.9790/4861-0440107>.
- [73] U.S. Eya, D. D. O., Eze, F. C., Echendu, K. O. and Mbamara, Synthesis and optical properties of chemically deposited cadmium sulphide thin films, *Niger. J. Sol. Energy* . 27 (2016) 85–93.
- [74] V.V.P. Munaga, T. Krishnan, R.K. Borra, Structural, surface morphological, optical and thermoelectric properties of sol–gel spin coated Zn doped CdS thin films, *SN Appl. Sci.* 2 (2020). <https://doi.org/10.1007/s42452-020-2358-3>.
- [75] P.U. Asogwa, OPTICAL AND STRUCTURAL PROPERTIES OF CHEMICAL BATH DEPOSITED CdSe NANOPARTICLE THIN FILMS FOR PHOTOVOLTAIC APPLICATIONS, 2 (2010) 183–189.
- [76] T. Gao, Q.H. Li, T.H. Wang, CdS nanobelts as photoconductors, *Appl. Phys. Lett.* 86 (2005) 1–3. <https://doi.org/10.1063/1.1915514>.
- [77] A. Afal, S. Coskun, H. Emrah Unalan, All solution processed, nanowire enhanced ultraviolet photodetectors, *Appl. Phys. Lett.* 102 (2013).

- <https://doi.org/10.1063/1.4789757>.
- [78] D.S. Chuu, C.M. Dai, W.F. Hsieh, C.T. Tsai, Raman investigations of the surface modes of the crystallites in CdS thin films grown by pulsed laser and thermal evaporation, *J. Appl. Phys.* 69 (1991) 8402–8404. <https://doi.org/10.1063/1.347405>.
- [79] K. Deng, L. Li, CdS Nanoscale Photodetectors, (2014) 2619–2635. <https://doi.org/10.1002/adma.201304621>.
- [80] Z.R. Khan, Munirah, A. Aziz, M.S. Khan, Sol-gel derived CdS nanocrystalline thin films: Optical and photoconduction properties, *Mater. Sci. Pol.* 36 (2018) 235–241. <https://doi.org/10.1515/msp-2018-0028>.
- [81] C. Thirunavukkarasu, K.K. Saranya, B. Janarthanan, J. Chandrasekaran, Design , Fabrication and Working of In-House, (2016) 10017–10023. <https://doi.org/10.15680/IJIRSET.2015.0506068>.
- [82] J. Tauc, R. Grigorovici, A. Vancu, Optical Properties and Electronic Structure of Amorphous Germanium, *Phys. Status Solidi.* 15 (1966) 627–637. <https://doi.org/https://doi.org/10.1002/pssb.19660150224>.
- [83] Z. Makhdoumi-Kakhaki, A. Youzbashi, P. Sangpour, N. Naderi, A. Kazemzadeh, Effects of film thickness and stoichiometric on the electrical, optical and photodetector properties of CdS quantum dots thin films deposited by chemically bath deposition method at different bath temperature, *J. Mater. Sci. Mater. Electron.* 27 (2016) 12931–12939. <https://doi.org/10.1007/s10854-016-5430-4>.
- [84] R. Aggarwal, N. Sharma, R. Kumar, Investigating ions concentration effect on structural and optical characteristics of metal-sulphide's thinfilms for photonic devices, *J. Opt.* (2023). <https://doi.org/10.1007/s12596-023-01095-z>.
- [85] A. Chauhan, Powder XRD Technique and its Applications in Science and Technology, *J. Anal. Bioanal. Tech.* 5 (2014) 1–6. <https://doi.org/10.4172/2155-9872.1000212>.

- [86] A. Abdolazadeh Ziabari, F.E. Ghodsi, Growth, characterization and studying of sol-gel derived CdS nanocrystalline thin films incorporated in polyethyleneglycol: Effects of post-heat treatment, *Sol. Energy Mater. Sol. Cells.* 105 (2012) 249–262. <https://doi.org/10.1016/j.solmat.2012.05.014>.
- [87] H. Metin, R. Esen, Annealing effects on optical and crystallographic properties of CBD grown CdS films, *Semicond. Sci. Technol.* 18 (2003) 647–654. <https://doi.org/10.1088/0268-1242/18/7/308>.
- [88] C.D. Gutiérrez Lazos, E. Rosendo, H. Juárez, G. García Salgado, T. Díaz, M. Rubín Falfán, A.I. Oliva, P. Quintana, D.H. Aguilar, W. Cauich, M. Ortega, Y. Matsumoto, Hexagonal Phase of CdS Thin Films Obtained by Oscillating Chemical Bath, *J. Electrochem. Soc.* 155 (2008) D158. <https://doi.org/10.1149/1.2820620>.
- [89] N. Gupta, S. Choudhry, S.B. Bhardwaj, S. Kumar, S. Kumar, Relativistic Effects on Stimulated Brillouin Scattering of Self-Focused q-Gaussian Laser Beams in Plasmas with Axial Density Ramp, *J. Russ. Laser Res.* 42 (2021) 418–429. <https://doi.org/10.1007/s10946-021-09978-x>.
- [90] N. Gupta, S. Kumar, S.B. Bhardwaj, Stimulated Raman scattering of self focused elliptical q-Gaussian laser beam in plasma with axial temperature ramp: effect of ponderomotive force, *J. Electromagn. Waves Appl.* 36 (2022) 767–786. <https://doi.org/10.1080/09205071.2021.1983877>.
- [91] S. Chun, Y. Jung, J. Kim, D. Kim, The analysis of CdS thin film at the processes of manufacturing CdS/CdTe solar cells, *J. Cryst. Growth.* 326 (2011) 152–156. <https://doi.org/10.1016/j.jcrysgr.2011.01.086>.
- [92] M. Husham, Z. Hassan, M.A. Mahdi, A.M. Selman, N.M. Ahmed, Fabrication and characterization of nanocrystalline CdS thin film-based optical sensor grown via microwave-assisted chemical bath deposition, *Superlattices Microstruct.* 67 (2014) 8–16. <https://doi.org/10.1016/j.spmi.2013.12.010>.
- [93] O. Zelaya-Angel, J.J. Alvarado-Gil, R. Lozada-Morales, H. Vargas, A.

- Ferreira Da Silva, Band-gap shift in CdS semiconductor by photoacoustic spectroscopy: Evidence of a cubic to hexagonal lattice transition, *Appl. Phys. Lett.* 64 (1994) 291–293. <https://doi.org/10.1063/1.111184>.
- [94] E.M.K. Ikbali Ahamed, A.K. Sen Gupta, M.N.I. Khan, M.A. Matin, N. Amin, Effect of Annealing Temperature on the Structural and Optical Properties of CdS Thin Films Deposited by CBD, *2020 IEEE Reg. 10 Symp. TENSYP 2020*. 1 (2020) 1168–1171. <https://doi.org/10.1109/TENSYP50017.2020.9230777>.
- [95] F.T. Munna, P. Chelvanathan, K. Sobayel, K. Nurhafiza, D.K. Sarkar, M. Nour, H. Sindi, M. Rawa, K. Sopian, N. Amin, M. Akhtaruzzaman, Effect of zinc doping on the optoelectronic properties of cadmium sulphide (CdS) thin films deposited by chemical bath deposition by utilising an alternative sulphur precursor, *Optik (Stuttg)*. 218 (2020). <https://doi.org/10.1016/j.ijleo.2020.165197>.
- [96] V.K. Ashith, K. Priya, M.A. A V, R.A. Keshav, G.K. Rao, M. M G, The effects of Zn incorporation on electrical, photoluminescence and spectral sensitivity of SILAR deposited CdS thin films, *Mater. Res. Express*. 7 (2020). <https://doi.org/10.1088/2053-1591/ab5ec4>.
- [97] J.R. Jayaramaiah, R. Shamanth, V. Jayanth, K.S. Shamala, Optical investigation on zinc doped cadmium sulphide nanocrystalline thin films, *Curr. Appl. Phys.* 16 (2016) 799–804. <https://doi.org/10.1016/j.cap.2016.04.011>.
- [98] Q. An, X. Meng, P. Sun, High-Performance Fully Nanostructured Photodetector with Single-Crystalline CdS Nanotubes as Active Layer and Very Long Ag Nanowires as Transparent Electrodes, *ACS Appl. Mater. Interfaces*. 7 (2015) 22941–22952. <https://doi.org/10.1021/acsami.5b06166>.
- [99] D. Yoo, M.S. Choi, C. Chung, S.C. Heo, D. Kim, C. Choi, Characteristics of radio frequency-sputtered ZnS on the flexible polyethylene terephthalate

- (PET) substrate, *J. Nanosci. Nanotechnol.* 13 (2013) 7814–7819. <https://doi.org/10.1166/jnn.2013.8120>.
- [100] A.N. Banerjee, C.K. Ghosh, K.K. Chattopadhyay, H. Minoura, A.K. Sarkar, A. Akiba, A. Kamiya, T. Endo, Low-temperature deposition of ZnO thin films on PET and glass substrates by DC-sputtering technique, *Thin Solid Films*. 496 (2006) 112–116. <https://doi.org/10.1016/j.tsf.2005.08.258>.
- [101] I.M.S. Mohammed, G.M.M. Gubari, N.P. Huse, A.S. Dive, S.H. Han, R. Sharma, Effect of Cd/S ratio on growth and physical properties of CdS thin films for photosensor application, *J. Mater. Sci. Mater. Electron.* 31 (2020) 9989–9996. <https://doi.org/10.1007/s10854-020-03543-z>.
- [102] B. Barman, K. V. Bangera, G.K. Shivakumar, ZnxCd1-xS thin films: A study towards its application as a reliable photodetector, *Superlattices Microstruct.* 137 (2020) 106349. <https://doi.org/10.1016/j.spmi.2019.106349>.
- [103] J. Mathew, S. Devasia, S. Shaji, E.I. Anila, Metal–semiconductor–metal visible photodetector based on Al-doped (Cd:Zn)S nano thin films by hydrothermal synthesis, *Optik (Stuttg)*. 241 (2021) 166878. <https://doi.org/10.1016/j.ijleo.2021.166878>.
- [104] D.I. Halge, V.N. Narwade, P.M. Khanzode, S. Begum, I. Banerjee, J.W. Dadge, J. Kovac, A.S. Rana, K.A. Bogle, Development of highly sensitive and ultra-fast visible-light photodetector using nano-CdS thin film, *Appl. Phys. A Mater. Sci. Process.* 127 (2021) 1–11. <https://doi.org/10.1007/s00339-021-04611-9>.
- [105] M. Husham, Z. Hassan, A.M. Selman, N.K. Allam, Microwave-assisted chemical bath deposition of nanocrystalline CdS thin films with superior photodetection characteristics, *Sensors Actuators, A Phys.* 230 (2015) 9–16. <https://doi.org/10.1016/j.sna.2015.04.010>.
- [106] M. Shkir, M.T. Khan, I.M. Ashraf, A. Almohammed, E. Dieguez, S. AlFaify, High-performance visible light photodetectors based on inorganic

CZT and InCZT single crystals, *Sci. Rep.* 9 (2019) 1–9.
<https://doi.org/10.1038/s41598-019-48621-3>.

List of Conferences

- *International Conference on “Recent Advances in Fundamental and Applied Sciences” (RAFAS-2021), 25-26 June, 2021, Lovely Professional University, Punjab.*
- *International Conference On “Recent Advances in Functional Materials and sciences” held at Atma Ram Sanatana Dharma college, University of Delhi (RAFM-2022) 14-16 March 2022*
- *National conference on “Fundamental and Applied sciences” 20-21OCT 2022 held at Sardar Vallabhbhai National Institute of Technology, Surat*
- *Indo – Norwegian International online conference on “Functional materials for energy, environment and biomedical applications” (FARAON - 2022) held on 2- 4 Feb22*

List of Publication

1. ***“Investigating ions concentration effect on structural and optical characteristics of metal-sulphide’s thin films for photonic devices”***
Rekha Aggarwal, Rajesh Kumar
Journal of optics (2022), DOI: 10.1007/s12596-023-01095-z\
2. ***“Analysis of electrical, optical and structural behaviour of nanostructured CdS thin films for Photosensing devices”***
Rekha Aggarwal, Neha Sharma & Rajesh Kumar
Journal of Optics (2023), DOI: <https://doi.org/10.1007/s12596-022-00996-9>
3. ***“Structural and Optical studies of sol-gel driven spin-coated CdS-thin films”.***
Rekha Aggarwal, Deepak Kumar Kaushik
Journal of physics: Conference series, DOI: 10.1088/1742-6596/2267/1/012012
4. ***“Optimization of thermal annealing effect on sol-gel driven spin-coated CdS thin films”***
Rekha Aggarwal, Rajesh Kumar
JOURNAL OF APPLIED SPECTROSCOPY; Vol. 91, No.1 (January-February) 2024)